High Spatiotemporal Air Quality Measurements in Urban Environments

Dissertation zur Erlangung des Grades

„Doktor der Naturwissenschaften“

im Promotionsfach

Geographie

am Fachbereich Chemie, Pharmazie, Geographie und Geowissenschaften

der Johannes Gutenberg-Universität Mainz

Lorenz Oskar Harr

Mainz, den 04. April 2023

Betreuer der Dissertation

Tag der mündlichen Prüfung: 19. Juli 2023

D77 (Dissertation Universität Mainz))

Summary

Airborne pollutants and PM in particular are one of the greatest environmental threats to human health worldwide. The particles are small enough so that they can be inhaled and, depending on the particle size and composition, reach deep into lungs, where they cause inflammations on bronchi and alveoli. In the EU, stationary measurement networks have therefore been implemented to monitor $PM_{2.5}$ and PM_{10} concentrations. However, personal PM exposure cannot be properly assessed because these immobile monitoring systems cannot provide spatiotemporal PM values in high resolution. They are too sparsely deployed, even in highly populated urban environments. As a result, mobile monitoring is of increasing interest as it improves the horizontal and vertical coverage and allows to display the variability of PM concentrations and their emission sources. Recent developments of highly portable, and easy-to-use low-cost PM sensors further show that these sensors offer the opportunity to revolutionize mobile measurements in high spatiotemporal resolution, even though their measurement performances and resulting fields of applications are questionable.

This thesis addresses (i) potentials and limitations of the Alphasense's low-cost sensors OPC-N3 for mobile measurements to investigate PM exposure differences between children and adults, as well as seasonal changes in PM hotspots and their emission sources and (ii) opportunities offered by investigating PM distribution and attribution to emission sources at submicron resolution in urban environments.

The side-by-side calibrations of the low-cost sensors in the ambient air of Mainz showed that among each other there are good agreements in $PM_{2.5}$ concentration at RH < 85%. On this basis, mobile measurements by foot with the low-cost sensors demonstrated that children were exposed to significantly higher $PM_{2.5}$ than adults under anticyclonic conditions, regardless of the position on the walking route. A microclimate simulation with ENVI-met on the dispersion of exhaust particles showed that the higher PM exposure of children was partly attributed to traffic emissions. A shift in $PM_{2.5}$ hotspots across seasons was identified during mobile measurements on foot in spring and autumn. In spring, the particulate matter hotspots were located at a busy road and a construction site. The high concentrations could be clearly attributed to the high volume of traffic and construction site work. In autumn, on the other hand, the highest concentrations were found in pedestrian areas and a park, where cooking and smoking as well as whirled-up dust from unpaved roads were the main sources. However, to

determine the hotspots, only relative $PM_{2.5}$ concentrations were considered, since the absolute concentrations measured with the low-cost sensors significantly underestimated those of the nearest government monitoring station.

To determine reliable absolute concentrations of PM with high spatial and temporal resolution in the submicrometer particle range, mobile measurements were performed using a GRIMM 11-R reference instrument mounted on a cargo bike. It was demonstrated that concentrations for PM_1 and PM_{10} were significantly higher in the MO than in the AF. Although PNC decreased sharply with increasing D_P throughout the measured route, particles with $D_P < 0.3$ µm and 3–5 µm dominated the total dM at urban hotspots. This indicates traffic-related combustion processes and tire and brake abrasion as main sources. In contrast, natural dust with $D_P > 3$ µm was crucial for the elevated concentrations in the agricultural used part of the study route.

The results of this thesis are of great importance as it was shown that mobile measurements with modern low-cost sensors can be used to indicate PM hotspots and identify their emission sources in high spatiotemporal resolution. In turn, the more expensive cargo bicycle measurement system can provide an even deeper insight into the variability of PNC and PM distributions of particles with varying D_P and providing a new method for revealing patterns from different emission processes. This offers the opportunity to identify emission sources more clearly and enables more effective PM reduction in future urban transportation planning. Mobile measurement systems can therefore complement stationary measurements and, in particular, capture personal exposure in complex urban environments.

Zusammenfassung

Luftschadstoffe und Feinstaub im Besonderen stellen weltweit eine der größten Umweltgefahren für die menschliche Gesundheit dar. Die Partikel sind so klein, dass sie eingeatmet werden können und je nach Partikelgröße und -zusammensetzung bis tief in die Lunge gelangen können, wo sie Entzündungen an Bronchien und Alveolen verursachen. In der EU wurden deshalb von staatlichen Stellen zur Überwachung von $PM_{2.5}$ und PM_{10} stationäre Messnetze eingerichtet. Die persönliche Feinstaubbelastung kann mit dem Messnetz jedoch nicht korrekt erfasst werden, da die Messstationen keine Feinstaubwerte in hoher räumlicher wie zeitlicher Auflösung liefern können. Selbst in dicht besiedelten städtischen Gebieten reicht die Anzahl der Messstationen nicht aus. Infolgedessen sind mobile Messungen von zunehmendem Interesse, denn sie verbessern die horizontale und vertikale Abdeckung und ermöglichen es die Variabilität der Feinstaubkonzentrationen und ihre Emissionsquellen aufzuzeigen. Jüngste Entwicklungen von tragbaren und einfach zu bedienenden Low-Cost Feinstaubsensoren zeigen, dass diese Sensoren die Möglichkeit bieten könnten, mobile Messungen mit hoher räumlicher und zeitlicher Auflösung zu revolutionieren, auch wenn ihre Messqualität und die daraus resultierenden Anwendungsbereiche noch umstritten sind.

Diese Arbeit befasst sich mit (i) den Potentialen und Limitierungen der Low-Cost Sensoren OPC-N3 von Alphasense für mobile Messungen zur Untersuchung möglicher Unterschiede in der Feinstaubbelastung von Kindern und Erwachsenen sowie der saisonalen Veränderungen in Feinstaubhotspots und deren Emissionsquellen und (ii) den Möglichkeiten, die sich durch die Untersuchung der Feinstaubverteilung und der Zuordnung zu Emissionsquellen mit einer hohen Auflösung im Submikrometerbereich in städtischen Umgebungen ergeben.

Die nebeneinander durchgeführten Kalibrierungen der Low-Cost-Sensoren in der städtischen Umgebung von Mainz zeigten, dass es, bei einer relativen Feuchte < 85% , untereinander gute Übereinstimmungen in den Feinstaubkonzentrationen gibt. Auf dieser Grundlage konnte bei mobilen Messungen zu Fuß mit den Low-Cost-Sensoren nachgewiesen werden, dass Kinder bei stabilen Hochdruckwetterlagen einer signifikant höheren $PM_{2.5}$-Belastung ausgesetzt waren als Erwachsene, und zwar unabhängig von der Position auf der Messstrecke. Eine mikroklimatische Simulation mit ENVI-met zu der Ausbreitung von Abgaspartikeln konnte die höhere Feinstaubbelastung von Kindern mitunter auf Verkehrsemissionen zurückführen.

Eine Verschiebung der $PM_{2.5}$-Hotspots über die Jahreszeiten hinweg konnte bei mobilen Messungen zu Fuß im Frühjahr und im Herbst identifiziert werden. Im Frühjahr befanden sich die Feinstaub-Hotspots an einer stark befahrenen Straße und einer Baustelle. Die hohen Konzentrationen konnten dem hohen Verkehrsaufkommen und Baustellenarbeiten zugeordnet werden. Im Herbst wiederum, wurden die höchsten Konzentrationen in Fußgängerzonen und einem Park festgestellt, bei denen das Kochen und Rauchen sowie aufgewirbelter Staub unbefestigter Wege die Hauptquellen waren. Zur Bestimmung der Hotspots wurden dabei jedoch nur relative Feinstaubkonzentrationen betrachtet, da die mit den Low-Cost-Sensoren gemessenen, absoluten Konzentrationen diejenigen der nächstgelegenen, staatlichen Messstation deutlich unterschätzten.

Zur Bestimmung zuverlässiger absoluter Feinstaubkonzentrationen mit hoher räumlicher und zeitlicher Auflösung im Submikrometerbereich wurden mobile Messungen mit einem auf einem Lastenfahrrad montierten GRIMM 11-R-Referenzinstrumenten durchgeführt. Es zeigte sich, dass die Konzentrationen für PM_1 und PM_{10} in MO signifikant höher waren als in AF. Obwohl die PNC mit zunehmendem Partikeldurchmesser auf der ganzen Messstrecke stark abnahmen, dominierten Partikel mit Partikeldurchmessern < 0,3 µm und 3–5 µm den gesamten dM an städtischen Hotspots, was auf verkehrsbedingte Verbrennungsprozesse und Reifen- und Bremsabrieb als Hauptquellen hinweist. Im Gegensatz dazu war natürlicher Staub mit Partikeldurchmessern > 3 µm ausschlaggebend für erhöhte Konzentrationen im landwirtschaftlich genutzten Teil der Untersuchungsstrecke.

Die Ergebnisse dieser Arbeit sind von großer Bedeutung, da gezeigt werden konnte, dass bei mobilen Feinstaubmessungen moderne Low-Cost-Sensoren dazu genutzt werden können, Orte hoher Konzentrationen zu finden und deren Emissionsquellen mit hoher räumlicher und zeitlicher Auflösung zu identifizieren. Das teurere Messsystem ermöglicht sogar detaillierte Einblicke in die Variabilität der PNC und Konzentrationen Partikeln unterschiedlicher Durchmesser und kann somit eine neue Methode zur Bestimmung von Feinstaubverteilungen in urbanen Umgebungen bieten. Dies ermöglicht Emissionsquellen klarer zu identifizieren und kann eine effektive Planung der Feinstaubreduzierung in der zukünftigen städtischen Verkehrsentwicklung unterstützen. Die mobilen Messsysteme haben gezeigt, dass sie die Feinstaubbelastung auf Atemhöhe in komplexen städtischen Umgebungen erfassen können und eine sinnvolle Ergänzung zu den etablierten stationären Messstationen darstellen.

Acknowledgements

Not available online.

Table of Content

1 Introduction

Air pollution is the greatest single environmental risk and a major contributor to the public burden of disease (WHO, 2022). In 2019, air pollution, including household and ambient air pollution led to approx. 6.7 million premature deaths worldwide. Especially the deaths from ambient air pollution increased substantially and becomes predominant in the last centuries. While in 2000, ambient air pollution was responsible for 2.9 million premature deaths, the number of deaths increased up to 4.5 million in 2019 (Fuller et al., 2022). Although this process becomes particularly evident in East Asia, South Asia and Southeast Asia, ambient air pollution is also a serious threat in the European Union (EU) leading to approx. 790,000 premature deaths each year (Lelieveld et al., 2019).

Aware of this, the EU-parliament and -council declared in 2008 a directive to regulate ambient air pollution and improve the air quality to minimize harmful human health effects (European Parliament and Council, 2008). On this basis, directives in quality standards, exceedance levels and objectives were developed and established for a number of air pollutants. Besides the air pollutants such as nitrogen oxides (NO_X), sulfur dioxide (SO_2), carbon monoxide (CO) and ozone (O_3), particulate matter (PM) in particular was identified as important pollutant, since PM is considered to cause the most severe impacts on health (EEA, 2022).

PM contains a mixture of solid particles varying chemical compositions suspended in air. Microscopic particles with an aerodynamic diameter (D_P) $\leq$ 10 µm (PM_{10}) are of special interest, as they are small enough to be inhaled and cause severe health problems. Coarse PM with D_P between 2.5 µm and 10 µm penetrate the upper respiratory system, i.e., nose, mouth and throat, while fine particles with $D_P \leq 2.5$ µm ($PM_{2.5}$) and can reach deep into lungs and cause oxidative stress and inflammation on bronchi and alveoli. These inflammations can lead to cough, trigger asthma, chronic obstructive pulmonary diseases (COPD), cardiovascular disease (CVD) and, in most serious cases, PM exposure can lead to death (Gualtieri et al., 2011; Lelieveld et al., 2019; Torres-Ramos et al., 2011). Submicron aerosols (PM_1) are even worse, as they enhance the aforementioned negative health effects and poorer lung functions. (Jalava et al., 2015; Yang et al., 2020). However, not all people are equally affected. Children are particularly exposed to PM because they breathe more air per body size than adults and their respiratory systems are not yet fully developed. This danger increases the higher the absolute PM concentration (Alemany et al., 2018; Goldman, 1995; Mazur, 2003).

The absolute concentrations of PM depend on the number of emitters, the intensity of each emission and on the prevailing weather conditions. Besides the input of long-distanced transported aeolian mineral dust, e.g. dust from the Sahara to Central Europe, stable anti cyclonic weather conditions in spring and autumn are particularly prominent. Anticyclonic weather situations are characterized by temperature inversion with low windspeeds and little to no precipitation. This leads to a lower mixing layer height (MLH) and, in turn, to a low vertical dispersion of emitted air pollutants (Czernecki et al., 2017; Graham et al., 2020). As a result, emitted PM accumulates locally and causes high absolute concentrations (Tang et al., 2016; Wagner and Schäfer, 2017). The toxicity posed by PM depends, however not solely on the size and concentration, but also varies on the different chemical composition of PM. PM containing metallic elements from combustion processes, i.e., industrial fumes, domestic heating, traffic exhausts, gas and coal cookers and wildfires, as well as from abrasion from construction sites and tyre and brakes show more negative health effects in contrast to biogenic and inorganic components, i.e., parts of plants and pollen as well as mineral dust (e.g. Chen and Lippmann, 2009; Karagulian et al., 2019; Schlesinger, 2007).

For the fractions $PM_{2.5}$[1] and PM_{10}[2], the EU established Air Quality Standards in 2008. These restrictive guidelines lead to considerable success in reducing air pollution as the PM concentrations are constantly decreasing until today. In 2020, for instance, 99% ($PM_{2.5}$) and 89% (PM_{10}) of the EU population were living in areas where the respective exceeding levels were undercut. Following the recommendations of the WHO guidelines[3], however, 96% ($PM_{2.5}$) and 70% (PM_{10}) of the population in the EU in 2022 is still exposed to hazardous concentration levels (EEA, 2023).

As a result, PM concentrations and population exposure still need to be reduced. This is especially relevant for urban environments, as at least 74% of the EU population lives in cities (Eurostat, 2016). Therefore, the numbers of air quality monitoring stations increased from 1300 in 1990 to > 5000 measurement sites in 2020 (Sicard et al., 2021). This quantity of stations seems to provide good spatial coverage of monitoring across the EU, but the measuring sites are still several kilometers apart from each other, even in urban areas. Since the focus is on monitoring daily and annual exceedances of PM concentrations, only PM_{10}, $PM_{2.5}$ and (rarely)

[1] annual average concentration target: 20 µg/m³ (European Parliament and Council, 2008)
[2] annual average concentration target: 40 µg/m³; daily average concentration of 50 µg/m³ may not be exceeded more than 35 times a year (European Parliament and Council, 2008)
[3] $PM_{2.5}$: annual average concentration target: 5 µg/m³; 24h-average concentration: 15 µg/m³
PM_{10}: annual average concentration target: 15 µg/m³; 24h-average concentration: 45 µg/m³ (WHO, 2021)

PM_1 are measured at intervals > 30 min at one height of 1.5 – 4 m (European Parliament and Council, 2008). To study personal exposures in urban areas, the stationary monitoring is too sparse and the measurements do not have high enough temporal resolution. PM concentrations can vary spatially and vertically in a distance of a few meters due to varying building structures and the PM exposure can differ greatly within a few seconds due to changing intensity of emissions and its sources (e.g. Briggs et al., 2000; Bukowiecki et al., 2010; WHO, 2022). Estimates of spatial differences, e.g. the identification of PM hotspots, differences between busy streets within a street canyon and traffic-calmed streets in single-family residential areas or parks and pedestrian zones as well as the attribution of locally measured PM to emission sources in urban environments are not possible (e.g. Parkhurst et al., 1999; Snyder et al., 2013; Xu et al., 2017). Similarly, estimates of possible variations in vertical personal exposure of children and adults are not feasible due to measurements on only one height (e.g. Garcia-Algar et al., 2015; Kumar et al., 2008)

Mobile PM measurement devices offer the opportunity to close the spatial gap and complement stationary systems. These devices are monitoring systems that can be attached to means of transport such as trams, cars or bicycles and, equipped with GPS sensors, can provide location-accurate measurements (e.g. Aberer et al., 2010; Carreras et al., 2020; Castell et al., 2016). Besides portability, the measuring devices offer the possibility to carry out measurements of size distributed PNC and dM in high temporal resolution in an interval of up to 1 s and thus achieve a high spatiotemporal coverage, depending on the speed of movement during the measurement. However, mobile air quality measurements are very preparation- and labor-intensive due to sensitive devices and the mostly self-developed monitoring systems are therefore difficult to conduct (WMO, 2018).

Low-cost devices could bring therefore revolutionary advances in mobile PM measurements. In the last decade, many low-cost devices and sensors have entered the market as they are easy-to-use, affordable (< 1000 $ per device) and small in size (< 10 x 10 x 10 cm) and weight (< 105 g) (Alfano et al., 2020; Morawska et al., 2018). These advantages make them advantageous for mobile scientific studies as they can be easily mounted on a rack to monitor by foot or bike (e.g. Carreras et al., 2020; Garcia-Algar et al., 2015; Kumar et al., 2017) as well as for citizen science monitoring with multiple simultaneously used sensors (Fritz et al., 2019; Mead et al., 2013; West et al., 2020).

Despite these undeniable new possibilities and advantages, low-cost PM sensors have notable limitations. Although most sensors are factory calibrated and perform very well under

laboratory conditions for the common fractions $PM_{2.5}$ and PM_{10} (Morawska et al., 2018; Sousan et al., 2016), the measurements can be very inaccurate due to RH sensitivity of the sensors and changing PM compositions (Di Antonio et al., 2018). As significant inaccuracies can occur even between sensors of the same type (Crilley et al., 2020, 2018), studies on low-cost sensor testing and evaluating remain still popular (e.g. Báthory et al., 2022; Kaur and Kelly, 2022; Roberts et al., 2022).

Following section 2 presents an exploration study about potential personal $PM_{2.5}$ exposure differences of children and adults in the urban environment of Mainz under anticyclonic weather conditions at high spatiotemporal resolution. As there is only research on personal exposure differences using expensive reference instruments (Garcia-Algar et al., 2015; Goel and Kumar, 2016; Kumar et al., 2017; Sharma and Kumar, 2018), this study focuses on using two mobile, self-designed devices with Alphasense OPC-N3 low-cost sensors developed for the $PM_{2.5}$ and PM_{10} fractions to measures at children (1.0 m) and adults (1.6 m) breath levels on walking routes. The results were afterwards compared with a microclimate simulation by ENVI-met featuring specific weather conditions of the study period and according local traffic emission rates to specify the influence of traffic on exposure differences. The author supported substantially the work out of the concept and methodology and was responsible for the investigation and data curation. He wrote the majority of the manuscript and the visualization (excluding Fig. 2-7). The manuscript was published in *Urban Climate* 44 (2022) in July 2022 (Harr et al., 2022b).

In order to further assess the health risk to citizens, it is important to identify locations with high PM concentrations as well as their emission sources on pedestrian breath level during different times of the year. In the study introduced in section 3, mobile $PM_{2.5}$ measurements with Alphasense OPC-N3 low-cost sensors at breathing height of adults (1.6 m) were carried out simultaneously on foot on three routes in the urban area of Mainz in spring and autmn to identify spatially and seasonally variations in $PM_{2.5}$ and its sources. The obtained absolute $PM_{2.5}$ data was compared with stationary measurements to examine whether a previously side-by-side calibration would be sufficient to receive expectable absolute $PM_{2.5}$ concentrations. Furthermore, urban $PM_{2.5}$ hotspots and their emission sources were indicated using $PM_{2.5}$ / PM_{10} ratios as well as seasonal variabilities in hotspots were discussed. The author supported substantially the conceptualization, methodology, formal analysis, and was responsible for investigation and data curation. He wrote the majority of the manuscript including the figures. The manuscript was published in *Atmosphere* 13 694 (2022) in April 2022 (Harr et al., 2022a).

Emission sources can be of inhomogeneous particle D_P as they can be released by different processes, e.g. traffic emissions containing of exhaust and various non-exhaust emissions (Harrison et al., 2021; Squizzato et al., 2016). Low-cost sensors as Alphasense OPC-N3 were manufactured to measure primary $PM_{2.5}$ and PM_{10} which is why they were not able to resolve spatiotemporal patterns for varying particle D_P. The study in Section 4 shows a new approach to address the spatial distribution and attribution of PNC and concentrations at high, (sub-) micron particle resolution: Mobile measurements were conducted using a GRIMM 11-R laser aerosol spectrometer mounted on a mobile cargo bike platform. After comparing measured PM_1 and PM_{10} with stationary data, the spatial variability of these fractions was analyzed to identify hotspots, followed by a quantification of the measured PNC and dM in submicron resolution, and the identification of the emission sources at the hotspots along distinct source pattern. The author was largely involved in the conception, methodology and formal analysis and was responsible for the research and data maintenance. He wrote the manuscript including the graphics. The manuscript is under Review in *Atmospheric Environment*.

2 $PM_{2.5}$ exposure differences between children and adults

Harr Lorenz[1], Tim Sinsel[1], Helge Simon[1], Oliver Konter[1], Damian Dreiseitl[1], Philipp Schulz[1], Esper Jan[1,2]

[1]*Department of Geography, Johannes Gutenberg-University, Johann-Joachim-Becher-Weg 21, 55128 Mainz, Germany*

[2]*Global Change Research Institute of the Czech Academy of Sciences (CzechGlobe), 60300 Brno, Czech Republic*

Summary

Heights of children and adults vary substantially and can lead to different $PM_{2.5}$ exposure, as children's breath level are closer to emissions released near ground. This is especially the case in urban environments, where local, ground-level, traffic-related emissions can have a large impact on total concentrations. As there is only research on personal exposure differences using expensive reference instruments, and citizen sciences studies using low-cost sensors have greatly increased, this study focuses on using two mobile, self-designed devices with low-cost sensors to measure $PM_{2.5}$ at children (1.0 m) and adults (1.6 m) breath levels on walking routes in high spatiotemporal resolution. The results were then compared with an ENVI-met microclimate simulation that considers specific weather conditions of the study period and corresponding local traffic emission rates to specify the influence of traffic on exposure differences. The author conducted previously a side-by-side calibration to assess the measurement quality of the low-cost sensors and supported then substantially the work out of the concept and methodology. He was also responsible for the investigation, data curation and wrote the majority of the manuscript including the visualization (exclusive of Fig. 2-7).

“

2.1 Introduction

Various epidemiological studies provide evidence that air pollution exposure has negative effects on public health causing respiratory and cardiovascular diseases and even increase mortality (Feng et al., 2016; Lelieveld et al., 2019). Fine particles with a size < 2.5 µm can reach the lungs via the respiratory tract and cause airway inflammation followed by a decrease in lung function and even chronic obstructive pulmonary disease (Gualtieri et al., 2011; Lelieveld et al., 2019; Torres-Ramos et al., 2011).

Children are particularly exposed to ambient PM. As their breathe more air per body size and have a greater risk due to their smaller airways than adults (Goldman, 1995; Mazur, 2003). Their respiratory system is not completely developed, they are exposed to an increased risk of developing respiratory diseases and exacerbation of asthma (Habre et al., 2014; Nachman and Parker, 2012).

In urban environments, $PM_{2.5}$ concentration largely stems from locally emitted sources including traffic-related particles (exhausts, tyre and brake abrasion), house heating, construction sites, soil and biogenic compositions (Azarmi et al., 2016; Karagulian et al., 2019; Kumar et al., 2015). Factors influencing ambient concentrations include the number of emitters as well as mesoscale weather condition. Anticyclonic weather in European autumn and winter is characterized by low wind speeds and little to no precipitation (Czernecki et al., 2017; Graham et al., 2020). Mesoscale high pressure systems lower atmospheric MLH hindering vertical dispersion of air pollutants, which in turn causes an accumulation of locally emitted $PM_{2.5}$ within the planetary boundary layer (Tang et al., 2016; Wagner and Schäfer, 2017).

Several studies found that pollutant concentration decreases with increasing height above ground (Goel and Kumar, 2016; Imhof et al., 2005; Kumar et al., 2008; Zauli Sajani et al., 2018; Zhou et al., 2019). However, only a few studies examined vertical differences near the surface in heights < 2 m (Garcia-Algar et al., 2015; Goel and Kumar, 2016; Kumar et al., 2017; Sharma and Kumar, 2020), whereby these are particularly important when it comes to pedestrian exposure. The smaller size of children in comparison to adults means their breath levels are closer to pollutants emitted near ground, making them potentially more vulnerable to emissions by traffic-related exhausts and whirled up fine particles (Kumar et al., 2017; Sharma and Kumar, 2020).

To examine potentially varying exposure differences between adults and children, we measured $PM_{2.5}$ at two heights, 1.0 m and 1.6 m, in a dense urban environment featuring different traffic intensities. The measurements were conducted using self-designed monitoring systems hosting Alphasense OPC-N3 low-cost sensors (Alphasense, 2018). The sensors are easily portable due to their small size and weight, and perform well under laboratory conditions (Morawska et al., 2018; Sousan et al., 2016), making them suitable for studies about spatial PM exposure (Brattich et al., 2020; Bulot et al., 2019; Jovašević-Stojanović et al., 2019). However, under ambient air conditions in urban areas, the accuracy of measurements is negatively affected by changing particle compositions and even more so by changing RH (Alfano et al., 2020; Brattich et al., 2020; Crilley et al., 2018; Di Antonio et al., 2018). These limitations were addressed by calibrating the sensors and comparing the empirical findings with simulations from a microscale model considering particle advection and dispersion modelling was conducted (Singh et al., 2003).

The main objective of this study is to examine potential differences of $PM_{2.5}$ exposure between children and adults in an urban area at high spatiotemporal resolution. We (i) compare changes in $PM_{2.5}$ concentrations related to changing weather conditions, (ii) quantify the absolute and relative exposure differences between children and adults considering the position on the measurement route, and (iii) assess findings by comparing measured differences with microclimate simulation outputs.

2.2 Material and methods

2.2.1 Study characteristics

The study was conducted in Mainz-Neustadt, an urban area district of Mainz, the capital of Rhineland-Palatinate in South-West Germany (50.0 °N, 8.26 °E, Fig. 1a). Mainz is an inland city with approximately 220,000 inhabitants, located in a landscape of gently rolling hills to the west of the Rhine river. The climate is temperate with an annual average TA of 10.7 °C and precipitation of 620 mm (Koeppen Cfb). The winters are cool and dry. From November to March, the mean TA is 3.9 °C and mean precipitation is 48 mm (Deutscher Wetterdienst, 2021a, 2021b). The urban architecture of this densely populated area consists of compact midrise structures with a grid-based street layout (Stewart and Oke, 2012). The streets are mostly narrow (10 m wide) and feature low traffic intensity. The city quarter is surrounded by larger multi-lane roads with high traffic volume.

To capture local differences in $PM_{2.5}$ concentration, a clockwise circular, 5.5 km-long measurement track passes through both, the inner narrower low traffic parts as well as the larger roads of the Neustadt (Fig. 2-1 a). The track starts at Mainz main station (50.0017 °N, 8.2595 °E), then runs within the inner part of the district, passing social institutions, i.e., kindergartens, primary and secondary schools as well as nursing and retirement homes. After leaving the center of the quarter, the transect continues along roads with high intensity of traffic, first in southeast, then in southwest direction (Fig. 2-1Fig. 2-1 e) ending at the main station.

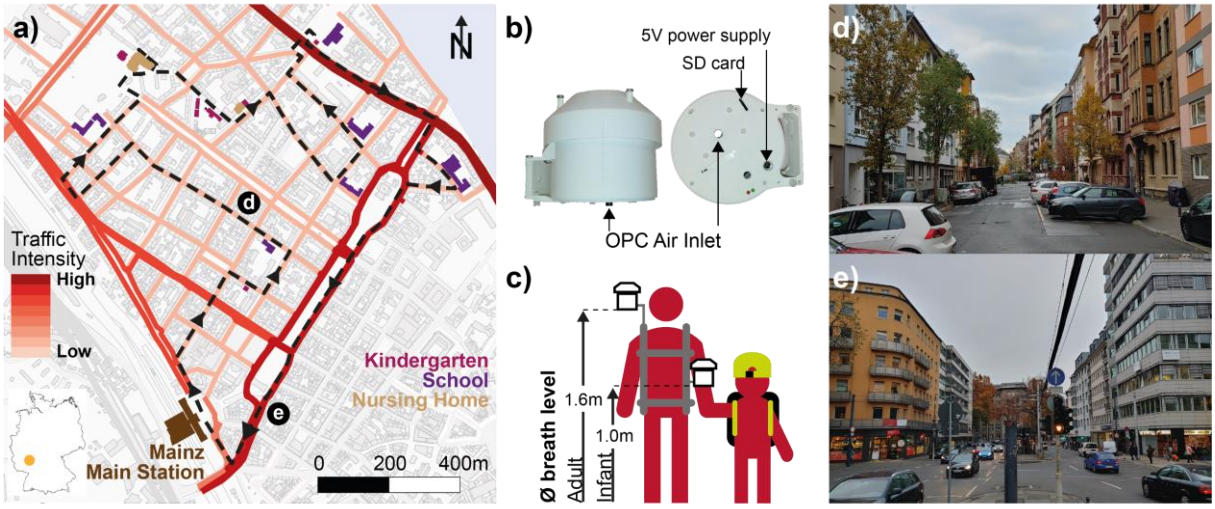

Fig. 2-1 Location of the study district Mainz-Neustadt including the start/end point Mainz main station (brown) of the measurement transect (dashed black line) with nearby social institutions, i.e., kindergartens (pink), primary and secondary schools (purple) and nursing homes (light brown). The streets within the district are colored depending on traffic intensity (**a)**. Design of the measurement devices (dimensions: 11.5 cm x 14 cm x 12.5 cm) (**b)**. Two devices mounted offset on the front of a wearable rack at breath levels of adults (1.6 m) and children (1.0 m), respectively (**c)**. Typical city block street canyons with low (**d)** and high traffic intensity (**e)**.

The measurement campaign took place from 20.11.2019 to 27.11.2019 (Wednesday to Wednesday). The measurement runs were conducted by foot starting at 3:15 pm and ending at ~ 4.30 pm every day covering the time of daily of kindergarten and school endings and start of the rush hour within the study area. For each run, two devices containing a PM sensor (Alphasense, 2018), a GPS module (Simcom, 2021), a ESP32 as microcontroller (Espressif, 2021) and a microSD card for saving the data were used (Fig. 2-1 b). The cover of the cases protruded all around over the side parts were similar to a radiation shield cap to support an unconstrained outflow of the air sample. The devices were mounted at the breath level of adults (1.6 m, device A) and children (1.0 m, device B). To reduce influences induced by the

measuring person, the devices were attached at the front of the body at a distance of 30cm (Fig. 2-1 c). Every run was filmed with a camera to facilitate detections of possible local emitters in the post-processing of the measuring campaign.

2.2.2 Meteorological data

A detailed description of the meteorology during the measurement period is needed as the local weather characteristics affect the type, number, and duration of PM concentrations (Cheng and Li, 2010; Graham et al., 2020; McGregor and Bamzelis, 1995). The central emission network of Rhineland-Palatinate kindly provided 3-min-arithmetic-means of TA, RH, precipitation, and atmospheric pressure (Fig. 2-A1), measured at the station Mainz-Zitadelle (49.9950 °N, 8.2739 °E) located ~ 1.2 km west of the study area, as well as 3-min-sums of precipitation, wind direction and speed at the station Mainz-Mombach (50.0180 °N, 8.2157 °E) located ~ 3 km west of the study area (ZIMEN, 2019). Data of the CIN and MLH, indicators for the stability of the air near the ground, were measured with a radiometer located ~ 500 m west of the study area (50.01406 °N 8.257 °E). These data were provided by the environmental meteorology unit of the environmental state office of Rhineland-Palatinate (Umweltmeteorologie RLP, 2019).

2.2.3 Calibration of $PM_{2.5}$ sensors

The $PM_{2.5}$ measurements on both breathing heights were conducted using an Alphasense OPC-N3 sensor (Alphasense, 2018). The OPC-N3 is a low-cost optical particle counter using the light scattering principle to count particles (Mie, 1908). The total number counted is processed internally in the sensor, categorized by estimated particle size in 24 classes using software bins (Alphasense, 2018; Bohren and Huffman, 1998) and converts the data into dM (Walser et al., 2017). During the default settings of the sensor's principles were made.

Both OPC-N3 sensors were manufacture-calibrated following the European Standard EN 481 (Crilley et al., 2018). However, to improve sensor accuracy, a field calibration in an environment comparable to the study area has been conducted (Alfano et al., 2020; Chatzidiakou et al., 2019; Crilley et al., 2020; Gysel et al., 2007; Hagler et al., 2018). This was done from 22.12.2019 to 31.12.2019 at the official measurement station Mainz-Zitadelle (49.9950 °N, 8.2739 °E) of ZIMEN. Both Alphasense devices were located side-by-side on the same height measuring $PM_{2.5}$ concentration at a 1 s interval. The data were then transformed into running 20 s-truncated arithmetic means and RH-corrected to mitigate the influence of fine

particle hygroscopy (Crilley et al., 2018; Petters and Kreidenweis, 2007). The correction is based on the *k*-Köhler-theory considering a particle hygroscopy of $k = 0.33$, density of particles of 1.65 g/cm³ (Crilley et al., 2020), and ambient RH recorded at the official station Mainz-Zitadelle.

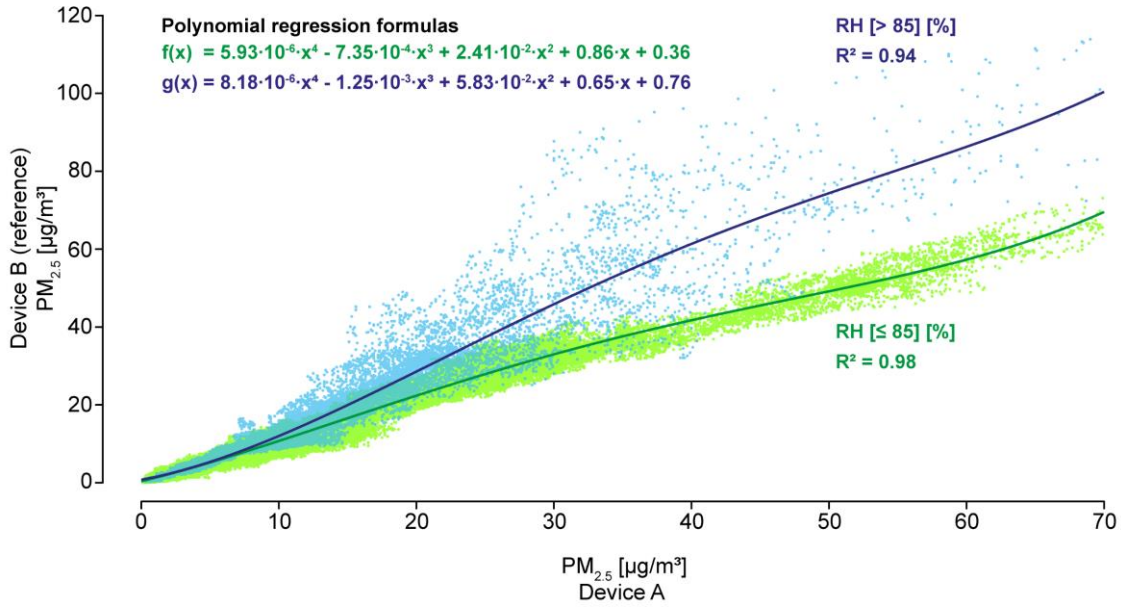

Fig. 2-2 Scatter plots and polynomial regression curves of devices A and B $PM_{2.5}$ measurements from the adjustment period 22.12.2019 to 31.12.2019. The green data and curve show the measurements for RH ≤ 85% and the blue data for RH > 85% (blue dots and line), as well as the regression equations and coefficients R^2, respectively.

The scatter plot between $PM_{2.5}$ data from devices A and B reveal high precision measurements when RH ≤ 85% as reflected by the explained variance ($R^2 = 0.98$) and data homoscedasticity (Fig. 2). This allowed a reliable comparison of $PM_{2.5}$ measurements by transforming the measurements of device A considering the 4th degree polynomial regression model shown as a green curve in Fig. 2. For the data recorded at RH > 85%, the $PM_{2.5}$ correlation and resulting correction are weaker (blue data, Fig. 2-2). The scatter plot includes an obvious heteroscedasticity for $PM_{2.5}$ > 10 µg/m³ largely driven by increased residuals in device A $PM_{2.5}$ concentrations. This increased variability of OPC-N3 devices is in line with results by Brattich et al., 2020 revealing similar biases for the predecessor device, OPC-N2, and identifying a systematic misclassification of PM sizes during high RH conditions. These results question the reliability of $PM_{2.5}$ data recorded at RH > 85%. Nevertheless, these measurements are fitted with a different model, shown as the blue curve in Fig. 2-2, considering the weak reliability for $PM_{2.5}$ > 10 µg/m³.

2.2.4 Post-processing analysis

After each measurement run, several post-processing steps were carried out to support the comparison between heights and among runs. The datasets of devices A and B were adjusted by time (Wickham, 2020), the $PM_{2.5}$ concentrations, recorded in a 1 s-interval, transformed into a running 20 s-truncated arithmetic mean, and the 10% highest values removed to mitigate the influence of local short-term emissions (e.g. smokers or street cleaning). Since the duration of the different runs varied slightly and minor inaccuracies affected the recorded GPS data, an additional synchronizing procedure was applied: We calculated a mean standard route considering a concave hull surrounding all runs and retrieving the mean by the skeleton algorithm of the GRASS GIS Processing Toolbox (Fortune, 1987; McCauley et al., 2020). A few remaining inaccuracies were re-digitized manually. The standard route was converted to points with a distance of 20 cm to each other (total n = 27515). Each point was assigned the appropriate $PM_{2.5}$ concentration, in which all values within a search radius of 15 m are averaged using an inverse distance weighting method (Shepard, 1968). If less than 10 measurements were found, the radius was increased to 50 m. The $PM_{2.5}$ data were adjusted using the same RH correction method as during the calibration (Crilley et al., 2020, 2018). To compare absolute $PM_{2.5}$ values, device A data were transformed considering the regression equation from a polynomial fit against the device B data (Fig. 2-2). The adjusted $PM_{2.5}$ data were analyzed using descriptive statistics, i.e., arithmetic mean, median, SD and CV. Cubic smoothing splines (degrees of freedom = 55, n = 27515) were calculated to reduce the sensitivity of $PM_{2.5}$ measurements to short-term extreme concentrations. The correlation coefficient R was used to quantify the relation between the measurements of the two heights and respective smoothing splines. To assess differences between 1.0 m and 1.6 m levels, the RMSE was calculated considering daily data, and residuals and relative differences were calculated in cases of pronounced differences in $PM_{2.5}$ concentrations. Welch's t-test was conducted to assess statistically significant differences in case of unequal variances.

2.2.5 Simulation setup

To examine whether traffic exhausts can be assigned as a cause for varying PM exposures along streets with high traffic intensities, a pollutant dispersion simulation for one exemplary day of the measurement period was conducted. This simulation was performed using the holistic ENVI-met microclimate model, which is able to simulate pollutant concentration distributions for specific meteorological conditions in complex urban environments (Bruse, 1999; Nachman

and Parker, 2012; Wania et al., 2012). The 24.11. was selected as is represents a day of average meteorological conditions and $PM_{2.5}$ concentrations after a short period of air mass exchange the day before. RH was < 85% during the time of the run, so the measurements should be reliable (Tab. 2-1). The modelled area covers the district of Mainz-Neustadt with a dimension of 280 x 250 x 26 grids at 5 x 5 x 2 m per grid (Tab. 2-1). The simulation started with full forcing at 11 am using the 30 min mean-meteorological parameters of that day as meteorological boundary conditions (Fig. 2-A1). Wind speed and direction were set constant to avoid instabilities in the model. Radiation was forced by only cloud coverage as measured values were not available.

Tab. 2-1 model parameters of the simulated emissions for 24.11.2019 in ENVI-met.

Start date and time (Local)	24.11.2019 11:00
Duration [h]	10
Wind Speed [m s^{-1}]	1.0
Wind Direction [°]	115
Meteorological Boundary Conditions	Full Forcing
Emission height [m]	0.2
Location Lat (Lower Left Corner)	50.01 °N
Location Lon (Lower Left Corner)	8.25 °E
Dimensions	280 x 250 x 26
Resolutions (X, Y, Z) [m]	5 x 5 x 2
Lowest Grid Cell Splitted	Yes
Telescoping: Factor & Starting Height	30% above 28 m
Height of 3D Model Domain [m]	221

The applied $PM_{2.5}$ emissions originating from vehicle exhausts were implemented as source emission profiles at a height of 20 cm in the model. The diurnal profiles of traffic exhaust emissions are based on the handbook of emission factors for Road Transport (Environmental Protection Agency of Germany, 2017) and the amounts of emitted $PM_{2.5}$ in the model area were related to the intensity of traffic per lane (Fig. 2-1). Detailed settings about the traffic emission profiles are described in Simon et al., 2019, where model area and traffic intensities were initially used. The relative differences of $PM_{2.5}$ concentrations were computed between 1.0 m and 1.8 m due to the simulations grid cell resolution of only 0.4 m to compare the model outputs to the measurement data.

2.3 Results

2.3.1 Weather conditions

During the measurement period, the weather situation was dominated by a continental anticyclone centered over Eastern Europe, ~ 2000 km away. On 20.11. and 22.11., Germany was located between a long wave trough in the west and a ridge in the east. This led to weak atmospheric pressure gradients (~Δ 10 hPa around 1003 hPa) and calm weather characterized by low wind speeds (< 0.8 m/s), small daily TA gradients (max. Δ 5.3 °C, 1.6 °C – 6.9 °C on 22.11.) and RH ranging from 72 – 90%. CIN was subjected to diurnal courses with increasing gradients (Δ 106 J/kg around 89 J/kg to Δ 163 J/kg around 181 J/kg) which led to lower maximum MLH, declining from 386 to 300 m a.g.l., and low stratus conditions in Mainz (Hoffmann, 2019). Starting on 22.11. ~ 2:30 pm, the anticyclonic influence was interrupted by weak cyclonal conditions, which led to a dissolution of low stratus in Mainz in the MO of 23.11. (Zeuschner, 2019). Wind speed rose to 1.6 m/s at 11 am, interrupted by an absence of wind at around 2:30 am. The atmospheric pressure gradient decreased slowly reaching a minimum of 982 hPa in the AF and TA increased up to 11.7 °C. However, the CIN gradient decreased (Δ83 J/kg 177 J/kg) but remained > 100 J/kg indicating that, at the end of 23.11., the ridge of the anticyclone became influential again. Starting on 24.11., the wind speed declined < 0.5 m/s and TA and the air pressure increased to maxima of 9.8 °C and 999 hPa, respectively. Moreover, RH rose to a maximum of 92.2% in the MO of 25.11. and remained > 83.5% thereafter. On 26.11., the weather changed from an anticyclonic to a calm cyclonic situation characterized by a slowly decreasing air pressure from 999 to 990 hPa, rising TA to 11.4 °C, and low wind speeds < 0.5 m/s. However, on 27.11., the last day of the study, wind speed increased again to a maximum of 1.1 m/s, while TA still increased (to 12.3 °C) and precipitation started, summing up to 13.4 mm. The influence of the anticyclone on the weather situation thus retreated.

2.3.2 Recorded $PM_{2.5}$ concentrations

Fig. 2-3 shows the $PM_{2.5}$ concentrations at the 1.0 and 1.6 m levels for every run of the measurement campaign. The absolute $PM_{2.5}$ concentrations at both levels differed substantially among runs over the course of the period from 20.11. to 27.11. Mean $PM_{2.5}$ concentrations at 1.0 m increased from 6.1 µg/m³ on 20.11. to 46.4 µg/m³ on 22.11., then declined massively to 2.7 µg/m³ on 23.11., reached a distinct peak of 67.8 µg/m³ on the next day and then decreased to 2.2 µg/m³ until 27.11. (0).

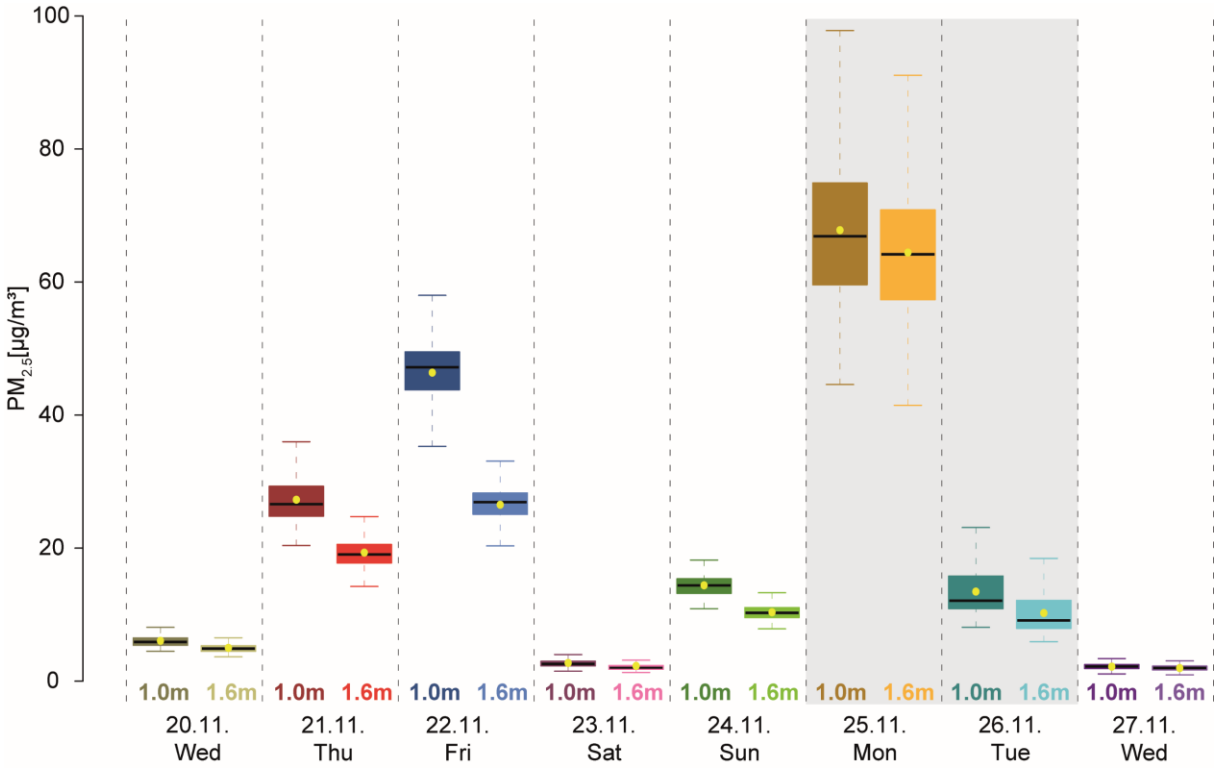

Fig. 2-3 $PM_{2.5}$ concentrations at the 1.0 and 1.6 m levels for every run from 20.11. to 27.11. visualized as boxplots with whiskers (length 1.5 * IQR), median (black bar) and mean (yellow dot). Grey background indicates RH > 85% during the run.

During all days, the $PM_{2.5}$ concentrations at 1.0 m were higher than on 1.6 m (Tab. 2). On 20.11., 21.11., 22.11. and 24.11. the IQR do not overlap, indicating that at least 75% of the $PM_{2.5}$ concentrations measured at 1.6m are lower than at least 75% of the $PM_{2.5}$ values at 1.0 m. The temporal distribution along the days (Fig. 4) shows that on 21.11., 22.11. and 24.11. the concentrations at the children breath level were constantly higher than at adult level (RMSE: 8.2 µg/m³, 20.1 µg/m³, 4.1 µg/m³, respectively).This is also the case for the run on 26.11. (RMSE: 3.4 µg/m³), but the data had to be adjusted using the equation for RH > 85% (Fig. 2; Tab. 3). On 20.11. and 23.11., the 1.0 m $PM_{2.5}$ concentrations were higher in 97% and 88% of all measurement points, independent of the position of the route (RMSE: 1.2 µg/m³, 1.5 µg/m³, respectively). For the remaining six days, the $PM_{2.5}$ concentrations were significantly higher at 1.0 m than at 1.6 m according to a Welch t-test ($p < 0.01$).

Tab. 2-2 $PM_{2.5}$ characteristics at 1.0 m (dark yellow) and 1.6 m (light yellow) for the 8-day measurement campaign.

date	**20.11.**		**21.11.**		**22.11.**		**23.11.**		**24.11.**		**25.11.**		**26.11.**		**27.11.**	
Mean $PM_{2.5}$ [µg/m³]	6.1	5.0	27.3	19.3	46.4	26.5	2.7	2.3	14.4	10.4	67.8	64.4	13.5	10.2	2.2	2.0
Median $PM_{2.5}$ [µg/m³]	5.9	4.9	26.6	19.1	47.3	26.9	2.6	2.0	14.4	10.3	66.9	64.2	12.1	9.1	2.2	2.0
SD [µg/m³]	1.2	1.1	3.6	2.4	4.7	2.4	0.9	1.4	1.4	1.1	10.6	9.9	3.8	3.3	0.5	0.4
CV	0.19	0.21	0.13	0.12	0.10	0.10	0.33	0.61	0.10	0.10	0.16	0.15	0.28	0.32	0.22	0.20

On 25.11., the $PM_{2.5}$ concentrations measured by device A were adjusted using the equation for RH > 85% (Fig. 2-2, Tab. 2-3). Considering the unexplained variance of the adjustment procedure (6%) as well as the uncertainties for $PM_{2.5}$ > 10 µg/m³, the recorded differences between children and adult breathing heights were insignificant on that day. On 27.11., the differences were not distinguishable due to low absolute $PM_{2.5}$ concentrations including 97% of measurements < 3 µg/m³ at 1 m, and 99% of measurements < 3 µg/m³ at 1.6 m, with the absolute differences (~ 0.2 µg/m³) approaching measurement accuracy.

Tab. 2-3 Meteorological conditions during the measurement campaign from 20.11. to 27.11. including Mean TA [°C], Mean RH [%], Precipitation Sum [mm], Atmospheric Pressure [hPA], Wind Speed [m/s], Wind Direction [°], Mean CIN [J/kg] and MLH [m] (Umweltmeteorologie RLP, 2019; ZIMEN, 2019).

date	**20.11.**	**21.11.**	**22.11.**	**23.11.**	**24.11.**	**25.11.**	**26.11.**	**27.11.**
TA [°C]	5.0	5.9	6.6	11.5	8.9	6.7	11.1	12.3
RH [%]	77.3	78.1	81	62.5	78	87	86	78
Precipitation [mm]	0	0.1	0	0	0	0	0	4.3
Atmospheric pressure [hPA]	1004	998	996	987	997	999	994	983
Wind direction [°]	116	152	119	90	142	-	-	129
Wind speed[m/s]	0.4	0.1	0.7	0.5	0.1	0	0	0.5
CIN [J/kg]	62	134	113	156	164	149	100	88
MLH [m]	289	239	301	130	116	183	74	54

2.3.3 Distribution of $PM_{2.5}$ along the route

The temporal variability of $PM_{2.5}$ measurements were low (CV < 0.22) as well as the differences in variability of both heights among the runs (CV difference max. 0.04; 0). Exceptions are the runs on 23.11. and 26.11.: the high CVs (1.0 m: 0.33; 1.6 m: 0.61) on 23.11. were affected by an oncoming person at the beginning of the run, holding a cigarette between 1.0 and 1.6 m, so the devices recorded the short-term pollution shortly one after the other. The higher variabilities

on 26.11. (1.0 m: 0.28; 1.6 m: 0.32) could not be attributed to single incidents, explanations could be RH > 85% as well as weakening of anticyclonic weather.

The distribution of the absolute $PM_{2.5}$ concentrations indicated common concentration patterns between the two measurement heights ($R_{Run\_all} > 0.8$) (Fig. 4). This coherence was reduced on days with low $PM_{2.5}$ concentrations, on 23.11. and 27.11., with R_{Run}= 0.29 and R_{Run} = 0.46, respectively, when random variability near the measurement accuracy adds uncertainty to the data. However, there is no common temporal pattern among the runs, as some timeseries increase throughout the run (21.11.), whereas other decrease (22.11.) or show no long-term trend (27.11.).

On 20.11. and 22.11., the differences between 1.0 and 1.6 m decline towards the end of the runs, whereas short-term $PM_{2.5}$ peaks are recorded on 20.11. at ~ 5250 m , 23.11. at ~ 350 m and ~ 5400 – 5500 m, and 27.11. at ~ 4300 m; Fig. 2-4). The causes for these peaks differ though, and may include ventilation of a cellar bar (20.11.), a smoking person and exceptional high traffic at the main station (23.11.), or were simply not detectable (27.11.). There are two distinct deviations including mean $PM_{2.5}$ > 10 µg/m³ detectable in all runs, however. These are located at the ‘Grüne Brücke’, a bridge crossing the ‘Rheinallee’ (Fig. 2-4 at 3300 – 3500 m; Fig. 2-7 dot 3) and the ‘Rheinallee’ close to the crossroad ‘Rheinallee/Kaiserstraße’ (Fig. 2-4 at 3800 – 4000 m; Fig. 2-7 dot 4).

The described trends in absolute $PM_{2.5}$ concentration among the runs change considerably when focusing on the absolute height differences between devices A and B (Fig. 2-5). The common $PM_{2.5}$ patterns of both measurement heights lead to the fact that the differences between top and bottom remain almost the same and thus strong deviations are largely leveled out. Only the mentioned deviations at the ‘Grüne Brücke’ and ‘Rheinallee’ were visible on 21.11., 22.11., 24.11. and 26.11.

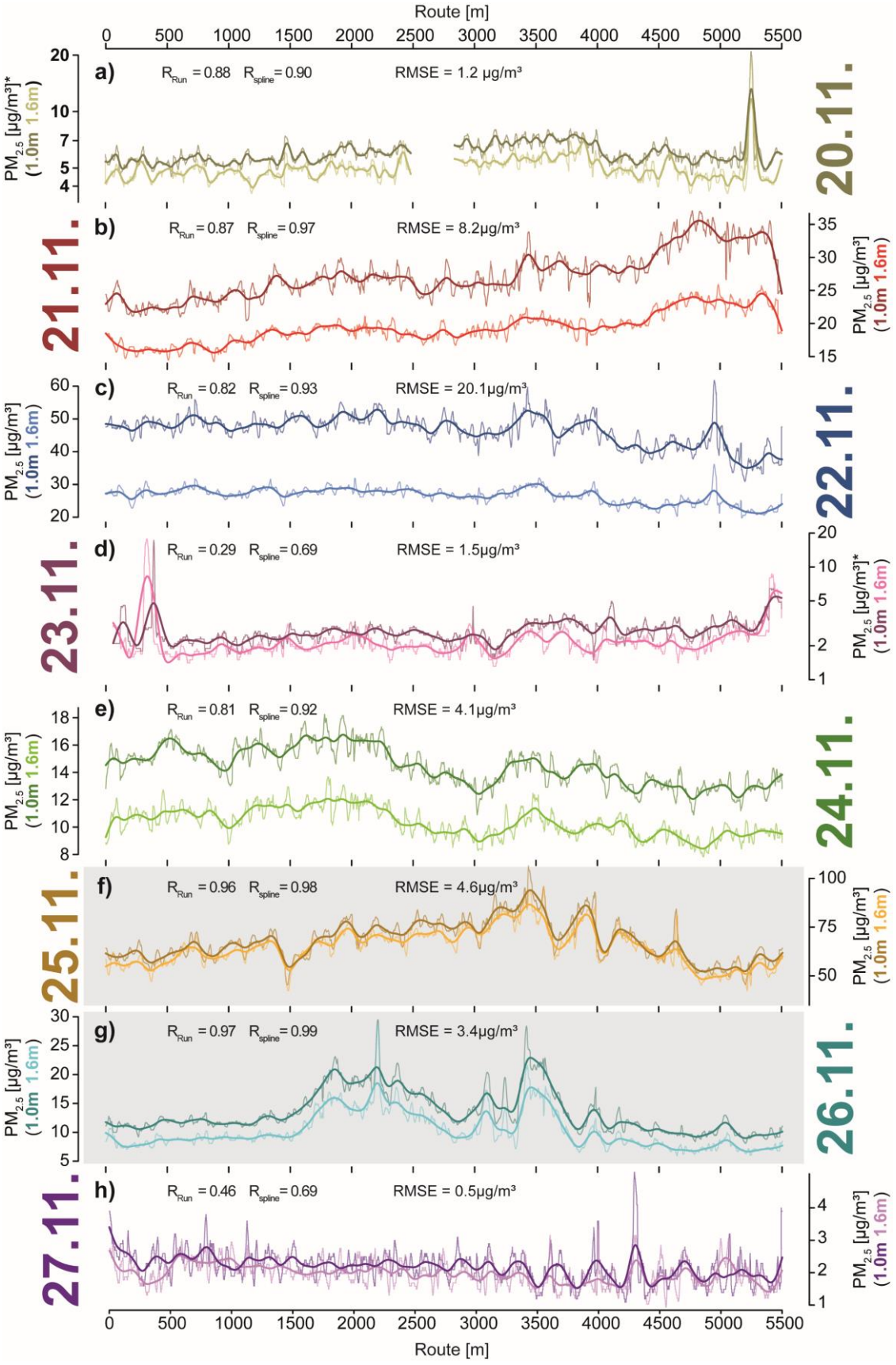

Fig. 2-4 Distribution of 20 s $PM_{2.5}$ concentrations at 1.0 m (dark curves) and 1.6 m level (bright curves) on days 20.11. (**a)** to 27.11.(**h)** along the route. Bold curves are smoothing splines (df = 55, n = 27515) and grey background indicates runs with RH > 85%. *Logarithmic y-axis used in panel (**a)** and (**d)**.

The $PM_{2.5}$ residuals persist on most days, except of 25.11. and 27.11. due to indistinguishable differences. However, the residuals differ among the days. The amount and variability of the absolute differences seem to be depended on the level of their absolute value. The higher the PM concentration was, the higher were the residuals and their absolute variability within a run. Only for 24.11. and 26.11. this hypothesis does not apply: The residual IQR of the run at 26.11. (1.0 µg/m³) were slightly larger than the IQR of the run at 24.11. (1.3 µg/m³) although the 26.11. residual mean was smaller (3.2 µg/m³).

To highlight the association between children and adult $PM_{2.5}$ exposures, splines of the relative differences between 1.0 and 1.6 m were calculated (Fig. 2-6). The ratios were largest on 22.11. reaching a maximum value exceeding 188%, nearly the double exposure for children. Following the residuals (Fig. 2-5), relative $PM_{2.5}$ differences correlate positively on the total amount of the measured $PM_{2.5}$, as is expressed by the lower ratios on 21.11. (141%), followed by 24.11. (139%), 26.11. (133%) and 20.11. (122%).

The IQR of the runs range from 11 – 16%, excluding the run at 23.11., affected by an oncoming smoking person. The relative differences of the run at 23.11. were exceptional, as the values varied massively around the 127% mean, expressed by an IQR of 29%. In contrast, the CV was lower, as this metric considers the (high) absolute mean value.

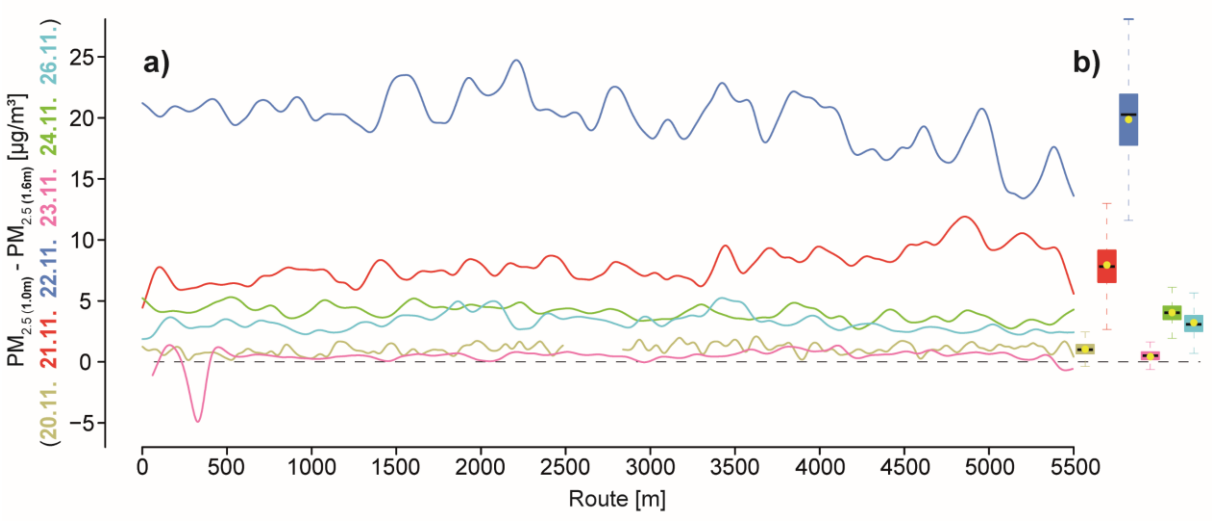

Fig. 2-5 Residuals of $PM_{2.5}$ concentrations between 1.0 and 1.6m for days of significant $PM_{2.5}$ height differences shown as smoothed deviations from 20 s $PM_{2.5}$ concentrations along the route (df = 55, n = 27515) (**a)**, and boxplots of the data (**b).**

The pronounced extremes of absolute $PM_{2.5}$ values at the 'Grüne Brücke' at 3300 – 3500 m are also seen in the height differences on 21.11., 22.11., 24.11. and 26.11. Similarly, the high absolute $PM_{2.5}$ values at the 'Rheinallee' at 3800 – 4000 m also appear on 21.11., 22.11., 23.11., 24.11., 26.11., in the relative difference between devices A and B. Data variability during days with substantial height differences showed no trends. Only on 22.11. the ratios were slightly decreasing along the measurement route.

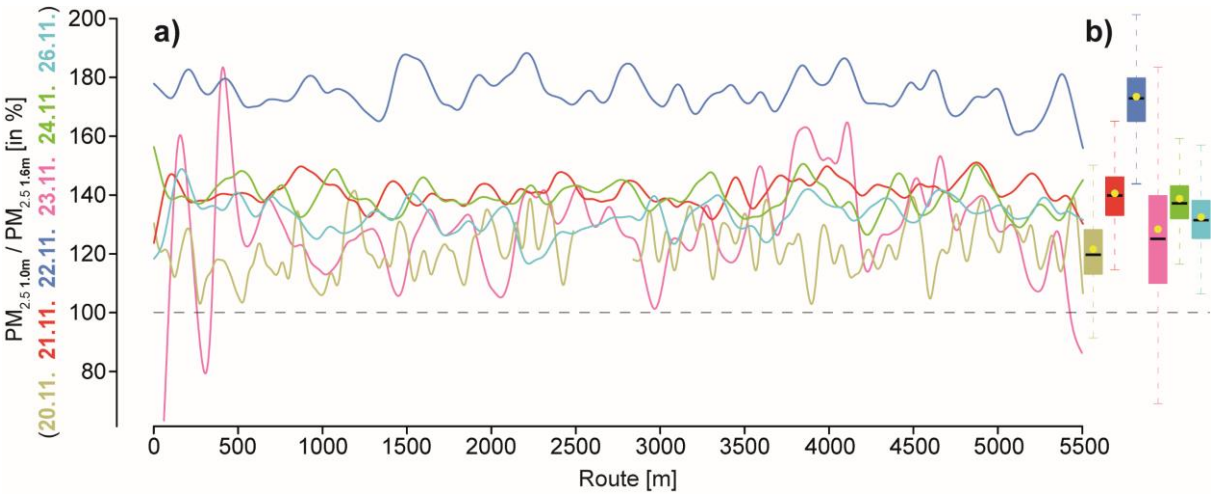

Fig. 2-6 Relative differences of $PM_{2.5}$ concentrations between 1.0 and 1.6 m for days of significant $PM_{2.5}$ height differences shown as smoothed deviations from 20 s $PM_{2.5}$ concentrations along the route (df = 55, n = 27515) (**a)**, and boxplots of the data (**b).**

2.3.4 Simulated *versus* measured concentrations

The simulated $PM_{2.5}$ exposures for the run on 24.11. showed similar results: The relative differences of $PM_{2.5}$ exposure between 1.0 and 1.8 m were positive across the model area (Fig. 2-7, without shading Fig. 2-A2). Ratios < 100% could only be found at the borders of the model probably due to boundary modelling artifacts. Relative differences > 110% were located on the roads with high traffic intensities (Fig. 2-1, e.g. Fig. 2-7 dot 4) and/or streets with the same direction as the wind (e.g. Fig. 2-7, dot 2). Following the measurement route, the simulation underestimated the measured relative differences by ~ 30% on average (Fig. 2-8). Starting with ~ 115% at Mainz main station, the simulated $PM_{2.5}$ exposures at 1.0 m were just < 5% higher than at 1.8 m in the inner part of Mainz-Neustadt and showed almost no variability in contrast to the measured $PM_{2.5}$ ratios. Areas close to streets featuring high traffic intensities showed larger relative differences of up to 127%.

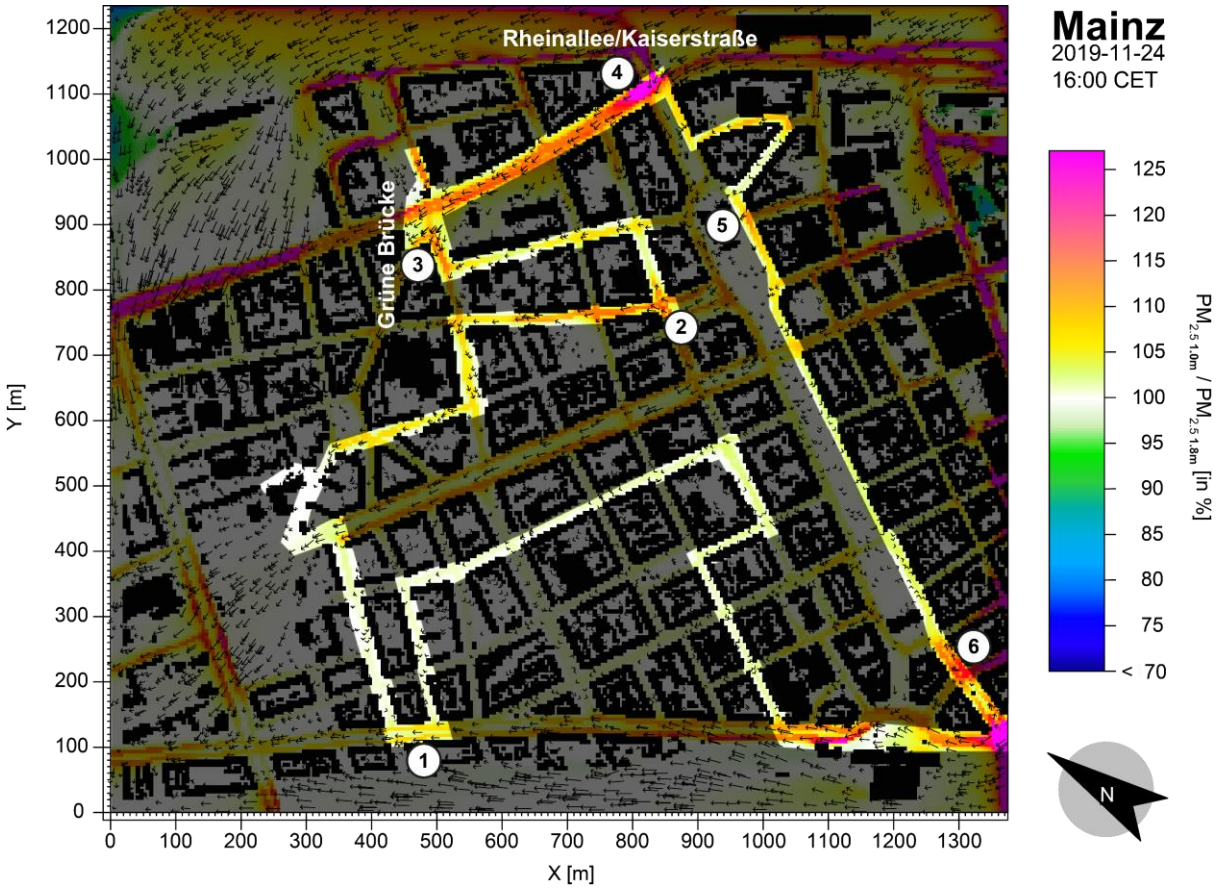

Fig. 2-7 Simulated relative differences distribution of $PM_{2.5}$ concentrations between 1.0 and 1.8 m in the study area with the measurement route highlighted. The colors display reduced (blue and green), equal (white) and increased (yellow to red/magenta) $PM_{2.5}$ exposure at 1.0 m level. The arrows represent horizontal wind speed and direction.

Comparing the relative differences of $PM_{2.5}$ between the model and measurements along the route (Fig. 2-8) confirms that the model predicts both lower values and a lower variability in general. For some locations however, the model simulates similar increases in relative differences when compared to the measurements (Fig. 2-8, marked 1 to 6). The relative differences of the simulation increased as the study route passed a street with higher traffic intensity at the western border of the district (Fig. 2-8, dot 1).

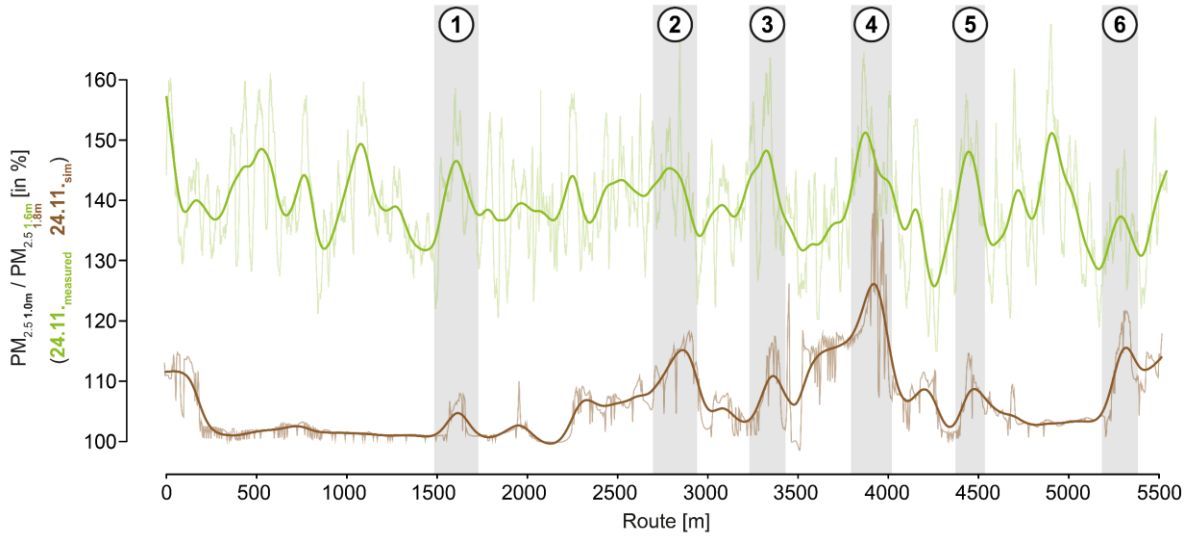

Fig. 2-8 Relative $PM_{2.5}$ exposure differences on 24.11. between 1.0 and 1.6 m as measured (green curves) and between 1.0 and 1.8 m as simulated (brown curves). Bold curves are smoothing splines (df=55, n=27515).

2.4 Discussion

2.4.1 Influence of weather conditions on $PM_{2.5}$ exposure

The continental anticyclonic conditions led to a mainly stable and calm weather throughout the study period (Fig. 2-A2). Several studies (Cheng and Li, 2010; Czernecki et al., 2017; Graham et al., 2020; Hamburger et al., 2011) showed that the longer the stability of anticyclonic weather endured, the higher $PM_{2.5}$ concentrations increased. Our work corroborates this finding: When the weather situation was stable with low wind speeds < 1 m/s and a lack of precipitation, the $PM_{2.5}$ values increased from 20.11. to 22.11. (Fig. 2-2; 0). From 22.11. to 23.11., the absolute $PM_{2.5}$ concentrations declined due to a short-term cyclonical influence with wind speeds > 1 m/s. Subsequent to this exchange of air masses, anticyclonic conditions fostered $PM_{2.5}$ increases on 24.11. and 25.11., until the influence weakened due to an upcoming cyclone with higher wind speed and minor precipitation towards the end of the measurement campaign. However, the concentrations recorded in this study exceeded the European law threshold of 25 µg/m³, as a benchmark for yearly mean $PM_{2.5}$ exposure (European Parliament and Council, 2008), in only three of eight runs. These effects were observed at both heights, which indicates that the changes in absolute $PM_{2.5}$ concentrations throughout the week were largely weather driven.

2.4.2 Local emissions and vertical $PM_{2.5}$ differences

We showed that in six of eight runs, $PM_{2.5}$ concentrations were significantly higher at the respiratory level of children than of adults. The exposure is at least 41% higher, and during the calm weather conditions on 22.11., grew up to 89% (75% on average), which means that children were exposed up to 24.7 µg/m³ higher $PM_{2.5}$ concentrations.

Our results are consistent with the findings of studies made by Garcia-Algar et al., 2015, Kumar et al., 2017 and Sharma and Kumar, 2020. Garcia-Algar et al., 2015 conducted a study measuring ultrafine particles at the height of strollers (0.55 m) and adults (1.70 m) by foot on three randomly chosen streets with high traffic intensity 20 times on 10 consecutive days in Barcelona, Spain. They showed that the exposure is 10% higher on stroller level. Kumar et al., 2017 measured $PM_{2.5}$ exposure to in-pram babies (0.7 m) and the carrying adult (1.4 and 1.6 m) also by foot 32 times on a predefined route (2.1 km) in Guilford, UK during MO (8 to 10 am) and AF (3 to 5pm). They found out that in the MO hours, the infants were 5% significantly lower exposed than adults. However, in the AF, the concentrations were 10% significantly higher for the children. Sharma and Kumar, 2020 reconducted this study in 2018 on a similar but shorter route (2.1 km) in Guildford, UK; showing that the $PM_{2.5}$ concentrations at 0.7 m were up to 44% higher in the AF. All of these three studies concluded that traffic-related sources were major factors (Garcia-Algar et al., 2015; Kumar et al., 2017; Sharma and Kumar, 2020). We also assume that our results are affected by the prevailing calm weather during the study period. McGregor and Bamzelis, 1995, for instance, showed that low wind speeds, caused by continental anticyclonic conditions, limited air mass exchange in Birmingham, UK and concluded that measured PM had to be emitted locally. The local, ambient $PM_{2.5}$ in the urban area of Mainz-Neustadt are likely emitted by combustion processes, i.e. traffic and domestic heating, whirled up dust, tyre and brake abrasion, as well as floating soil or biogenic compounds and deposited PM (Karagulian et al., 2015). Except domestic heating, all particle sources are close to the surface. In consequence, high traffic volumes are expected to cause high PM emissions near the ground. Moreover, the measurement runs (~3:15 pm to ~4:30 pm) took place during the daily AF rush hour, a time with higher traffic volume. The rush hour typically starts at ~3 pm with the daily end of service in the kindergartens and all-day schools but also with the end of working days within the study area. This means that parents are picking up their children, and people are commuting in the beginning rush hour traffic, thereby increasing $PM_{2.5}$ emissions. The increase of these means of mobility during the AF rush hour probably led to

higher $PM_{2.5}$ concentrations near ground and caused larger $PM_{2.5}$ exposure for children than for adults within the study area.

Additionally, we observed that the absolute and the relative differences in $PM_{2.5}$ exposure between both levels depended on the total amount of $PM_{2.5}$. The higher the concentration of PM, the higher the absolute and relative differences (Fig. 2-5/2-6). As stated before, in the case of emissions in calm weather situations with low wind speeds, $PM_{2.5}$ will remain near the ground. The absolute and relative $PM_{2.5}$ differences between 1.0 and 1.6 m increase with increasing $PM_{2.5}$ concentrations.

The absolute and relative difference between both heights were largely independent of the position on the study route. Even in areas with low traffic, the differences were at the same level as in streets with high traffic intensity. The lack of spatial variability in $PM_{2.5}$ differences is expressed by high correlations ($R > 0.8$) and similar CV of each run's measurements. Both heights had similar courses in $PM_{2.5}$ concentration, so strong deviations were leveled out after calculating differences.

There are two locations that stood out for relative and absolute $PM_{2.5}$ concentrations: 'Grüne Brücke' (Fig. 2-4/2-6 at 3400 – 3500 m; Fig. 2-7/2-8 dot 3) and 'Rheinallee' close to the crossroad 'Rheinallee/Kaiserstraße' (Fig. 2-4/2-6 at 3900 – 4000 m; Fig. 2-7/2-8 dot 4). The 'Grüne Brücke' is a pedestrian bridge with extensive planting crossing the 'Rheinallee', a road with high traffic intensity (Fig. 2-1). When the wind arrives from an easterly direction, the bridge and adjacent buildings of the 'Josefstraße' form a barrier for particles perpendicular to the 'Rheinallee' (Tab. 2-3). On days with high absolute $PM_{2.5}$ concentrations (21.11., 22.11., 24.11.), the traffic-related $PM_{2.5}$ accumulated and additionally increased the height differences due to a lack of vertical air exchange. These findings corroborate with Gallagher et al., 2015 showing that surrounding buildings are solid barriers for air flow hindering PM to disperse within street canyons. The second site at the 'Rheinallee' is bounded by 5-story-high blocks on two sides in north-south direction, with the northern block tapering down to the intersection 'Rheinallee/Kaiserstraße'. The intersection itself is free of buildings in the northeast direction. As a result, during easterly winds, traffic-related particles are pushed into the 'Rheinallee' and accumulate behind the crossroad, similar to 'Grüne Brücke'.

Nevertheless, the $PM_{2.5}$ differences at both sites were not significantly higher than other extrema during the runs. The relative differences varied more strongly among the days than along the study route. A reason for this is that the absolute and relative differences between

1.0 and 1.6 m levels seem to depend on the absolute $PM_{2.5}$ concentrations controlled by the changing weather conditions throughout the measurement campaign (Fig. 2-5). These results may be significant for health risk analyses of children. Due to their still developing respiratory tract, any given $PM_{2.5}$ concentration leads to higher levels of exposure for children compared to adults (Habre et al., 2014; Nachman and Parker, 2012) (Habre et al., 2014; Nachman and Parker, 2012). Our data show that the absolute $PM_{2.5}$ concentrations at children breathing height were consistently higher than at adult breathing height, independent of the measurement location. This in turn leads to a disproportionately higher exposure of children, and therefore a higher chance to develop respiratory diseases such as asthma, regardless of the particular site of the children in an urban environment (Khreis et al., 2017). However, our study includes only eight measurement runs using low-cost measurement hardware, which is still at a relatively early stage of development when compared to the established and officially used PM measurement technologies. Further research over longer periods and using advanced hardware is needed to improve our understanding of $PM_{2.5}$ exposure differences between children and adults.

2.4.3 Influence of traffic-exhaust emissions on $PM_{2.5}$

The recorded higher $PM_{2.5}$ exposure of children is supported by the microclimate model simulation. Fed with meteorological parameters from 24.11. as boundary conditions, the model simulated $PM_{2.5}$ exposure at 4 pm higher at 1.0 than at 1.8 m. These differences were also independent of the location on the route (Fig. 2-7). The relative differences between children and adult breathing heights are plausible as $PM_{2.5}$ was emitted at 0.2 m height in the model. At least six local maxima of simulated relative differences could be allocated to real-world, recorded maxima, even though the horizontal resolution of the model is only 5 x 5 m (Fig. 2-7). These sites are located nearby streets with high traffic intensities and where the horizontal dispersion of traffic-related particles is limited by high-rising buildings and narrow streets (Fig. 2-7, dots 1-6).

$PM_{2.5}$ maxima appear related to the low horizontal wind speeds in the simulation combined with the low irradiation due to a closed cloud cover causing lowered thermal convection and, in consequence, low vertical exchange of emitted $PM_{2.5}$. These findings were limited on traffic-related locations. Within areas of lower traffic occurrences, i.e. the middle of the study area (250 – 1500 m on the route; Fig. 2-8), the relative differences show little variability. However, the variance of relative differences was also low at the ‘Kaiserstraße’ featuring a wide road with

fewer obstacles supporting the dispersion of emission, resulting in lower concentrations (4700-5250 m on the route). These findings correspond to results of Paas and Schneider, 2016 demonstrating that the simulated dispersion of PM_{10} was also underpredicted throughout the study area. It should be noted though that the simulation represents a snapshot of relative differences for a distinct time. Local variabilities of $PM_{2.5}$ pollution (e.g. higher number of busses and trucks or a traffic jam at the certain time of measurement) cannot be represented, so that a reduced variability and fewer maxima were expected. Furthermore, emission sources like tyre and brake abrasions as well as whirled up $PM_{2.5}$ are not simulated, but have a distinct impact on $PM_{2.5}$ (Karagulian et al., 2019; Sharma and Kumar, 2020). On the other hand, the modelled maxima were more pronounced compared to mean $PM_{2.5}$ levels, which could be affected by the larger vertical difference of 0.8 m due to the grid cell size. Nevertheless, all relative differences were > 30% lower than the measurements. These underestimated differences could additionally be related to the fact that the model started with a clean atmosphere including no background concentration of PM and only traffic-related $PM_{2.5}$ as an emission source. However, the results of the simulation corroborated that $PM_{2.5}$ emitted by vehicle exhausts alone are a cause of the measured relative differences in $PM_{2.5}$ exposure.

2.5 Conclusion

Our results show that the absolute $PM_{2.5}$ exposure at both heights was related to the stability of the prevailing weather condition, particularly to wind speeds. We conclude that in six out of eight measurement runs, children were significantly more exposed to $PM_{2.5}$ than adults, independent of the position along the measurement runs. Relative $PM_{2.5}$ differences ranged from 122% (20.11.) to 175% (22.11.) among the runs. The absolute and relative height differences were positively correlated with $PM_{2.5}$ concentrations. Relative differences also varied more strongly among days than along the study route, whereby the latter showed a tendency towards lower variability with increasing absolute concentrations. Explanatory approaches include accumulation processes of local, near ground emitters causing higher exposure differences between 1.0 and 1.6 m, when the absolute $PM_{2.5}$ increase. On the other hand, deviations in absolute $PM_{2.5}$ was leveled out in differences due to similar progression at both heights. However, two sites with local $PM_{2.5}$ concentration maxima (‘Grüne Brücke’, ‘Rheinallee’) are still visible in absolute and relative differences.

A simulation of traffic-related $PM_{2.5}$ exposure within the study area shows similar results, whereby at least six local maxima of simulated relative differences can be attributed to measured maxima. Height differences in areas with low traffic intensity cannot be displayed by the model, which is why we suggest that other sources including tyre and brake abrasion as well as whirled up, play an important role in $PM_{2.5}$ traffic emission.

In general, the study demonstrated that highly time-resolved measurements, and subsequent comparisons, of $PM_{2.5}$ exposure with low-cost OPC-N3 sensors are appropriate after initial calibration during RH < 85% conditions.

2.6 Acknowledgements

We thank the environmental state office of Rhineland-Palatinate, particularly Michael Weißenmayer and Margit von Döhren from Referat 60, Matthias Zimmer and Matthias Voigt from Referat 63, for providing data of the official meteorological measurement stations and the radiometer. The authors thank the municipality of Mainz "Grün und Umweltamt" for providing GIS data for the microclimate simulations. We are also grateful to Klaus E. Rogge for discussions about statistical analysis and to Christian Gnaneswaran for supporting the measurements by foot.

2.7 References

Alfano, B., Barretta, L., Del Giudice, A., Vito, S., Di Francia, G., Esposito, E., Formisano, F., Massera, E., Miglietta, M.L., Polichetti, T., 2020. A Review of Low-Cost Particulate Matter Sensors from the Developers' Perspectives. Sensors (Basel) 20. https://doi.org/10.3390/s20236819

Alphasense, 2018. Technical Information Release December 2018: Alphasense Particle Counter OPC-N Range Product Update . URL http://www.alphasense.com/WEB1213/wp-content/uploads/2019/02/OPC-N3-information-update-Dec-18.pdf

Azarmi, F., Kumar, P., Marsh, D., Fuller, G., 2016. Assessment of the long-term impacts of PM10 and PM2.5 particles from construction works on surrounding areas. Environ Sci Process Impacts 18, 208–21. https://doi.org/10.1039/c5em00549c

Bohren, C.F., Huffman, D.R., 1998. Absorption and Scattering of Light by Small Particles. Wiley. https://doi.org/10.1002/9783527618156

Brattich, E., Bracci, A., Zappi, A., Morozzi, P., Di Sabatino, S., Porcù, F., Di Nicola, F., Tositti, L., 2020. How to Get the Best from Low-Cost Particulate Matter Sensors: Guidelines and Practical Recommendations. Sensors (Basel) 20. https://doi.org/10.3390/s20113073

Bruse, M., 1999. Die Auswirkungen kleinskaliger Umweltgestaltung auf das Mikroklima: Entwicklung des prognostischen numerischen Modells ENVI-met zur Simulation der Wind-, Temperatur- und Feuchteverteilung in städtischen Strukturen. Bochum.

Bulot, F.M.J., Johnston, S.J., Basford, P.J., Easton, N.H.C., Apetroaie-Cristea, M., Foster, G.L., Morris, A.K.R., Cox, S.J., Loxham, M., 2019. Long-term field comparison of multiple low-cost particulate matter sensors in an outdoor urban environment. Sci Rep 9, 7497. https://doi.org/10.1038/s41598-019-43716-3

Chatzidiakou, L., Krause, A., Popoola, O.A.M., Di Antonio, A., Kellaway, M., Han, Y., Squires, F.A., Wang, T., Zhang, H., Wang, Q., Fan, Y., Chen, S., Hu, M., Quint, J.K., Barratt, B., Kelly, F.J., Zhu, T., Jones, R.L., 2019. Characterising low-cost sensors in highly portable platforms to quantify personal exposure in diverse environments. Atmos Meas Tech 12, 4643–4657. https://doi.org/10.5194/amt-12-1-2019

Cheng, Y.-H., Li, Y.-S., 2010. Influences of Traffic Emissions and Meteorological Conditions on Ambient PM10 and PM2.5 Levels at a Highway Toll Station. Aerosol Air Qual. Res. 10, 456–462. https://doi.org/10.4209/aaqr.2010.04.0025

Crilley, L.R., Shaw, M., Pound, R., Kramer, L.J., Price, R., Young, S., Lewis, A.C., Pope, F.D., 2018. Evaluation of a low-cost optical particle counter (Alphasense OPC-N2) for ambient air monitoring. Atmos. Meas. Tech. 11, 709–720. https://doi.org/10.5194/amt-11-709-2018

Crilley, L.R., Singh, A., Kramer, L.J., Shaw, M.D., Alam, M.S., Apte, J.S., Bloss, W.J., Hildebrandt Ruiz, L., Fu, P., Fu, W., Gani, S., Gatari, M., Ilyinskaya, E., Lewis, A.C., Ng'ang'a, D., Sun, Y., Whitty, R.C.W., Yue, S., Young, S., Pope, F.D., 2020. Effect of aerosol composition on the performance of low-cost optical particle counter correction factors. Atmos. Meas. Tech. 13, 1181–1193. https://doi.org/10.5194/amt-13-1181-2020

Czernecki, B., Półrolniczak, M., Kolendowicz, L., Marosz, M., Kendzierski, S., Pilguj, N., 2017. Influence of the atmospheric conditions on PM10 concentrations in Poznań, Poland. J Atmos Chem 74, 115–139. https://doi.org/10.1007/s10874-016-9345-5

Deutscher Wetterdienst, 2021a. Temperatur: vieljährige Mittelwerte 1981 - 2010 . URL https://www.dwd.de/DE/leistungen/klimadatendeutschland/mittelwerte/temp_8110_fest_html.html%3Fview%3DnasPublication

Deutscher Wetterdienst, 2021b. Niederschlag: vieljährige Mittelwerte 1981 - 2010 . URL https://www.dwd.de/DE/leistungen/klimadatendeutschland/mittelwerte/nieder_8110_fest_html.html?view=nasPublication&nn=16102

Di Antonio, A., Popoola, O.A.M., Ouyang, B., Saffell, J., Jones, R.L., 2018. Developing a Relative Humidity Correction for Low-Cost Sensors Measuring Ambient Particulate Matter. Sensors (Basel) 18. https://doi.org/10.3390/s18092790

Environmental Protection Agency of Germany, 2017. The Handbook of Emission Factors for Road Transport (HBEFA) . URL https://www2.dmu.dk/AtmosphericEnvironment/Docs/NO2scheme.pdf

Espressif, 2021. ESP32 . URL https://www.espressif.com/en/products/socs/esp32

European Parliament and Council, 2008. Directive 2008/50/EC of the european Parliament and of the council of 21 May 2008 on ambient air quality and cleaner air for Europe . URL https://eur-lex.europa.eu/eli/dir/2008/50/oj

Feng, S., Gao, D., Liao, F., Zhou, F., Wang, X., 2016. The health effects of ambient PM2.5 and potential mechanisms. Ecotoxicol Environ Saf 128, 67–74. https://doi.org/10.1016/j.ecoenv.2016.01.030

Fortune, S., 1987. A sweepline algorithm for Voronoi diagrams. Algorithmica 2, 153–174. https://doi.org/10.1007/BF01840357

Gallagher, J., Baldauf, R., Fuller, C.H., Kumar, P., Gill, L.W., McNabola, A., 2015. Passive methods for improving air quality in the built environment: A review of porous and solid barriers. Atmospheric Environment 120, 61–70. https://doi.org/10.1016/j.atmosenv.2015.08.075

Garcia-Algar, O., Canchucaja, L., d'Orazzio, V., Manich, A., Joya, X., Vall, O., 2015. Different exposure of infants and adults to ultrafine particles in the urban area of Barcelona. Environ Monit Assess 187, 4196. https://doi.org/10.1007/s10661-014-4196-5

Goel, A., Kumar, P., 2016. Vertical and horizontal variability in airborne nanoparticles and their exposure around signalised traffic intersections. Environ Pollut 214, 54–69. https://doi.org/10.1016/j.envpol.2016.03.033

Goldman, L.R., 1995. Children--unique and vulnerable. Environmental risks facing children and recommendations for response. Environ Health Perspect 103 Suppl 6, 13–8. https://doi.org/10.1289/ehp.95103s613

Graham, A.M., Pringle, K.J., Arnold, S.R., Pope, R.J., Vieno, M., Butt, E.W., Conibear, L., Stirling, E.L., McQuaid, J.B., 2020. Impact of weather types on UK ambient particulate matter concentrations. Atmospheric Environment: X 5, 100061. https://doi.org/10.1016/j.aeaoa.2019.100061

Gualtieri, M., Ovrevik, J., Mollerup, S., Asare, N., Longhin, E., Dahlman, H.-J., Camatini, M., Holme, J.A., 2011. Airborne urban particles (Milan winter-PM2.5) cause mitotic arrest and cell death: Effects on DNA, mitochondria, AhR binding and spindle organization. Mutat Res 713, 18–31. https://doi.org/10.1016/j.mrfmmm.2011.05.011

Gysel, M., Crosier, J., Topping, D.O., Whitehead, J.D., Bower, K.N., Cubison, M.J., Williams, P.I., Flynn, M.J., McFiggans, G.B., Coe, H., 2007. Closure study between chemical composition and hygroscopic growth of aerosol particles during TORCH2. Atmos. Chem. Phys. 7, 6131–6144. https://doi.org/10.5194/acp-7-6131-2007

Habre, R., Moshier, E., Castro, W., Nath, A., Grunin, A., Rohr, A., Godbold, J., Schachter, N., Kattan, M., Coull, B., Koutrakis, P., 2014. The effects of PM2.5 and its components from indoor and outdoor sources on cough and wheeze symptoms in asthmatic children. J Expo Sci Environ Epidemiol 24, 380–7. https://doi.org/10.1038/jes.2014.21

Hagler, G.S.W., Williams, R., Papapostolou, V., Polidori, A., 2018. Air Quality Sensors and Data Adjustment Algorithms: When Is It No Longer a Measurement? Environ Sci Technol 52, 5530–5531. https://doi.org/10.1021/acs.est.8b01826

Hamburger, T., McMeeking, G., Minikin, A., Birmili, W., Dall'Osto, M., O'Dowd, C., Flentje, H., Henzing, B., Junninen, H., Kristensson, A., Leeuw, G., Stohl, A., Burkhart, J.F., Coe, H., Krejci, R., Petzold, A., 2011. Overview of the synoptic and pollution situation over Europe during the EUCAARI-LONGREX field campaign. Atmos. Chem. Phys. 11, 1065–1082. https://doi.org/10.5194/acp-11-1065-2011

Hoffmann, J., 2019. DWD. SXEU31 DWAV 200800. Synoptische Übersicht Kurzfrist. . URL https://www.wetterzentrale.de/article.php?id=70603&lang=1

Imhof, D., Weingartner, E., Vogt, U., Dreiseidler, A., Rosenbohm, E., Scheer, V., Vogt, R., Nielsen, O.J., Kurtenbach, R., Corsmeier, U., Kohler, M., Baltensperger, U., 2005. Vertical distribution of aerosol particles and NOx close to a motorway. Atmospheric Environment 39, 5710–5721. https://doi.org/10.1016/j.atmosenv.2004.07.036

Jovašević-Stojanović, M., Davidovic, M., Tasic, V., Bartonova, A., Ristovski, Z., 2019. Current Status of Applicability of Low-Cost Particulate Matter Sensors for Ambient Air Pollution and Exposure Assessment.

Karagulian, F., Barbiere, M., Kotsev, A., Spinelle, L., Gerboles, M., Lagler, F., Redon, N., Crunaire, S., Borowiak, A., 2019. Review of the Performance of Low-Cost Sensors for Air Quality Monitoring. Atmosphere 10, 506. https://doi.org/10.3390/atmos10090506

Karagulian, F., Belis, C.A., Dora, C.F.C., Prüss-Ustün, A.M., Bonjour, S., Adair-Rohani, H., Amann, M., 2015. Contributions to cities' ambient particulate matter (PM): A systematic review of local source contributions at global level. Atmospheric Environment 120, 475–483. https://doi.org/10.1016/j.atmosenv.2015.08.087

Khreis, H., Kelly, C., Tate, J., Parslow, R., Lucas, K., Nieuwenhuijsen, M., 2017. Exposure to traffic-related air pollution and risk of development of childhood asthma: A systematic review and meta-analysis. Environ Int 100, 1–31. https://doi.org/10.1016/j.envint.2016.11.012

Kumar, P., Fennell, P., Britter, R., 2008. Measurements of particles in the 5-1000 nm range close to road level in an urban street canyon. Science of The Total Environment 390, 437–47. https://doi.org/10.1016/j.scitotenv.2007.10.013

Kumar, P., Khare, M., Harrison, R.M., Bloss, W.J., Lewis, A.C., Coe, H., Morawska, L., 2015. New directions: Air pollution challenges for developing megacities like Delhi. Atmospheric Environment 122, 657–661. https://doi.org/10.1016/j.atmosenv.2015.10.032

Kumar, P., Rivas, I., Sachdeva, L., 2017. Exposure of in-pram babies to airborne particles during morning drop-in and afternoon pick-up of school children. Environ Pollut 224, 407–420. https://doi.org/10.1016/j.envpol.2017.02.021

Lelieveld, J., Klingmüller, K., Pozzer, A., Pöschl, U., Fnais, M., Daiber, A., Münzel, T., 2019. Cardiovascular disease burden from ambient air pollution in Europe reassessed using novel hazard ratio functions. Eur Heart J 40, 1590–1596. https://doi.org/10.1093/eurheartj/ehz135

Mazur, L.J., 2003. Pediatric environmental health. Curr Probl Pediatr Adolesc Health Care 33, 6–25. https://doi.org/10.1067/mps.2003.1

McCauley, J.D., Aime, A., Blazek, R., Metz, M., 2020. GRASS GIS 7.9.dev Reference Manual: v.voronoi . URL https://grass.osgeo.org/grass79/manuals/v.voronoi.html

McGregor, G.R., Bamzelis, D., 1995. Synoptic typing and its application to the investigation of weather air pollution relationships, Birmingham, United Kingdom. Theor Appl Climatol 51, 223–236. https://doi.org/10.1007/BF00867281

Mie, G., 1908. Beiträge zur Optik trüber Medien, speziell kolloidaler Metallösungen. Ann. Phys. 330, 377–445. https://doi.org/10.1002/ANDP.19083300302

Morawska, L., Thai, P.K., Liu, X., Asumadu-Sakyi, A., Ayoko, G., Bartonova, A., Bedini, A., Chai, F., Christensen, B., Dunbabin, M., Gao, J., Hagler, G.S.W., Jayaratne, R., Kumar, P., Lau, A.K.H., Louie, P.K.K., Mazaheri, M., Ning, Z., Motta, N., Mullins, B., Rahman, M.M., Ristovski, Z., Shafiei, M., Tjondronegoro, D., Westerdahl, D., Williams, R., 2018. Applications of low-cost sensing technologies for air quality monitoring and exposure assessment: How far have they gone? Environ Int 116, 286–299. https://doi.org/10.1016/j.envint.2018.04.018

Nachman, K.E., Parker, J.D., 2012. Exposures to fine particulate air pollution and respiratory outcomes in adults using two national datasets: a cross-sectional study. Environ Health 11, 25. https://doi.org/10.1186/1476-069X-11-25

Paas, B., Schneider, C., 2016. A comparison of model performance between ENVI-met and Austal2000 for particulate matter. Atmospheric Environment 145, 392–404. https://doi.org/10.1016/j.atmosenv.2016.09.031

Petters, M.D., Kreidenweis, S.M., 2007. A single parameter representation of hygroscopic growth and cloud condensation nucleus activity. Atmos. Chem. Phys. 7, 1961–1971. https://doi.org/10.5194/acp-7-1961-2007

Sharma, A., Kumar, P., 2020. Quantification of air pollution exposure to in-pram babies and mitigation strategies. Environ Int 139, 105671. https://doi.org/10.1016/j.envint.2020.105671

Shepard, D., 1968. A two-dimensional interpolation function for irregularly-spaced data, in: Blue, R.B., Rosenberg, A.M. (Eds.), Proceedings of the 1968 23rd ACM National Conference On -. ACM Press, New York, New York, USA, pp. 517–524. https://doi.org/10.1145/800186.810616

Simcom, 2021. Sim28 . URL https://www.simcom.com/product/SIM28.html

Simon, H., Fallmann, J., Kropp, T., Tost, H., Bruse, M., 2019. Urban Trees and Their Impact on Local Ozone Concentration—A Microclimate Modeling Study. Atmosphere 10, 154. https://doi.org/10.3390/atmos10030154

Singh, R.B., Huber, A.H., Braddock, J.N., 2003. Development of a microscale emission factor model for particulate matter for predicting real-time motor vehicle emissions. J Air Waste Manag Assoc 53, 1204–17. https://doi.org/10.1080/10473289.2003.10466288

Sousan, S., Koehler, K., Hallett, L., Peters, T.M., 2016. Evaluation of the Alphasense Optical Particle Counter (OPC-N2) and the Grimm Portable Aerosol Spectrometer (PAS-1.108). Aerosol Sci Technol 50, 1352–1365. https://doi.org/10.1080/02786826.2016.1232859

Stewart, I.D., Oke, T.R., 2012. Local Climate Zones for Urban Temperature Studies. Bulletin of the American Meteorological Society 93, 1879–1900. https://doi.org/10.1175/BAMS-D-11-00019.1

Tang, G., Zhang, Jinqiang, Zhu, X., Song, T., Münkel, C., Hu, B., Schäfer, K., Liu, Z., Zhang, Junke, Wang, L., Xin, J., Suppan, P., Wang, Y., 2016. Mixing layer height and its implications for air pollution over Beijing, China. Atmos. Chem. Phys. 16, 2459–2475. https://doi.org/10.5194/acp-16-2459-2016

Torres-Ramos, Y.D., Montoya-Estrada, A., Guzman-Grenfell, A.M., Mancilla-Ramirez, J., Cardenas-Gonzalez, B., Blanco-Jimenez, S., Sepulveda-Sanchez, J.D., Ramirez-Venegas, A., Hicks, J.J., 2011. Urban PM2.5 induces ROS generation and RBC damage in COPD patients. Front Biosci (Elite Ed) 3, 808–17. https://doi.org/10.2741/e288

Umweltmeteorologie RLP, 2019. URL https://luft.rlp.de/de/umweltmeteorologie/

Wagner, P., Schäfer, K., 2017. Influence of mixing layer height on air pollutant concentrations in an urban street canyon. Urban Climate 22, 64–79. https://doi.org/10.1016/j.uclim.2015.11.001

Walser, A., Sauer, D., Spanu, A., Gasteiger, J., Weinzierl, B., 2017. On the parametrization of optical particle counter response including instrument-induced broadening of size spectra and a self-consistent evaluation of calibration measurements. Atmos. Meas. Tech. 10, 4341–4361. https://doi.org/10.5194/amt-10-4341-2017

Wania, A., Bruse, M., Blond, N., Weber, C., 2012. Analysing the influence of different street vegetation on traffic-induced particle dispersion using microscale simulations. J Environ Manage 94, 91–101. https://doi.org/10.1016/j.jenvman.2011.06.036

Wickham, H., 2020. Package "plyr": Tools for Splitting, Applying and Combining Data; Version 1.8.6 . URL http://had.co.nz/plyr

Zauli Sajani, S., Marchesi, S., Trentini, A., Bacco, D., Zigola, C., Rovelli, S., Ricciardelli, I., Maccone, C., Lauriola, P., Cavallo, D.M., Poluzzi, V., Cattaneo, A., Harrison, R.M., 2018. Vertical variation of PM2.5 mass and chemical composition, particle size distribution, NO2, and BTEX at a high rise building. Environ Pollut 235, 339–349. https://doi.org/10.1016/j.envpol.2017.12.090

Zeuschner, J., 2019. DWD. SXEU31 DWAV 230800. Synoptische Übersicht Kurzfrist. . URL https://www.wetterzentrale.de/article.php?id=70739&lang=1

Zhou, S., Wu, L., Guo, J., Chen, W., Wang, X., Zhao, J., Cheng, Y., Huang, Z., Zhang, J., Sun, Y., Fu, P., Jia, S., Chen, Y., Kuang, J., 2019. Vertical distribution of atmospheric particulate matters within urban boundary layer in southern China: size-segregated chemical composition and secondary formation through cloud processing and heterogeneous reactions. https://doi.org/10.5194/acp-2019-155

ZIMEN, 2019. Luft-Überwachung in Rheinland-Pfalz. State Office of Rhineland-Palatinate .

2.8 Appendix

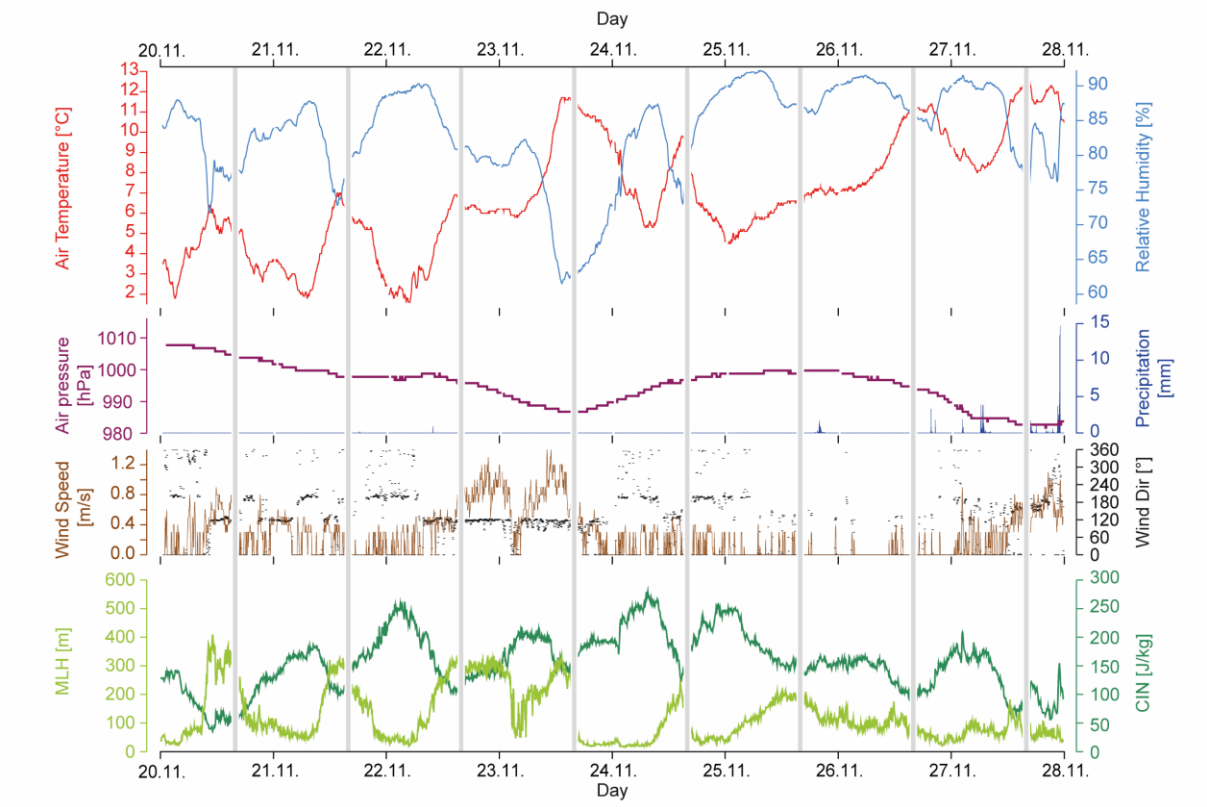

Fig. 2-A1 weather conditions during measurement period. Grey bars represent daily measurement periods. TA, RH and air pressure were measured at 2m a.g.l. at the measurement station Mainz-Zitadelle, wind speed and direction 10m a.g.l and precipitation 2m a.g.l. at the measurement station Mainz-Mombach. The MLH and the CIN were measured with a radiometer at the headquarter of the state office for environment in Mainz.

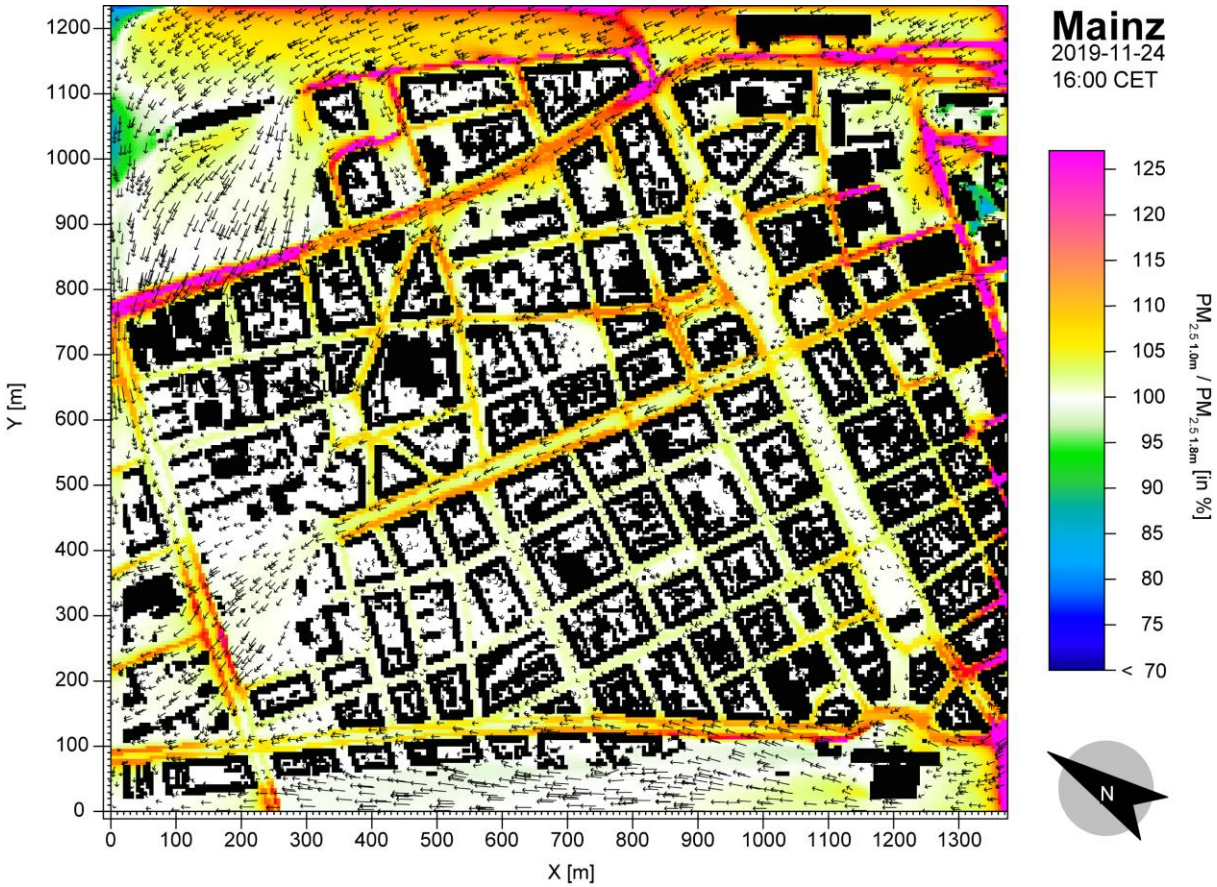

Fig. 2-A2 Simulated relative differences distribution of $PM_{2.5}$ concentrations between 1.0m and 1.8m in the study area.

"(Harr et al., 2022).

3 Seasonal Changes in Urban $PM_{2.5}$ Hotspots and Sources from Low-Cost Sensors

Lorenz Harr [1,*], Tim Sinsel [1], Helge Simon [1] and Jan Esper [1,2]

[1] *Department of Geography, Johannes Gutenberg-University, Johann-Joachim-Becher-Weg 21, 55128 Mainz, Germany;*

[2] *Global Change Research Institute of the Czech Academy of Sciences (CzechGlobe), 60300 Brno, Czech Republic*

Summary

To better assess the health risk for citizens, it is important to identify locations with high PM concentrations as well as their emission sources at the breathing height of pedestrians at different times of the year. As mobile measurements with low-cost sensors could improve spatial coverage, $PM_{2.5}$ measurements with Alphasense OPC-N3 low-cost sensors were carried out at adult breathing height (1.6 m) simultaneously on foot on three routes in the urban area of Mainz in spring and autumn to identify spatial and seasonal variations of $PM_{2.5}$ and their sources. The obtained absolute $PM_{2.5}$ data were compared with stationary measurements to check whether prior side-by-side calibration is sufficient to provide expectable absolute $PM_{2.5}$ concentrations. In addition, urban $PM_{2.5}$ hotspots and their emission sources were revealed using $PM_{2.5}/PM_{10}$ ratios, and seasonal variations in hotspots were discussed. The author was significantly involved in the conceptualization, methodology, formal analysis, and responsible for investigation and data curation. He wrote most of the manuscript including the creation of the figures.

Atmosphere 13 (2022) 694, April 2022 – published

“

3.1 Introduction

The global perception of air quality and air pollutants such as PM has increased partly due to the COVID-19 pandemic (Maione et al., 2021; Mirabelli et al., 2020). While coarse particles with an D_P between 2.5 and 10 µm ($PM_{2.5–10}$) are inhalable, fine particles with D_P < 2.5 µm can reach the bronchial system and cause airway inflammation, lung disfunction, and chronic obstructive pulmonary disease (Gualtieri et al., 2011; Lelieveld et al., 2019; Torres-Ramos et al., 2011).

However, the toxicity of particles is not only determined by their absolute concentration but also varies between different types of PM, e.g., metallic elements of residual oil fly ash have more adverse health effects than biogenic or inorganic components (Chen and Lippmann, 2009; Karagulian et al., 2019; Schlesinger, 2007). PM elements can be detected via chemical analyses, though in the absence of these measures, the origin of particles can be attributed by calculating the ratio of $PM_{2.5}/PM_{10}$ (Parkhurst et al., 1999; Xu et al., 2017). Whereas a weighting towards $PM_{2.5}$ indicates emissions from combustion processes, i.e., vehicle exhausts and house heating, a low ratio indicates natural emissions as sources, i.e., pollen and leaf particles and/or fugitive or re-suspended road dust from tire and brake abrasion, for instance (Evagelopoulos et al., 2019; Karagulian et al., 2019; Querol et al., 2001; Xu et al., 2017).

In urban areas, $PM_{2.5}/PM_{10}$ ratios can rapidly change over time due to short-term variation in emission intensity, e.g., rush hour or non-rush hour, but also in response to changing weather situations. Stationary anti-cyclonic weather in Central Europe is associated with low wind speeds and limited precipitation (Czernecki et al., 2017; Graham et al., 2020) as well as, particularly in autumn and winter, high CIN causing low MLH. The vertical air exchange is thus reduced, leading to an accumulation of fine particles near ground and a high $PM_{2.5}$ apportionment > 60% relative to PM_{10}, which is generally in contrast to $PM_{2.5}/PM_{10}$ ratios < 0.5 typically recorded in spring and summer (Speranza et al., 2016; Tang et al., 2016; Wagner and Schäfer, 2017).

To monitor the seasonal variability of the $PM_{2.5}$ and PM_{10}, 30 to 60 min mean data are provided by the official stationary measurement networks in Europe (ZIMEN, 2021a). However, highly temporal changes < 30 min cannot be detected, and more importantly, spatial variability of particle concentrations and their sources cannot be represented due to the immobility of permanent network facilities. Spatiotemporal differences in personal exposure can therefore not

be represented. In contrast, mobile measurements provide the possibility to extend the spatial coverage of stationary measurements, particularly at the pedestrian breath level (WMO, 2018). A cost-effective solution for mobile measurements is the use of so-called low-cost monitoring systems (Alfano et al., 2020). These devices are also highly portable due to their small weight and size and can be easily mounted on vehicles or racks carried by a person (Al-Ali et al., 2010). We used Alphasense OPC-N3 sensors (Alphasense, 2018), demonstrated to perform well under laboratory conditions (Morawska et al., 2018; Sousan et al., 2016), to measure different types of particles at high temporal resolution of 1 s. However, in urban outdoor environments, the accuracy of these data is adversely affected by changes in particle composition and RH (Brattich et al., 2020; Crilley et al., 2018; Di Antonio et al., 2018).

The goal of this study was to demonstrate seasonal and spatial variability of $PM_{2.5}$ concentrations in a Central European city (Mainz, Germany) using mobile low-cost instruments at high spatiotemporal resolution. We (i) compared these measurements with long-term stationary data, (ii) identified $PM_{2.5}$ hotspots and their source, and (iii) investigated seasonal changes in source regimes throughout the study area. We expected to find (i) similar peak $PM_{2.5}$ values in March and September, (ii) highest polluted locations nearby streets with high traffic intensity and close to anthropogenic sources, and (iii) higher $PM_{2.5}/PM_{10}$ ratios in spring than in late summer due to prevailing anti cyclonic weather regimes in the colder season.

3.2 Materials and Methods

3.2.1 Study Sites and Sensors

The study was conducted on five consecutive weekdays in September (14.09.20–18.09.20) and March (01.03.21–05.03.21) in Mainz, the capital and largest city (approx. 220,000 habitants) of Rhineland-Palatinate in south-west Germany (50.0 °N, 8.26 °E, Fig. 3-1). Located in a slightly hilly landscape along the river Rhine, Mainz is an inland town and one of the cities with the highest PM concentrations in Germany (ZIMEN, 2021b). The climate is moderate with an annual average TA of 10.7 °C and precipitation of 620 mm (Koeppen Cfb) (Deutscher Wetterdienst, 2021a, 2021b).

The study route includes three urban quarters of different characteristics: Altstadt, Hartenberg, and Neustadt (Fig. 3-1). The Altstadt quarter is the old part of the town characterized by compact low- to midrise buildings, mostly paved streets, and pedestrian zones (Stewart and Oke, 2012). The urban architecture of the Hartenberg quarter, on the contrary, is a district with

open low- to midrise buildings, a small grove, and low motorized traffic. The Neustadt quarter is characterized by mainly five-story-high buildings and narrow streets (~10 m wide), small parks (< 150 m across), and low traffic intensity in a grid-based street layout. Large multi-lane roads with high traffic intensities surround this quarter as well as the Altstadt.

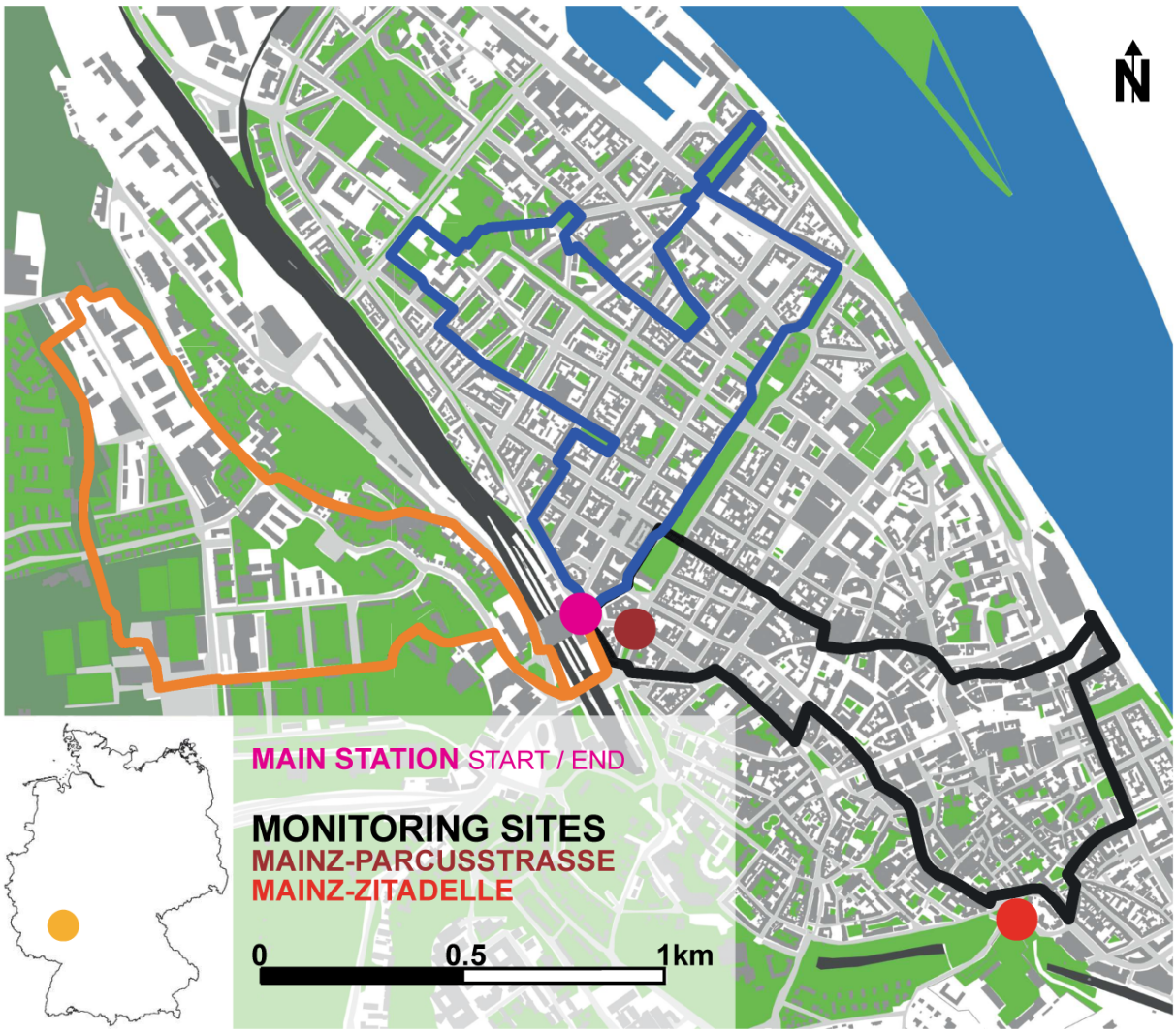

Fig. 3-1 Study tracks in the Mainz Altstadt, Hartenberg, and Neustadt (black, orange, and blue lines, respectively), their joint start and end point at the main station (magenta), and the monitoring sites of the ZIMEN network at Mainz-Parcusstraße (dark red) and Mainz-Zitadelle (red) of the ZIMEN network, and map of Germany showing the location of Mainz (orange).

The total length of the study route was ~15 km or ~3 h walking by foot. To mitigate potential changes of local concentrations during such a long time span, we divided the route into three circular tracks, each leading through one of the districts. Each track was 5 km long (~1 h by foot) and shared the same starting and ending point at the Mainz train station (50.0017 °N, 8.2595 °E; Fig. 3-1magenta dot). The division into district tracks also supported multiple

measurements per day. We conducted four measurement runs on each track, before and during the MO and AF rush hours starting at 6 am, 07:30 am, 4 pm and 05:30 pm, with the exception of 14.09.20 when we only measured in the AF. For each track, one device was used comprised of a PM sensor Alphasense OPC-N3 (Alphasense, 2018), a ESP32 controller (Espressif, 2021), a GPS module (Simcom, 2021), and a microSD card to save measurement data (Fig. 3-2a). The sensors were mounted at adult breath height (1.6 m) on the front of a wearable rack to reduce influences of the person carrying the device (Fig. 3-2b). To support the detection of local emitters during post-processing, every run was filmed with a camera attached to the rack.

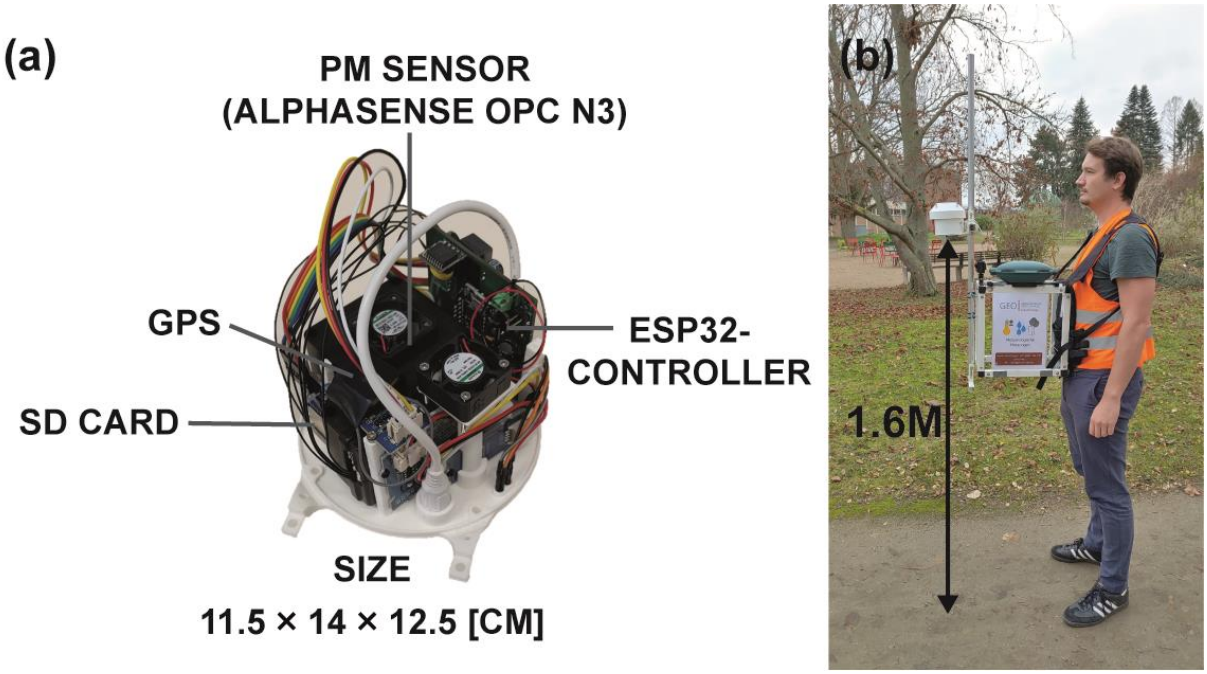

Fig. 3-2 (**a**) Design and components of the measurement device (dimensions: 11.5 cm × 14 cm × 12.5 cm), and (**b**) picture of a person carrying the rack.

3.2.2 Inter-Sensor Variability

The Alphasense OPC-N3 sensors are low-cost optical particle counters following a light scattering principle (Mie, 1908). The detected particles are put into bins considering their estimated size (Bohren and Huffman, 1998) and subsequently converted into dM (Walser et al., 2017). The measurement range of the Alphasense OPC-N3 for particles is 0.35 to 40 µm (Alphasense, 2018). The handy OPC-N3 units are suitable for a mobile measurement rack, affordable (~300 €), and perform well under laboratory conditions (Sousan et al., 2021) considering the European EN 481 standard and manufacture calibration (Crilley et al., 2018). However, to further assess accuracy and address inter-sensor variability, a stationary field

calibration in an environment similar to the study area is recommended (Alfano et al., 2020; Chatzidiakou et al., 2019; Crilley et al., 2020; Gysel et al., 2007; Hagler et al., 2018; WMO, 2018). Such a calibration was conducted on the Hartenberg district from 18–22.11.20, 05-08.01.21, and 20–23.02.21. Since there were no reference devices that feature a comparable temporal resolution (< 20 s), we adjusted two PM sensors to one other sensor: in our case, the sensors used in the Altstadt and Neustadt were adjusted to the Hartenberg sensor (Fig. 3-3). The devices were co-located on the same height side-by-side to measure $PM_{2.5}$ concentrations in a 1 s interval. The resulting data were then processed into 20 s arithmetic means, whereby the 10% highest and lowest values were truncated to mitigate the influence of short-term emissions (e.g., smokers).

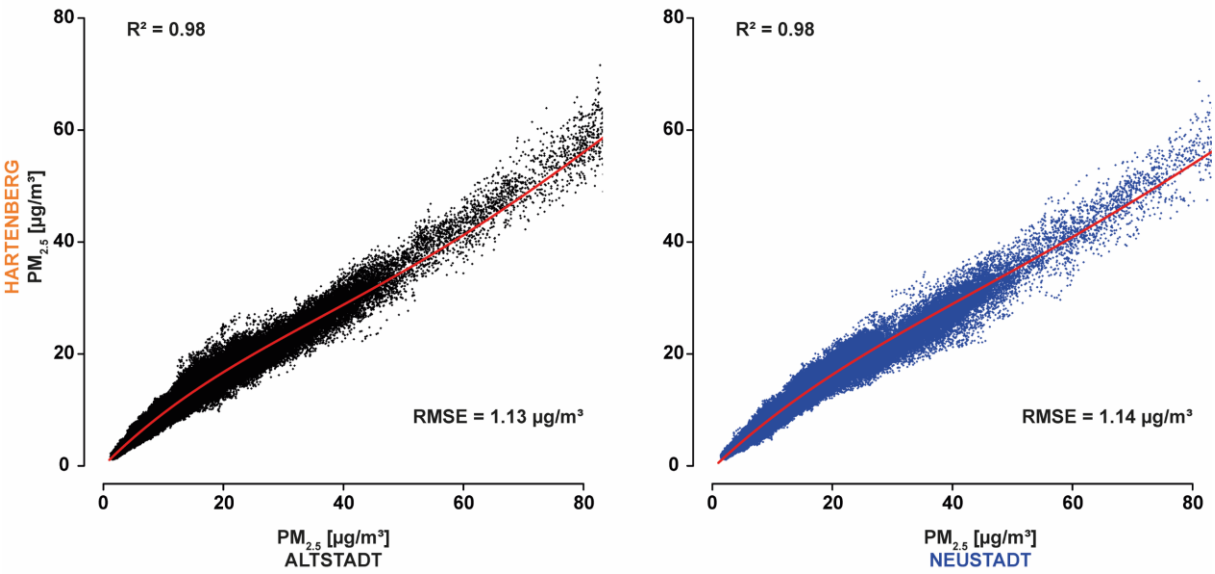

Fig. 3-3 Scatterplots and polynomial regressions of the moving 20 s truncated arithmetic mean $PM_{2.5}$ adjustments of the sensors used on the Altstadt (left panel) and Neustadt tracks (right panel) to the Hartenberg sensor including R^2 coefficients and RMSE for the adjustment periods from 18–22.11.20, 05–08.01.21, and 20–23.02.21.

Scatterplots of data measured in the Altstadt and Neustadt compared to Hartenberg showed that the cross-sensor accuracy was high. In addition to an explained variance exceeding 0.98, the data were homoscedastic and low RMSE reached 1.13 µg/m^3 and 1.14 µg/m^3, respectively. However, 4th degree polynomial (instead of linear) regression models were most suited to transform the measurements and produce statistically reliable data.

3.2.3 Data Post-processing

To enable the comparison across different runs and tracks, several steps of post-processing had to be undertaken. At first, the recorded 1 s interval PM datasets were averaged calculating moving 20 s truncated arithmetic means, similar to the procedure used for calibration. A spatial synchronization of the data of the individual tracks was applied to adjust slight variations in run duration and minor inaccuracies of the GPS data. This was done by manually setting an ideal route for every subtrack and converting the data into points with a distance of 50 cm to each other. Each point was allocated to its appropriate data by calculating an average of the 10 closest original datapoints using an inverse distance weighting method (Shepard, 1968). The data of each track and run were then converted considering the polynomial regression equation obtained from the calibration trials. To reduce the effect of particle hygroscopy, a RH correction for data recorded at RH > 60% according to Crilley et al., 2018 was applied. The correction formula is based on the κ-Köhler theory, with $\kappa = 0.33$ as a composition of hygroscopic particles in the ambient air and a dry particle density of 1.65 g/cm^3 (Crilley et al., 2020). Ambient RH measurements were taken from the long-term station Mainz-Zitadelle of the ZIMEN network. The processed data were then analyzed using descriptive statistics, i.e., arithmetic mean, median, and SD. In order to validate our absolute $PM_{2.5}$ measurements for $PM_{2.5}$ hotspot identification, a comparison of the mean $PM_{2.5}$ values of each track and run in September and March against the regular long-term station data from Mainz-Parcusstraße, which is characterized by urban traffic, and Mainz Zitadelle, which resembles the urban background, was performed. These two measurement stations are part of the ZIMEN network, which carries out measurements with Thermo Fisher SHARP 5030 instruments (Thermo Fisher Science, 2011) to monitor $PM_{2.5}$ and PM_{10} on behalf of the state.

For the detection of highly polluted spots, the following steps were conducted. To counteract time-related fine particulate gradients, the data of each run were linearly detrended. Subsequently, the measurements of the simultaneously conducted runs in each district were combined and highly polluted locations (spots with 10% highest $PM_{2.5}$ values) were identified: we determined highly polluted locations, for each period and season, by overlaying the extreme data of the respective runs and looking for matches. A match was recorded if the same location within a radius of 20 m indicated a pollution hotspot (i.e., 10% highest values) in several runs. After identifying highly polluted locations, we calculated $PM_{2.5}/PM_{10}$ ratios for the September and March data to evaluate emission sources.

3.3 Results and Discussion

3.3.1 Absolute $PM_{2.5}$ Concentrations in September and March

In September, the uncorrected mean $PM_{2.5}$ concentrations were in line with the ZIMEN measurements and showed a diurnal pattern in $PM_{2.5}$ characterized by 50 to 220% higher concentrations in the MO compared to the AF runs. This pattern was recorded during the first three days of the September campaign and followed by declining concentrations toward the end of the week (0, for median PM_{10} concentrations, see Fig. 3-A4).

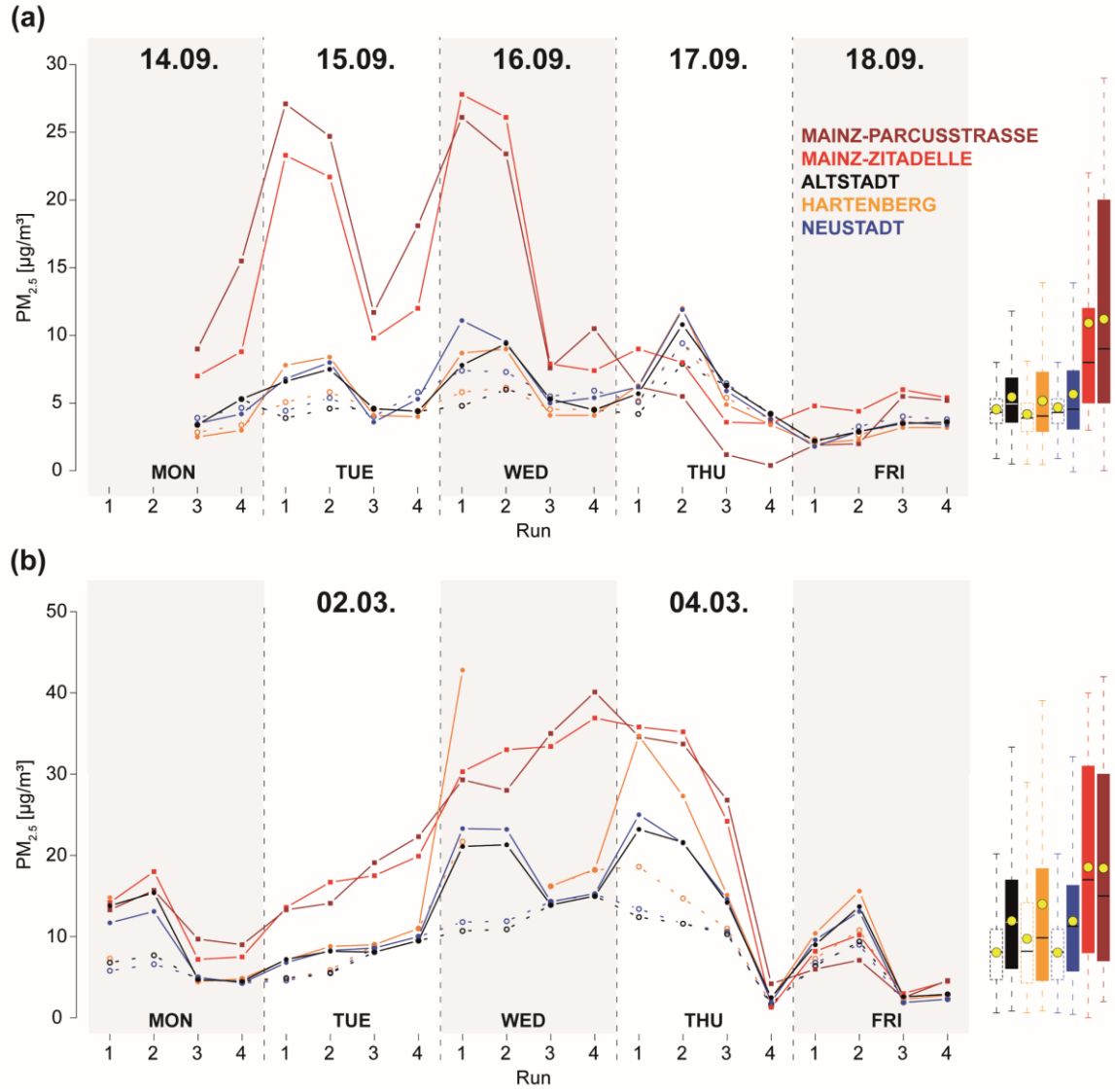

Fig. 3-4 Mean $PM_{2.5}$ concentrations in the Altstadt, Hartenberg, Neustadt (black, blue, and orange colors, respectively), and ZIMEN data from the Mainz-Parcusstraße and Mainz-Zitadelle (dark red and red colors, respectively) during the study periods in (a) September and (b) March with corresponding boxplots and arithmetic means (yellow dots). The unfilled dots symbolize the RH-corrected $PM_{2.5}$ measurements, and the filled dots symbolize PM2.5 concentrations without RH correction.

This change in $PM_{2.5}$ variability could be associated to changes in the weather regime: the first three days were characterized by warm late summer weather conditions consisting of high daily maximum TA > 30 °C, moderate mean RH < 57%, and low maximum windspeeds < 1.0 m/s mainly from southeast directions (0; Fig. 3-A1). These stable conditions were also expressed by a low mean MLH < 200 m and high mean CIN with daily amplitudes up to 340 J/kg, which provided meteorologically favorable conditions for increased PM concentrations (Graham et al., 2020). However, our measurements mainly underestimated the $PM_{2.5}$ concentrations of the ZIMEN network in this period, particularly during the MO runs of 15.09.20 and 16.09.20 and after consideration of the RH correction. These differences exceeded 23 µg/m^3 in absolute values equal to 700% (both on 1509.20, first run). Right after the 4th run on 16 September 2020, the weather changed. Air pressure increased to 1015 hPa accompanied by rising windspeeds (max: < 1.7 m/s), higher mean MLH value, lower CIN (69 J/kg), lower TA, and mean RH < 60% during last six runs of the September campaign which is why no RH correction was applied for this period (Fig. 3-A1). During this time, the differences between our and the ZIMEN data decreased. Whereas our measurements showed still slightly higher $PM_{2.5}$ concentrations on the 17.09.20, differences did not exceed 3.0 µg/m^3 thereafter.

In March, the $PM_{2.5}$ concentrations were higher than in September. The differences between ZIMEN and our uncorrected measurements were moderate (< 5.2 µg/m^3) during the first four runs. Thereafter, when stable weather conditions set in (Tab. 3-1, Fig. 3-A2) and $PM_{2.5}$ concentrations increased, a substantially larger underestimation up to 25.1 µg/m^3 of the ZIMEN was recorded. An exception was run one on 03.01.21 on the Hartenberg, where we measured > 12 µg/m^3 higher concentrations on average, though this seemed to be a single outlier that we could not explain. After 03.03.21, the $PM_{2.5}$ concentrations decreased due to a change in weather, upcoming north wind (max. 3.2 m/s), and a short-term shower, followed by decreasing of TA and RH. The differences between the ZIMEN measurements and those conducted by us were again small.

In both study periods, the differences in absolute $PM_{2.5}$ between our runs and the stationary data were large and could not be explained by spatial variability. Our findings confirm the results of, e.g., Li et al., 2020 and Sousan et al., 2016, who identified this underestimation of OPC-N3 sensors compared to reference instruments. A stronger underestimation of the RH-corrected $PM_{2.5}$ concentration could be explained by the fact that any correction lowers the values (Crilley et al., 2020). Furthermore, the missing diurnal pattern during the first 3 – 4 days in September could be related to higher RH in the AF causing larger corrections. In March,

however, the uncorrected measurements still showed diurnal patterns, whereas both the RH-corrected and ZIMEN data did not. The RH correction looked more suitable in the spring campaign, possibly because the prevailing higher RH resulted in corrections and hence stronger underestimations. The overall substantial underestimations and incomprehensible differences between mobile and stationary data led to the conclusion that our PM sensors cannot be used to assess absolute $PM_{2.5}$ concentrations. For this reason, we used relative instead of absolute $PM_{2.5}$ data to evaluate highly polluted areas.

Tab. 3-1 Meteorological conditions during the study measurement periods in September and March including mean TA [°C], mean RH [%], precipitation sum [mm], atmospheric pressure [hPA], wind speed [m/s], wind direction [°], mean CIN [J/kg], and mean MLH [m]. Adapted with permission from Umweltmeteorologie RLP, 2021; ZIMEN, 2021b.

Date	14.09.	15.09.	16.09.	17.09.	18.09.	01.03.	02.03.	03.03.	04.03.	05.03.
TA (°C)	23.0	23.3	23.8	19.5	18.8	7.7	9.2	8.2	9.6	5.8
RH (%)	53.6	56.6	57.1	51.2	46	66.8	62.7	71.5	71.7	59.4
Precipitation (mm)	0.3	0	0.1	1.1	1.9	0	0	0	9.5	0
Atmospheric pressure (hPA)	1013	1009	1007	1013	1012	1021	1020	1017	1008	1014
Wind direction (°)	56	63	147	105	100	143	122	148	225	166
Wind speed (m/s)	0.2	0.1	0.4	0.6	0.6	0.5	0.3	0.2	0.6	1.1
CIN (J/kg)	177	171	171	60	85	163	148	219	110	27
MLH (m)	170	165	115	312	249	135	163	102	226	455

3.3.2 Highly Polluted Places and Sources

The identification of highly polluted sites, i.e., sites with the highest 10% of $PM_{2.5}$ concentrations throughout the entire study area, was conducted using 35 of 38 runs. Two runs were excluded due to sensor malfunctions (run two on 01.03.21 and run two on 03.03.21) and one run was omitted because of onsetting rain causing strongly lowered PM, which did not allow reasonable spatial comparisons of that run (run three on 04.03.21).

Our result showed that no location was consistently identified as a highly polluted area throughout the entire measurement period (Fig. 3-5). This result was unexpected as our measurements took place along roads and large intersections with high vehicle traffic, reported to be main source of fine particle concentrations in urban areas (Kumar et al., 2017). On the contrary, locations with high levels of $PM_{2.5}$ could be identified on all three tracks. While all $PM_{2.5}$ hotspots were recorded in the Neustadt district during the September MO runs, the AF runs also included highly polluted places in the Altstadt. For the early MO runs in March, hotspots were solely detected in the Hartenberg, and in later runs, the highly polluted places

were recorded on all tracks yet focused in the Hartenberg and Neustadt districts. People were thus exposed to high particle concentrations at varying places in different urban settings depending on the daytime and season.

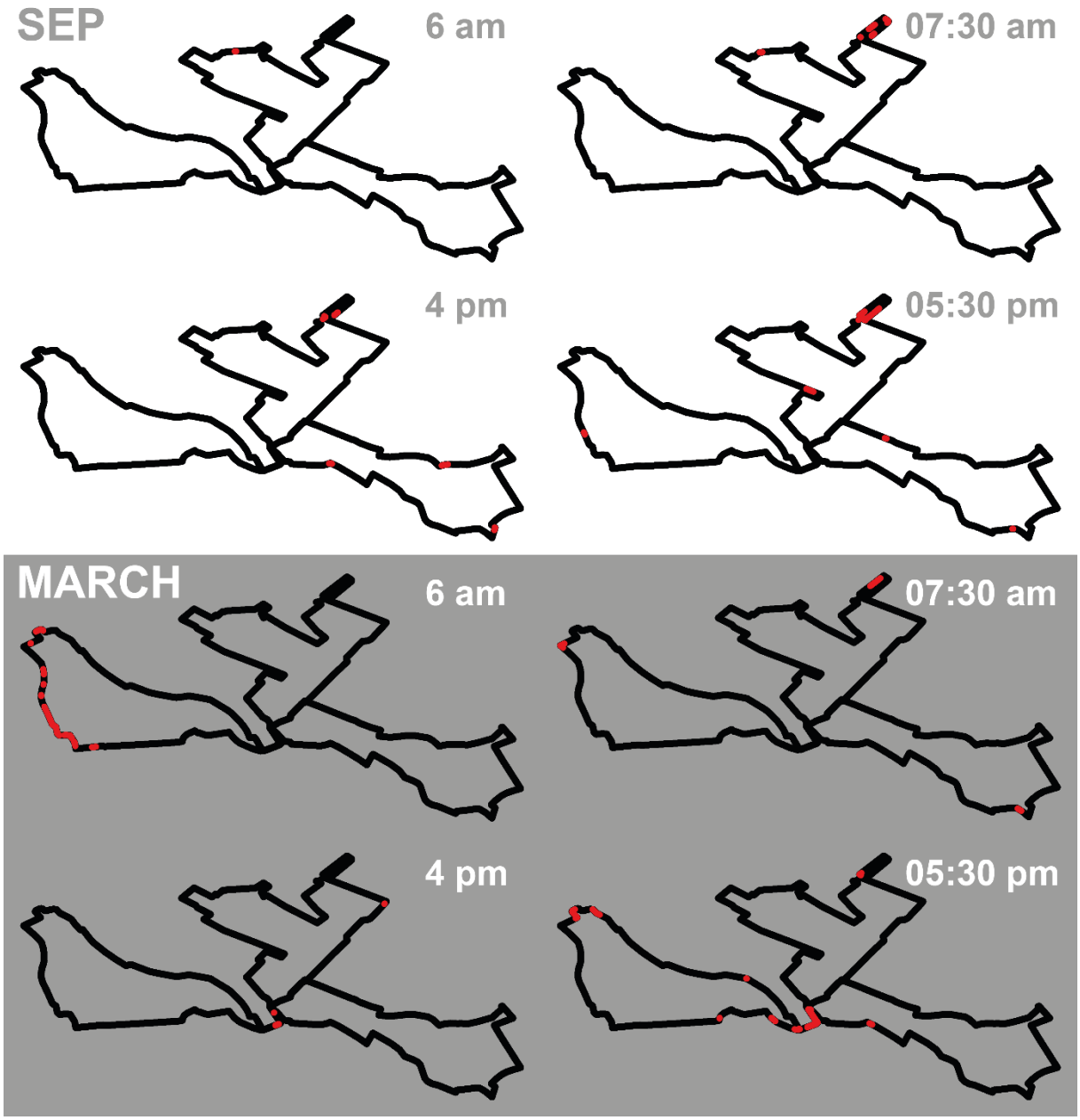

Fig. 3-5 Locations showing the 10% highest $PM_{2.5}$ concentrations (red dots) throughout the runs during the September and March campaigns.

However, there were locations where pedestrians were exposed more frequently. In > 50% of the September runs, we identified 21 different spots showing recurring high $PM_{2.5}$ concentrations throughout all tracks (Fig. 3-6, left panel). The larger number of hotspots in September could be assigned to the low absolute $PM_{2.5}$ concentrations and minor differences among districts (0). At low particle concentrations, local emissions have a large influence on absolute $PM_{2.5}$ peaks, and the mitigated track differences further the spread of hotspots. In March, there were at least seven highly polluted locations, mostly recorded on the overall more polluted Hartenberg track. However, when increasing the threshold to define highly polluted areas to > 60% of the runs, the number of hotspots declined massively to only five locations (Fig. 3-6, right panel; Fig. 3-A3). The remaining September hotspots were in a Neustadt park and the Altstadt pedestrian zone, whereas the two remaining March hotspots were located near a major housing construction site in Hartenberg and a traffic-loaded bridge near the train station.

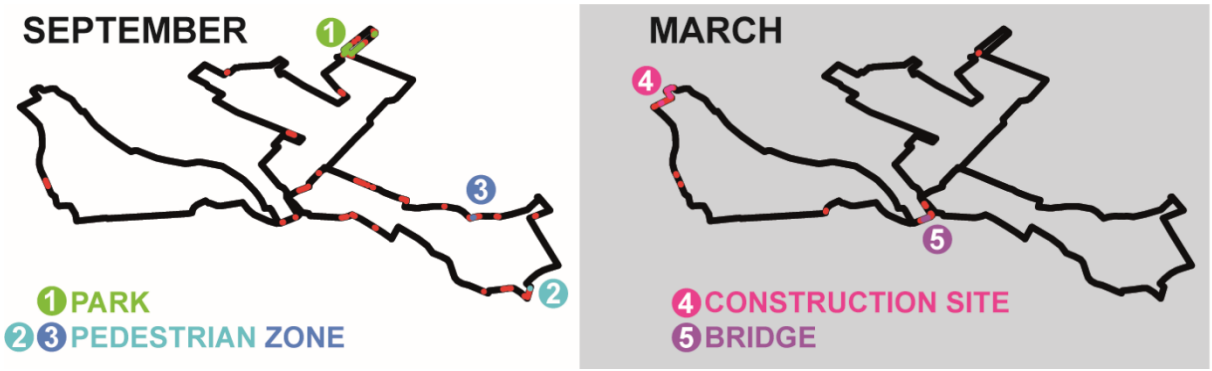

Fig. 3-6 Locations with 10% highest $PM_{2.5}$ in > 60% of all runs in September (left panel) and March (right panel). Colors refer to parks (green), pedestrian zone (blue and cyan), construction site (magenta), and a bridge (violet).

The March hotspots could clearly be attributed to anthropogenic sources: the origin of the particles at the bridge could be assigned to vehicles, as there was a high intensity of traffic on the multi-lane road crossing the bridge; the emission sources of the construction site were seemingly related to building processes and frequent construction vehicles (Karagulian et al., 2019; Yue et al., 2010). These conclusions were supported by low apportionment of $PM_{2.5}$ in PM_{10} at these locations (Fig. 3-7). While the high $PM_{2.5}/PM_{10}$ ratio at the bridge near the main station (0.73) indicated the particle source to originate predominantly from anthropogenic emissions due to combustion processes of vehicles, the lower ratio (0.63) and high variability (IQR = 0.13) at the construction sites pointed to a mixture of resuspended dust and particles from combustion processes.

The three September hotspots were particularly surprising, as there was no motorized traffic present at the time. This is in contrast to our hypothesis that the hotspots were related to heavy traffic streets as the main driver of high $PM_{2.5}$ concentrations in urban areas (Kumar et al., 2017). The high values in the pedestrian zones could nevertheless be of anthropogenic origin, emitted by the exhaust systems of the restaurant kitchens blowing fine particles during deep-frying and roasting onto the streets (Kang et al., 2019). Particles were likely additionally emitted in the outdoor areas of the restaurants (Fig. 3-A3, panel 3) due to smoking activities as reported by Birmili et al., 2013. High $PM_{2.5}/PM_{10}$ ratios > 0.6 at these locations support the conclusion that anthropogenic sources were the main emitters, as does the fact that these sites were identified as $PM_{2.5}$ hotspots in the AF runs, i.e., at times when restaurants were highly frequented.

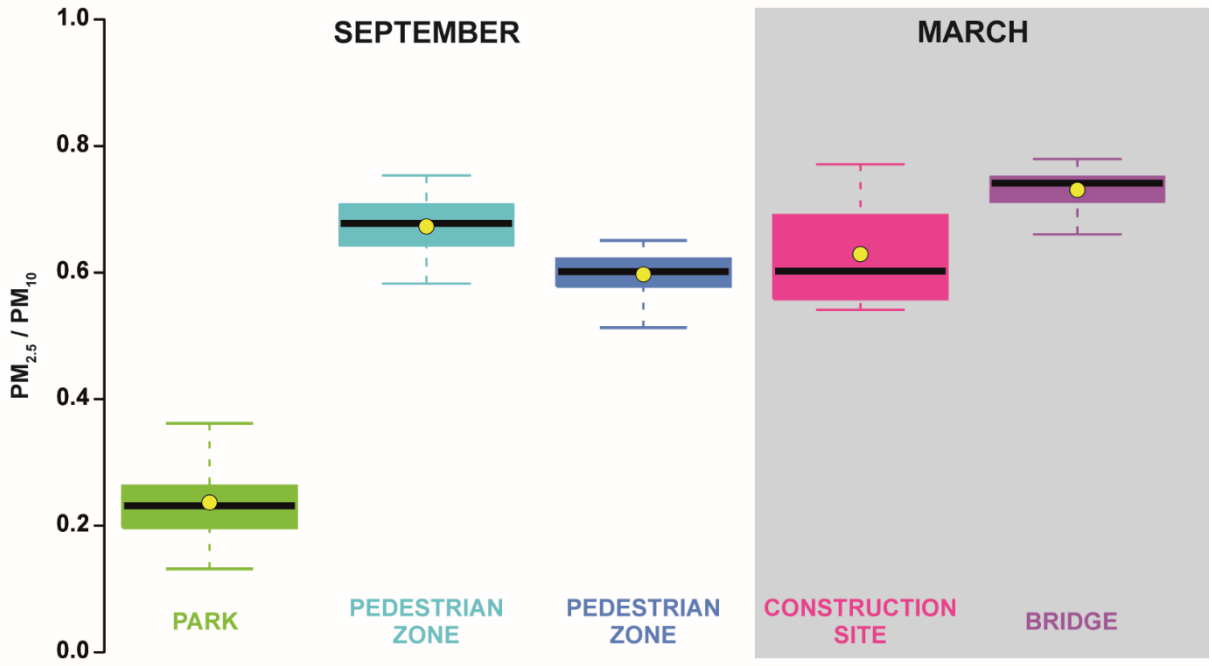

Fig. 3-7 $PM_{2.5}/PM_{10}$—ratio boxplots of the $PM_{2.5}$ hotspots in the park (green) and pedestrian zones (cyan and blue) for September (green, cyan, and blue colors) and the construction site (magenta) and motorized road (violet) for March. Yellow dots indicate mean values.

The particle sources in the park could not be attributed to combustion processes as in the other hotspots. The much lower mean $PM_{2.5}/PM_{10}$ ratio = 0.24 and small IQR = 0.07 pointed to a homogenous particle composition during September at this location (Fig. 3-7). These values were either related to fugitive dust (Evagelopoulos et al., 2019), i.e., impervious areas and footpaths containing loose top material, or to re-suspended road dust from the multi-lane road

right next to the park. The spatial distribution of the $PM_{2.5}/PM_{10}$ ratios for September indicated that horizontal transport of fine particles from the close road was unlikely (Fig. 3-8). Ratios < 0.5 are rather indicative of locations with ongoing road and construction works and of parks with loose gravel on the walkways. Since there was no roadwork near to the park during the measurement campaign, whirled up dust from graveled and unpaved walkways was the most plausible local emissions. These findings corroborate with Paas and Schneider, 2016 who attributed higher mean concentrations in a green area to re-suspended dried-out grass and unsurfaced footpath particles.

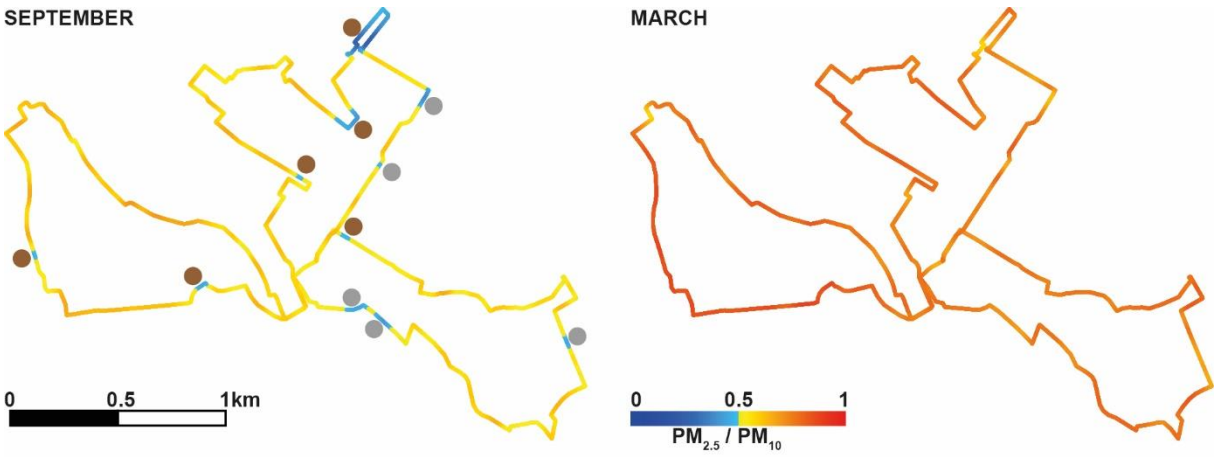

Fig. 3-8 Spatial patterns of mean $PM_{2.5}/PM_{10}$ ratios in September and March. Bluish colors indicate ratios between 0 to 0.5. The dots mark important particle sources including unpaved surfaces (brown) and construction sites (grey).

The comparison of highly polluted locations in September and March showed that the hotspots varied within the study area and that the underlying particle source changed. The data were additionally characterized by a substantial increase in $PM_{2.5}/PM_{10}$ ratios from 0.56 to 0.76 between autumn and spring, averaged over the study area (Fig. 3-8). This seasonal change is in line with Speranza et al., 2016 reporting ratios of < 0.5 during warmer seasons (spring–summer) and ratio of > 0.5 during colder seasons (autumn – winter). In our case, the increase in $PM_{2.5}$ ratio was likely additionally affected by a pronounced cool thermal inversion (Tab. 3-1; Fig. 3-A2). These conditions constrained the vertical mixing of air, which led to an increase in fine particle concentrations at ground level. The prevailing low wind speeds subsequently amplified dry deposition of coarse particles, which in turn increased the $PM_{2.5}$ apportionment in PM_{10} (Blanco-Becerra et al., 2015; Huang et al., 2014; Wallace and Kanaroglou, 2009).

3.4 Conclusion

Using mobile low-cost devices containing Alphasense OPC-N3 sensors, small-scale $PM_{2.5}$ hotspots along a 15 km transect in an urban area were identified. Three sensors showed a high agreement among each other but severely underestimated the measured $PM_{2.5}$ concentrations of the ZIMEN network, particularly after applying a widely used RH correction (Crilley et al., 2020). Absolute $PM_{2.5}$ values were not considered, but additional calibration against high-resolution reference instruments could possibly improve the data accuracy of OPC-N3 sensors.

The identification of (relatively) heavily polluted locations revealed persisting $PM_{2.5}$ hotspots in > 60% of all runs, though the locations varied between the September and March study periods. The March hotspots were most likely triggered by local anthropogenic emissions including traffic emissions and construction work. This conclusion was supported by $PM_{2.5}/PM_{10}$ ratios > 0.6 indicating combustion processes as the main particle source. The September hotspots, however, were located in areas dominated by pedestrians, and the PM sources were attributed to restaurant cooking exhaust air and outdoor seating activities. Exceptionally low $PM_{2.5}/PM_{10}$ ratios of 0.24 recorded in a park pointed to particles originating from locally emitted natural dust from unpaved footpaths, bare soils, and gravel surfaces. The $PM_{2.5}/PM_{10}$ ratios also increased from September to March as additional heating due to cooler TA and stable weather conditions prevailed during the spring campaign. The composition of sources can be further differentiated by analyzing the chemical composition of particles, which we recommend for further studies. The work detailed here revealed the capability of low-cost sensors to identify small-scale $PM_{2.5}$ hotspots and sources. While the accuracy of absolute $PM_{2.5}$ concentrations was insufficient, highly resolved spatiotemporal measurements may complement the stationary data and support the identification of highly polluted areas in the urban environment.

3.5 Acknowledgements

We thank several students of the Johannes Gutenberg University in Mainz including Joelle Juretzek, Leonard Köster, and Jan-Erik Schmitz for supporting the mobile measurements. We are grateful to the environmental state office of Rhineland-Palatinate, particularly Michael Weißenmayer and Margit von Döhren from Referat 60 and Matthias Zimmer and Matthias Voigt from Referat 63, for providing data of the official meteorological measurement stations and radiometer as shown in Tab. 3-1, 0, Fig. 3-5, Fig. 3-A1 and Fig. 3-A2.

3.6 Funding

Jan Esper received support from the Gutenberg Research College, SustES (CZ.02.1.01/0.0/0.0/16_019/0000797), and ERC (AdG 882727).

3.7 References

Al-Ali, A.R., Zualkernan, I., Aloul, F., 2010. A Mobile GPRS-Sensors Array for Air Pollution Monitoring. IEEE Sensors J. 10, 1666–1671. https://doi.org/10.1109/JSEN.2010.2045890

Alfano, B., Barretta, L., Del Giudice, A., Vito, S., Di Francia, G., Esposito, E., Formisano, F., Massera, E., Miglietta, M.L., Polichetti, T., 2020. A Review of Low-Cost Particulate Matter Sensors from the Developers' Perspectives. Sensors (Basel) 20. https://doi.org/10.3390/s20236819

Alphasense, 2018. Technical Information Release December 2018: Alphasense Particle Counter OPC-N Range Product Update . URL http://www.alphasense.com/WEB1213/wp-content/uploads/2019/02/OPC-N3-information-update-Dec-18.pdf

Birmili, W., Rehn, J., Vogel, A., Boehlke, C., Weber, K., Rasch, F., 2013. Micro-scale variability of urban particle number and mass concentrations in Leipzig, Germany. metz 22, 155–165. https://doi.org/10.1127/0941-2948/2013/0394

Blanco-Becerra, L.C., Gáfaro-Rojas, A.I., Rojas-Roa, N.Y., 2015. Influence of precipitation scavenging on the PM2.5PM10 ratio at the Kennedy locality of Bogotá, Colombia. Rev. Fac. Ing. Antioquia. https://doi.org/10.17533/udea.redin.n76a07

Bohren, C.F., Huffman, D.R., 1998. Absorption and Scattering of Light by Small Particles. Wiley. https://doi.org/10.1002/9783527618156

Brattich, E., Bracci, A., Zappi, A., Morozzi, P., Di Sabatino, S., Porcù, F., Di Nicola, F., Tositti, L., 2020. How to Get the Best from Low-Cost Particulate Matter Sensors: Guidelines and Practical Recommendations. Sensors (Basel) 20. https://doi.org/10.3390/s20113073

Chatzidiakou, L., Krause, A., Popoola, O.A.M., Di Antonio, A., Kellaway, M., Han, Y., Squires, F.A., Wang, T., Zhang, H., Wang, Q., Fan, Y., Chen, S., Hu, M., Quint, J.K., Barratt, B., Kelly, F.J., Zhu, T., Jones, R.L., 2019. Characterising low-cost sensors in highly portable platforms to quantify personal exposure in diverse environments. Atmos Meas Tech 12, 4643–4657. https://doi.org/10.5194/amt-12-1-2019

Chen, L.C., Lippmann, M., 2009. Effects of metals within ambient air particulate matter (PM) on human health. Inhal Toxicol 21, 1–31. https://doi.org/10.1080/08958370802105405

Crilley, L.R., Shaw, M., Pound, R., Kramer, L.J., Price, R., Young, S., Lewis, A.C., Pope, F.D., 2018. Evaluation of a low-cost optical particle counter (Alphasense OPC-N2) for ambient air monitoring. Atmos. Meas. Tech. 11, 709–720. https://doi.org/10.5194/amt-11-709-2018

Crilley, L.R., Singh, A., Kramer, L.J., Shaw, M.D., Alam, M.S., Apte, J.S., Bloss, W.J., Hildebrandt Ruiz, L., Fu, P., Fu, W., Gani, S., Gatari, M., Ilyinskaya, E., Lewis, A.C., Ng'ang'a, D., Sun, Y., Whitty, R.C.W., Yue, S., Young, S., Pope, F.D., 2020. Effect of aerosol composition on the performance of low-cost optical particle counter correction factors. Atmos. Meas. Tech. 13, 1181–1193. https://doi.org/10.5194/amt-13-1181-2020

Czernecki, B., Półrolniczak, M., Kolendowicz, L., Marosz, M., Kendzierski, S., Pilguj, N., 2017. Influence of the atmospheric conditions on PM10 concentrations in Poznań, Poland. J Atmos Chem 74, 115–139. https://doi.org/10.1007/s10874-016-9345-5

Deutscher Wetterdienst, 2021a. Temperatur: vieljährige Mittelwerte 1981 - 2010 . URL https://www.dwd.de/DE/leistungen/klimadatendeutschland/mittelwerte/temp_8110_fest_html.html%3Fview%3DnasPublication

Deutscher Wetterdienst, 2021b. Niederschlag: vieljährige Mittelwerte 1981 - 2010 . URL https://www.dwd.de/DE/leistungen/klimadatendeutschland/mittelwerte/nieder_8110_fest_html.html?view=nasPublication&nn=16102

Di Antonio, A., Popoola, O.A.M., Ouyang, B., Saffell, J., Jones, R.L., 2018. Developing a Relative Humidity Correction for Low-Cost Sensors Measuring Ambient Particulate Matter. Sensors (Basel) 18. https://doi.org/10.3390/s18092790

Espressif, 2021. ESP32 . URL https://www.espressif.com/en/products/socs/esp32

Evagelopoulos, V., Zoras, S., Triantafyllou, A.G., Albanis, T.A., 2019. PM10-PM2.5 TIME SERIES AND FRACTAL ANALYSIS: c. Global NEST Journal 8, 234–240. https://doi.org/10.30955/gnj.000372

Graham, A.M., Pringle, K.J., Arnold, S.R., Pope, R.J., Vieno, M., Butt, E.W., Conibear, L., Stirling, E.L., McQuaid, J.B., 2020. Impact of weather types on UK ambient particulate matter concentrations. Atmospheric Environment: X 5, 100061. https://doi.org/10.1016/j.aeaoa.2019.100061

Gualtieri, M., Ovrevik, J., Mollerup, S., Asare, N., Longhin, E., Dahlman, H.-J., Camatini, M., Holme, J.A., 2011. Airborne urban particles (Milan winter-PM2.5) cause mitotic arrest and cell death: Effects on DNA, mitochondria, AhR binding and spindle organization. Mutat Res 713, 18–31. https://doi.org/10.1016/j.mrfmmm.2011.05.011

Gysel, M., Crosier, J., Topping, D.O., Whitehead, J.D., Bower, K.N., Cubison, M.J., Williams, P.I., Flynn, M.J., McFiggans, G.B., Coe, H., 2007. Closure study between chemical composition and hygroscopic growth of aerosol particles during TORCH2. Atmos. Chem. Phys. 7, 6131–6144. https://doi.org/10.5194/acp-7-6131-2007

Hagler, G.S.W., Williams, R., Papapostolou, V., Polidori, A., 2018. Air Quality Sensors and Data Adjustment Algorithms: When Is It No Longer a Measurement? Environ Sci Technol 52, 5530–5531. https://doi.org/10.1021/acs.est.8b01826

Huang, R.-J., Zhang, Y., Bozzetti, C., Ho, K.-F., Cao, J.-J., Han, Y., Daellenbach, K.R., Slowik, J.G., Platt, S.M., Canonaco, F., Zotter, P., Wolf, R., Pieber, S.M., Bruns, E.A., Crippa, M., Ciarelli, G., Piazzalunga, A., Schwikowski, M., Abbaszade, G., Schnelle-Kreis, J., Zimmermann, R., An, Z., Szidat, S., Baltensperger, U., El Haddad, I., Prévôt, A.S.H., 2014. High secondary aerosol contribution to particulate pollution during haze events in China. Nature 514, 218–22. https://doi.org/10.1038/nature13774

Kang, K., Kim, H., Kim, D.D., Lee, Y.G., Kim, T., 2019. Characteristics of cooking-generated PM10 and PM2.5 in residential buildings with different cooking and ventilation types. Sci Total Environ 668, 56–66. https://doi.org/10.1016/j.scitotenv.2019.02.316

Karagulian, F., Barbiere, M., Kotsev, A., Spinelle, L., Gerboles, M., Lagler, F., Redon, N., Crunaire, S., Borowiak, A., 2019. Review of the Performance of Low-Cost Sensors for Air Quality Monitoring. Atmosphere 10, 506. https://doi.org/10.3390/atmos10090506

Kumar, P., Rivas, I., Sachdeva, L., 2017. Exposure of in-pram babies to airborne particles during morning drop-in and afternoon pick-up of school children. Environ Pollut 224, 407–420. https://doi.org/10.1016/j.envpol.2017.02.021

Lelieveld, J., Klingmüller, K., Pozzer, A., Pöschl, U., Fnais, M., Daiber, A., Münzel, T., 2019. Cardiovascular disease burden from ambient air pollution in Europe reassessed using novel hazard ratio functions. Eur Heart J 40, 1590–1596. https://doi.org/10.1093/eurheartj/ehz135

Li, J., Mattewal, S.K., Patel, S., Biswas, P., 2020. Evaluation of Nine Low-cost-sensor-based Particulate Matter Monitors. Aerosol Air Qual. Res. 20, 254–270. https://doi.org/10.4209/aaqr.2018.12.0485

Maione, M., Mocca, E., Eisfeld, K., Kazepov, Y., Fuzzi, S., 2021. Public perception of air pollution sources across Europe. Ambio 50, 1150–1158. https://doi.org/10.1007/s13280-020-01450-5

Mie, G., 1908. Beiträge zur Optik trüber Medien, speziell kolloidaler Metallösungen. Ann. Phys. 330, 377–445. https://doi.org/10.1002/ANDP.19083300302

Mirabelli, M.C., Ebelt, S., Damon, S.A., 2020. Air Quality Index and air quality awareness among adults in the United States. Environ Res 183, 109185. https://doi.org/10.1016/j.envres.2020.109185

Morawska, L., Thai, P.K., Liu, X., Asumadu-Sakyi, A., Ayoko, G., Bartonova, A., Bedini, A., Chai, F., Christensen, B., Dunbabin, M., Gao, J., Hagler, G.S.W., Jayaratne, R., Kumar, P., Lau, A.K.H., Louie, P.K.K., Mazaheri, M., Ning, Z., Motta, N., Mullins, B., Rahman, M.M., Ristovski, Z., Shafiei, M., Tjondronegoro, D., Westerdahl, D., Williams, R., 2018. Applications of low-cost sensing technologies for air quality monitoring and exposure assessment: How far have they gone? Environ Int 116, 286–299. https://doi.org/10.1016/j.envint.2018.04.018

Paas, B., Schneider, C., 2016. A comparison of model performance between ENVI-met and Austal2000 for particulate matter. Atmospheric Environment 145, 392–404. https://doi.org/10.1016/j.atmosenv.2016.09.031

Parkhurst, W.J., Tanner, R.L., Weatherford, F.P., Valente, R.J., Meagher, J.F., 1999. Historic PM2.5/PM10 Concentrations in the Southeastern United States-Potential Implications of the Revised Particulate Matter Standard. J Air Waste Manag Assoc 49, 1060–1067. https://doi.org/10.1080/10473289.1999.10463894

Querol, X., Alastuey, A., Rodriguez, S., Plana, F., Ruiz, C.R., Cots, N., Massague, G., Puig, O., 2001. PM10 and PM2.5 source apportionment in the Barcelona Metropolitan area, Catalonia, Spain. Atmospheric Environment 35, 6407–6419. https://doi.org/10.1016/S1352-2310(01)00361-2

Schlesinger, R.B., 2007. The health impact of common inorganic components of fine particulate matter (PM2.5) in ambient air: a critical review. Inhal Toxicol 19, 811–32. https://doi.org/10.1080/08958370701402382

Shepard, D., 1968. A two-dimensional interpolation function for irregularly-spaced data, in: Blue, R.B., Rosenberg, A.M. (Eds.), Proceedings of the 1968 23rd ACM National Conference On -. ACM Press, New York, New York, USA, pp. 517–524. https://doi.org/10.1145/800186.810616

Simcom, 2021. Sim28 . URL https://www.simcom.com/product/SIM28.html

Sousan, S., Koehler, K., Hallett, L., Peters, T.M., 2016. Evaluation of the Alphasense Optical Particle Counter (OPC-N2) and the Grimm Portable Aerosol Spectrometer (PAS-1.108). Aerosol Sci Technol 50, 1352–1365. https://doi.org/10.1080/02786826.2016.1232859

Sousan, S., Regmi, S., Park, Y.M., 2021. Laboratory Evaluation of Low-Cost Optical Particle Counters for Environmental and Occupational Exposures. Sensors (Basel) 21. https://doi.org/10.3390/s21124146

Speranza, A., Caggiano, R., Margiotta, S., Summa, V., Trippetta, S., 2016. A clustering approach based on triangular diagram to study the seasonal variability of simultaneous measurements of PM10, PM2.5 and PM1 mass concentration ratios. Arab J Geosci 9. https://doi.org/10.1007/s12517-015-2158-z

Stewart, I.D., Oke, T.R., 2012. Local Climate Zones for Urban Temperature Studies. Bulletin of the American Meteorological Society 93, 1879–1900. https://doi.org/10.1175/BAMS-D-11-00019.1

Tang, G., Zhang, Jinqiang, Zhu, X., Song, T., Münkel, C., Hu, B., Schäfer, K., Liu, Z., Zhang, Junke, Wang, L., Xin, J., Suppan, P., Wang, Y., 2016. Mixing layer height and its implications for air pollution over Beijing, China. Atmos. Chem. Phys. 16, 2459–2475. https://doi.org/10.5194/acp-16-2459-2016

Thermo Fisher Science, 2011. Model 5030i SHARP: Instruction Manual . URL https://tools.thermofisher.com/content/sfs/manuals/EPM-manual-Model%205030i%20SHARP.pdf

Torres-Ramos, Y.D., Montoya-Estrada, A., Guzman-Grenfell, A.M., Mancilla-Ramirez, J., Cardenas-Gonzalez, B., Blanco-Jimenez, S., Sepulveda-Sanchez, J.D., Ramirez-Venegas, A., Hicks, J.J., 2011. Urban PM2.5 induces ROS generation and RBC damage in COPD patients. Front Biosci (Elite Ed) 3, 808–17. https://doi.org/10.2741/e288

Umweltmeteorologie RLP, 2021. URL https://luft.rlp.de/de/umweltmeteorologie/

Wagner, P., Schäfer, K., 2017. Influence of mixing layer height on air pollutant concentrations in an urban street canyon. Urban Climate 22, 64–79. https://doi.org/10.1016/j.uclim.2015.11.001

Wallace, J., Kanaroglou, P., 2009. The effect of temperature inversions on ground-level nitrogen dioxide (NO2) and fine particulate matter (PM2.5) using temperature profiles from the Atmospheric Infrared Sounder (AIRS). Sci Total Environ 407, 5085–95. https://doi.org/10.1016/j.scitotenv.2009.05.050

Walser, A., Sauer, D., Spanu, A., Gasteiger, J., Weinzierl, B., 2017. On the parametrization of optical particle counter response including instrument-induced broadening of size spectra and a self-consistent evaluation of calibration measurements. Atmos. Meas. Tech. 10, 4341–4361. https://doi.org/10.5194/amt-10-4341-2017

WMO, 2018. Low-cost sensors for the measurement of atmospheric composition: overview of topic and future applications.

Xu, G., Jiao, L., Zhang, B., Zhao, S., Yuan, M., Gu, Y., Liu, J., Tang, X., 2017. Spatial and Temporal Variability of the PM2.5/PM10 Ratio in Wuhan, Central China. Aerosol Air Qual. Res. 17, 741–751. https://doi.org/10.4209/aaqr.2016.09.0406

Yue, D.L., Hu, M., Wu, Z.J., Guo, S., Wen, M.T., Nowak, A., Wehner, B., Wiedensohler, A., Takegawa, N., Kondo, Y., Wang, X.S., Li, Y.P., Zeng, L.M., Zhang, Y.H., 2010. Variation of particle number size distributions and chemical compositions at the urban

and downwind regional sites in the Pearl River Delta during summertime pollution episodes. Atmos. Chem. Phys. 10, 9431–9439. https://doi.org/10.5194/acp-10-9431-2010

ZIMEN, 2021a. - Luft-Überwachung in Rheinland-Pfalz -: Zentrales Immissionsmessnetz - ZIMEN - . URL https://luft.rlp.de/de/startseite/

ZIMEN, 2021b. Jahresbericht 2020: Zentrales Immissionsmessnetz - ZIMEN - . URL https://luft.rlp.de/fileadmin/luft/ZIMEN/Jahresberichte/ZIMEN-Jahresbericht_2020.pdf

3.8 Appendix

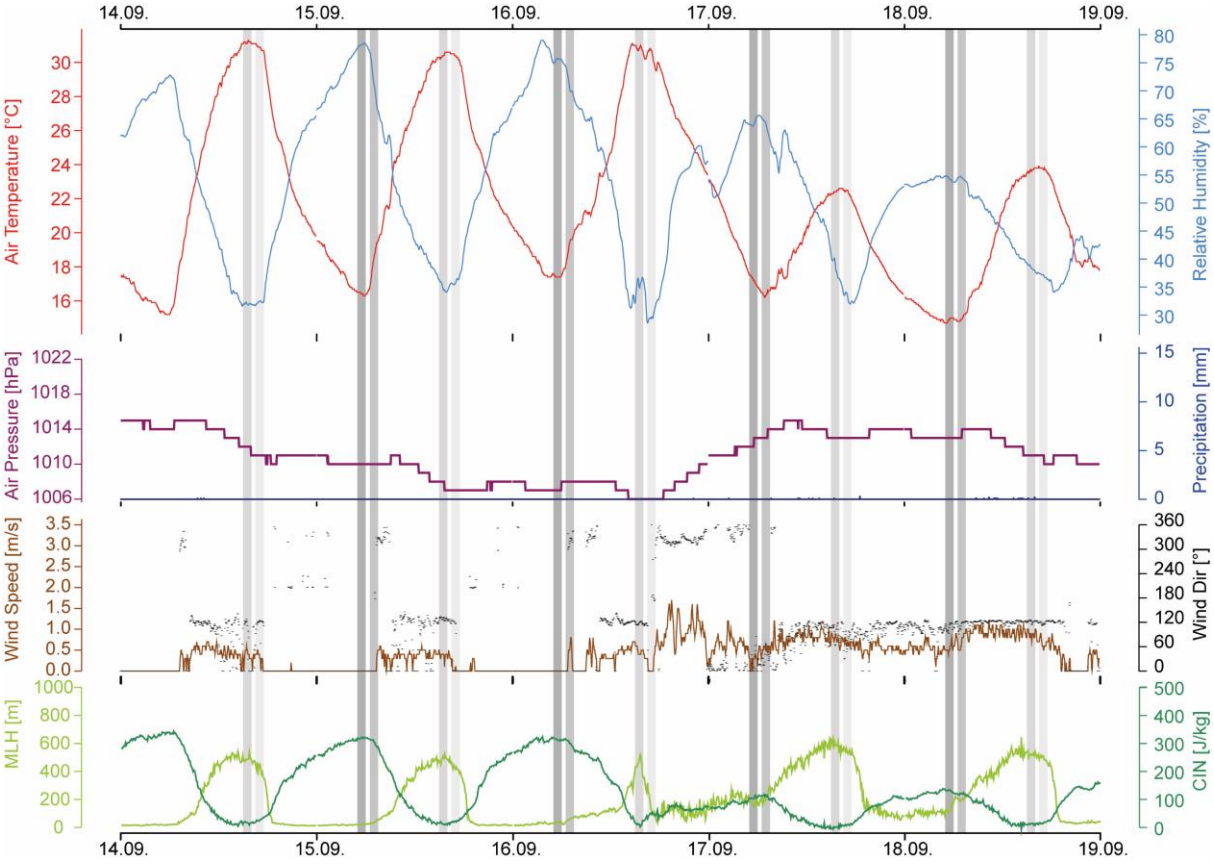

Fig. 3-A1 weather conditions during September measurement period. Grey bars represent daily measurement runs. RH, TA, and air pressure were measured at 2 m a.g.l. at the measurement station Mainz-Zitadelle, wind direction and speed at 10 m a.g.l and precipitation at 2 m a.g.l. at the measurement station Mainz-Mombach. CIN and MLH were measured with a radiometer at the headquarter of the state office for environment in Mainz.

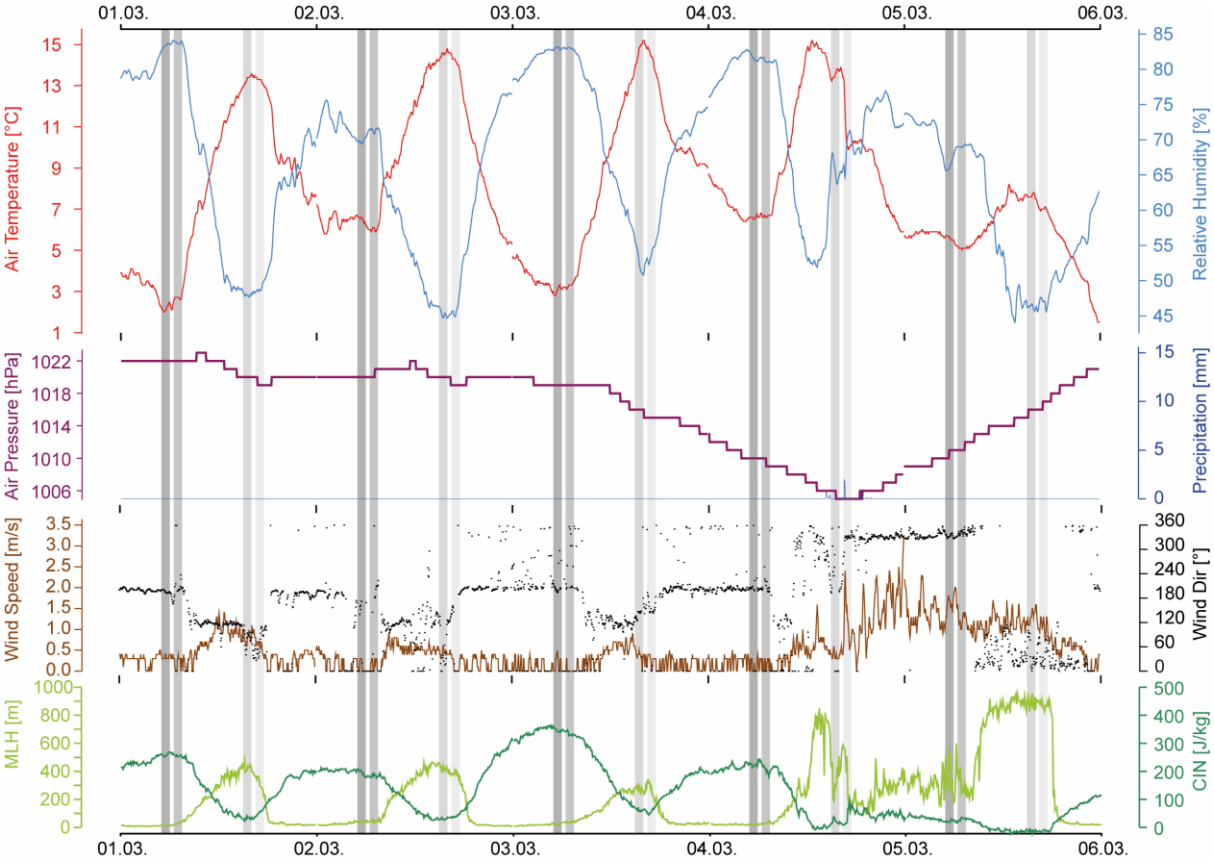

Fig. 3-A2 weather conditions during March measurement period. Grey bars represent daily measurement runs. RH, TA, and air pressure were measured at 2 m a.g.l. at the measurement station Mainz-Zitadelle, wind direction and speed at 10 m a.g.l and precipitation at 2 m a.g.l. at the measurement station Mainz-Mombach. CIN and MLH were measured with a radiometer at the headquarter of the state office for environment in Mainz.

Fig. 3-A3 Pictures of the high polluted areas during the measurement campaigns in September (panels 1-3) and March (panels 4 and 5)

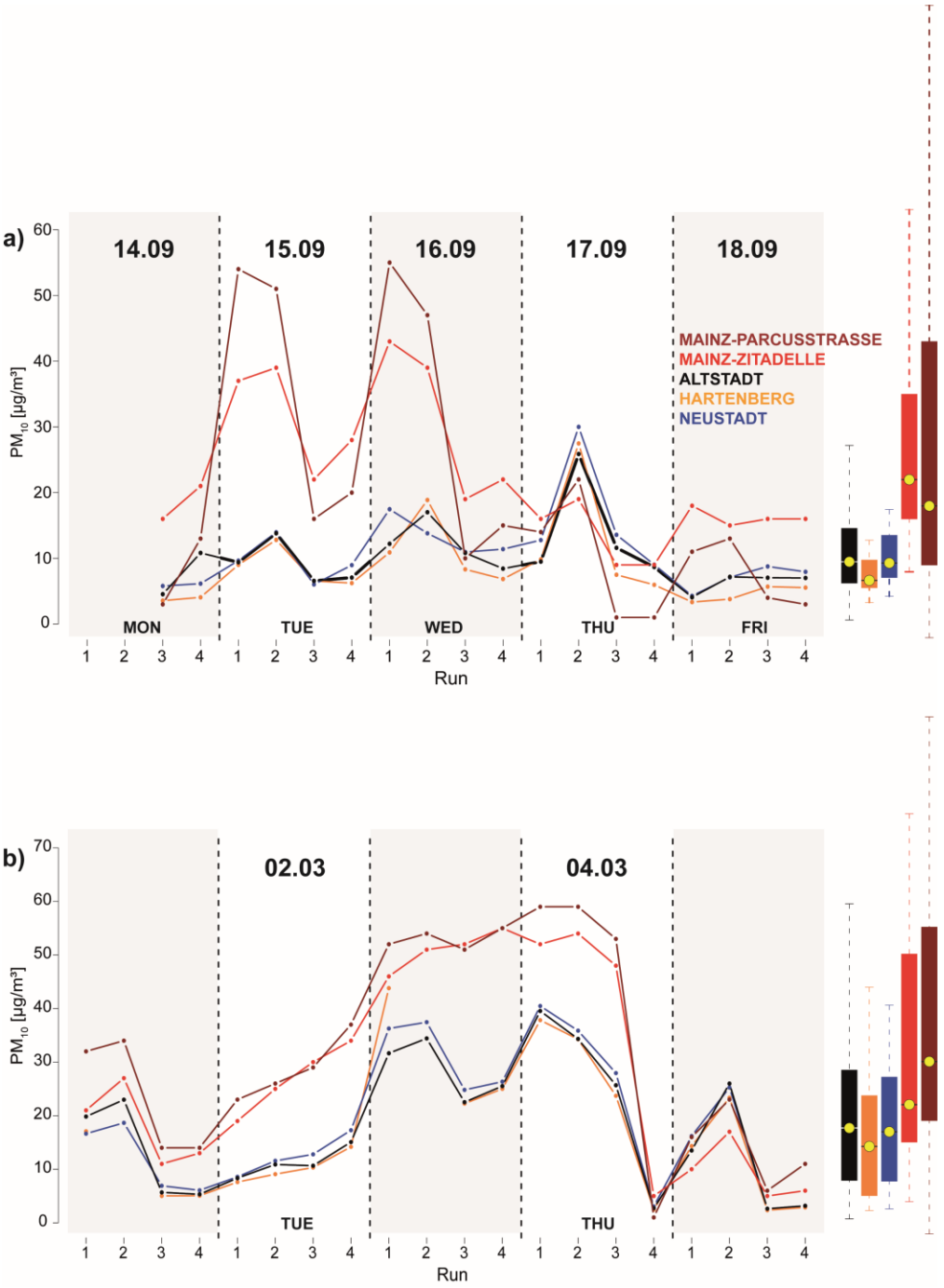

Fig. 3-A4 Mean PM_{10} concentrations in the Altstadt, Hartenberg, Neustadt (black, blue and orange colors) and ZIMEN data from the Mainz-Parcusstraße and Mainz-Zitadelle (dark red and red colors) during the study periods in **a** September and **b** March with according boxplots.

"(Harr et al., 2022).

4 Distribution and attribution of particulate matter in urban environments

Harr Lorenz[1], Tim Sinsel[1], Helge Simon[1], Max Carl Arne Torbenson[1], Esper Jan[1,2]

[1]*Department of Geography, Johannes Gutenberg-University, Johann-Joachim-Becher-Weg 21, 55128 Mainz, Germany*

[2]*Global Change Research Institute of the Czech Academy of Sciences (CzechGlobe), 60300 Brno, Czech Republic*

Summary

The results of Section 3 demonstrate that the Alphasense OPC-N3 low-cost sensors do not provide accurate absolute $PM_{2.5}$ values. Since emission sources can be of inhomogeneous particle D_P as they can be emitted by different processes, e.g. traffic emissions containing of exhaust and various non-exhaust emissions, the low-cost sensors were not able to properly resolve absolute PM for varying particle D_P. The following study shows a new approach to address high spatiotemporal patterns of the distribution and attribution of PNC and concentrations at high, (sub-) micron particle resolution: Mobile measurements were performed using a GRIMM 11-R laser aerosol spectrometer mounted on a mobile cargo bike platform. After comparing the measured PM_1 and PM_{10} with stationary data, the spatial variability of these fractions was analyzed to detect locations of high concentrations. Subsequently, the measured PNC and dM were quantified in submicron resolution and the emission sources at the hotspots were identified along unique source patterns. The author was largely responsible for the conception, methodology, formal analysis as well as for the research and data maintenance. He wrote the manuscript including all figures.

Atmospheric Environment – In Review

4.1 Introduction

Ambient air pollution is identified as one of the major health risks worldwide (WHO, 2022). Air pollutants such as PM cause cardiovascular and respiratory diseases, which can lead to premature deaths (Lelieveld et al., 2019). While PM_{10} – particles with D_P of < 10 µm – is inhalable and reaches in to lungs, fine particles with D_P < 2.5 µm ($PM_{2.5}$) can get to the bronchial system and cause lung disfunction as well as chronic obstructive pulmonary disease (Gualtieri et al., 2011; Torres-Ramos et al., 2011). For these reasons, both particle fractions are regulated by the EU with a permissible annual mean concentration of 20 and 40 µg/m³ for $PM_{2.5}$ and PM_{10}, respectively, as well as with daily thresholds of 50 µg/m³ for PM_{10} which must not be exceeded more than 35 times a year (European Parliament and Council, 2008). Finer particles like PM_1 – particles with D_P < 1 µm – are not regulated, although high PM_1 exposure is even worse than PM_{10} and $PM_{2.5}$: PM_1 can reach deeper into the lungs causing poorer lung functions, cytotoxicity effects and inflammation, particularly affecting children (Jalava et al., 2015; Yang et al., 2020).

In urban environments, the level of PM depends largely on regional background concentrations and local emission sources, including mineral and biogenic components, but also of anthropogenic origins, i.e. domestic heating, industrial fumes and particularly traffic (e.g. Azarmi et al., 2016; Karagulian et al., 2015; Minguillón et al., 2012; Titos et al., 2014). Traffic-related emissions are not of homogenous particle sizes, since they are released by different processes: While combustion exhausts of motorized vehicles mainly emit particles with D_P < 1 µm (Squizzato et al., 2016; Titos et al., 2014), non-exhaust particles – i.e. road wear, (resuspended) road dust as well as tyre and brake abrasion – contribute to dM of particles with D_P 1 – 10 µm (Harrison et al., 2021; Piscitello et al., 2021) with D_P of tyre and brake abrasion mainly ranging between 2 – 5 µm and 1 – 6 µm, respectively (Fussell et al., 2022; Hussein et al., 2008; Oroumiyeh and Zhu, 2021).

A distinction of emission sources by particle size is therefore only possible if the particles were measured in (sub-) micron resolution. Official stationary monitoring networks in Europe, however, were not able to resolve particle sizes in this range since they were providing only PM_{10}, $PM_{2.5}$ and (rarely) PM_1 data according to the legal requirements (European Parliament and Council, 2008). In addition, the immobility of the stations and their temporal measurement resolution of > 30 min averages (ZIMEN, 2022) make it unfeasible to record variations in urban PM concentrations, for example induced by changes in traffic intensity or varying street

characteristics, e.g. between street canyons and open arrangements of buildings (Bukowiecki et al., 2010; Gallagher et al., 2015).

These spatiotemporal gaps can be closed by mobile measurements that allow spatial coverage to be extended both horizontally and vertically, for example to breathing height level of pedestrians. Mobile PM measurements were mainly conducted by foot and bicycle (e.g. Carreras et al., 2020; Garcia-Algar et al., 2015; Harr et al., 2022a; Sharma and Kumar, 2020). While studies by foot only allow high spatiotemporal measurements in short time intervals (> 1s) along a max. 5 km long track within an hour (Harr et al., 2022b), measurements by bike give the possibility to cover a larger area at the same time, e.g. areas of different characteristics like urban, suburban, and rural within the same run.

The main objective of this study is to analyze the spatiotemporal variability of high-resolution PM to determine its emission sources in an urban environment. We (i) compare measured PM_1 and PM_{10} with stationary data, (ii) analyze their spatial variability to identify hotspots, (iii) quantify the measured PNC and dM per D_P, and (iv) discuss the relative differences per D_P to identify emission sources at the hotspots.

4.2 Material and methods

4.2.1 Study Site

The measurements were conducted from 28th May to 5th August 2021 in Mainz, the capital and largest city (approx. 220,000 inhabitants) of the southwestern German federal state Rhineland-Palatinate (50.0 °N, 8.26 °E, Fig. 4-1). Mainz is an inland town located in a gently hilly landscape along the River Rhine, which features a moderate climate with an annual average TA of 10.7 °C and precipitation of 620 mm (Koeppen Cfb; Deutscher Wetterdienst, 2021a, 2021b). The city's basin location hinders large-scale air exchange and results in Mainz being one of the most polluted cities in Germany (ZIMEN, 2021a). The 14 km long, circular study route led on paved roads through areas of different characteristics: While the starting and ending point at the campus of the university (49.9932 °N, 8.242 °E; Fig. 4-1 (1)) was characterized by large low-rise buildings and low traffic, the route passed streets with predominantly compact midrise buildings and multi-lane roads of high traffic intensity in the city center (Fig. 4-1 (2,3)). The route exited downtown via the steep and narrow, three-stories high street canyon ‘Gaustraße’ (< 10 m wide, building-height-to-width ratio ~1) (Fig. 4-1 (4)) onto the high traffic multi-lane road ‘Pariser Straße’ leading out of town (Stewart and Oke, 2012; Fig. 4-1 (6)). At the town

sign, the route continued through a suburban area with low-rise buildings and low traffic followed by an agricultural area in the west of the city (Fig. 4-1 (7)), before returning to the starting/ending point at the campus. We conducted two measurement runs every day starting at 7:30 am and 4:30 pm to cover MO and AF rush hour times.

Fig. 4-1 Bicycle track in Mainz (black line) with photographs from the starting and ending point at the university (**1**), the Kaiserstraße (**2**), Rheinallee (**3**), Gaustraße (**4**), Fichteplatz (**5**), Pariser Straße (**6**) and agricultural area (**7**). The monitoring sites at Mainz-Zitadelle and Friedrichsfeld are highlighted by black dots. Insert map shows the location of Mainz (orange) in Germany. © OpenStreetMap

The mobile measurements were conducted with a full-suspension electro cargo bike. The electric assistance allowed measurements to be made at a constant, average speed of 17 km/h and the suspension avoided vibrations which could interfere with the measurements. The bike was equipped with a GPS device powered by an USB-Powerbank and a camera with which each run was filmed to facilitate the identification of local emitters during the post analysis process (Fig. 4-2). As PM sensor, a GRIMM 11-R laser aerosol spectrometer was mounted in a box on the cargo platform, with the front orientated air inlet at a height of 1.6 m, corresponding to the average breathing height of adults. The GRIMM 11-R is an optical particle counter

following the light scatter principle (Mie, 1908) and is able to count particle sizes from 0.25 µm to 32 µm with 31 size bins in high temporal resolution of 6 s (GRIMM Aerosol Technik GmbH & Co. KG, 2015). The instrument is calibrated by the manufacturer to a filter-based reference instrument (Peters et al., 2006). As the GRIMM 11-R is intended for indoor use, it should only be used at RH < 95% and under precipitation-free conditions, as condensation could significantly damage the unit's optical chamber.

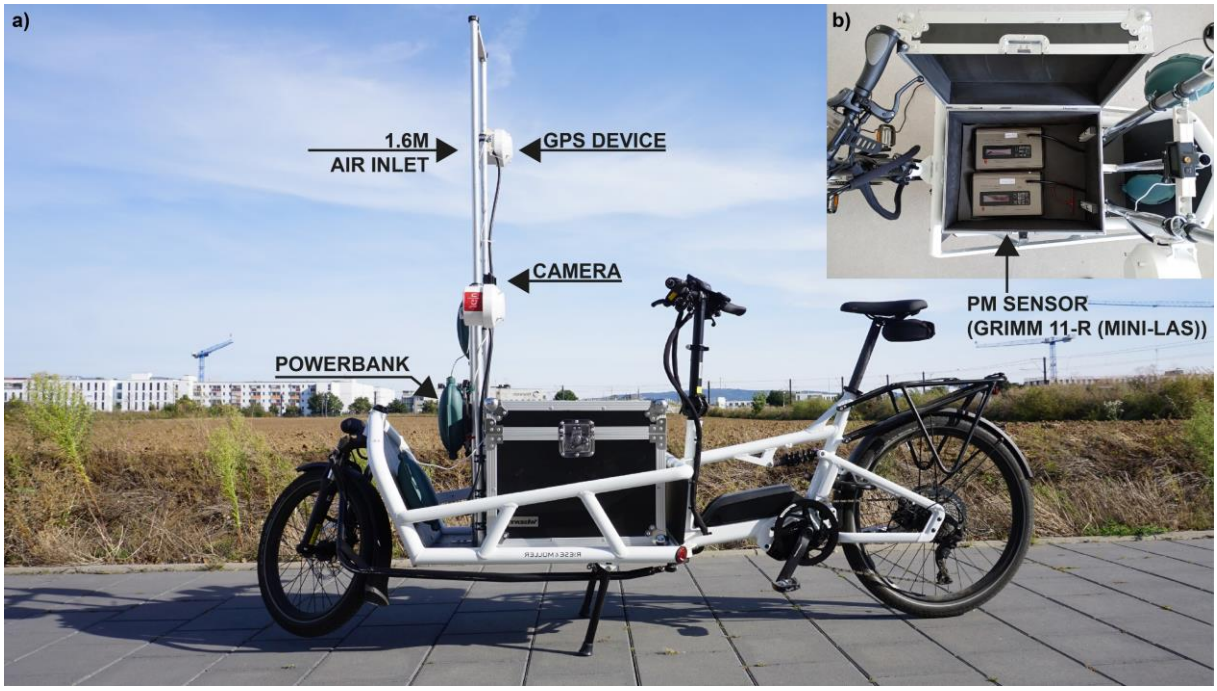

Fig. 4-2 Photographs of the electro cargo bike with GPS device, powerbank, camera (**a**) and the box containing PM sensors, GRIMM 11-R PM sensors (**b**).

4.2.2 Post-processing analysis

Several post-processing steps had to be conducted to enable a reliable spatial analysis of each run's measurement. At first, the GRIMM measurements were merged with the GPS data. To avoid slight spatial inaccuracies and minor variations between the runs, a spatial synchronization to a manually set ideal route was applied. An ideal route was converted into datapoints with a distance of 10 m and assigned the 10 closest original measurement points to each point using inverse distance weighting (Shepard, 1968). The PM data were subsequently linearly detrended to mitigate potential time-related changes in particle concentrations along the study route (Harr et al., 2022a). The differences between MO and AF concentrations in PM_1 and PM_{10} were tested on significance using a Monte Carlo simulation approach in which for

1000 iterations 100 AF and MO datapoints were randomly taken to calculate paired Mann-Whitney U tests. We then calculated the QCD to quantify the variation of particle concentrations along the study route, since this measure of variation is less sensitive to outliers than the commonly used CV (Bonett, 2006).

To specify the particle distribution of the PNC and dM of the mean MO and AF runs, the standard PM categories of PM_1, $PM_{2.5}$, and PM_{10} were considered too imprecise. We hence focused on the originally measured PNC and dM instead, which is divided into 31 D_P bins ranging from < 0.25 µm to 32 µm (GRIMM Aerosol Technik GmbH & Co. KG, 2015). These datasets were then used to calculate median PNC and dM for each particle D_P category at each datapoint along the study route for the average of all MO and AF runs, respectively. A normalization of the dM data was performed with dM/dlog (D_P) to reduce possible bias in the D_P masses due to unequal bin widths at each point on the track. Finally, relative differences between dM and dM_{MEDIAN} of each D_P were calculated to indicate the relative particle distribution for each particle bin size along the study route.

4.3 Results and Discussion

4.3.1 Mean PM_1 and PM_{10}

During the study period, 97 of 140 possible measurement runs (50 MO and 47 AF runs) could be conducted, 43 measurement runs were omitted due to unstable weather (Fig. 4-A1). These unsteady weather conditions – precipitation was 27% higher than in the reference period 1991-2020 (DWD, 2022) – led to cleaner air with relatively low particle concentrations overall: There was no run in which mean PM_{10} exceeded the daily threshold of 50 µg/m³ stated in the European law (European Parliament and Council, 2008). Nonetheless, the median PM_1 and PM_{10} concentrations recorded with the cargo bike were in line with the measurements at the stationary monitoring station Mainz-Zitadelle, provided by the ZIMEN network (ZIMEN, 2022; Fig. 3). The absolute differences between mobile and stationary measurements, however, were higher in PM_{10} ($mean_{DIFF\_PM10}$ = 1.3 µg/m³; sd_{DIFF_PM10} = 4.9 µg/m³) than in PM_1 ($mean_{DIFF\_PM1}$ = 0.7 µg/m³; sd_{DIFF_PM1} = 1.3 µg/m³). The differing concentration levels could be caused by coarse particles emitted in the various local environments along the study route, e.g. road dust in the city vs. resuspended natural dust at the agricultural field (Kerschbaumer and Lutz, 2008). The comparison of mobile and stationary measurements underlines the feasibility

of collecting reliable PM data with our mobile measurement setup by bike using GRIMM 11-R in urban environments.

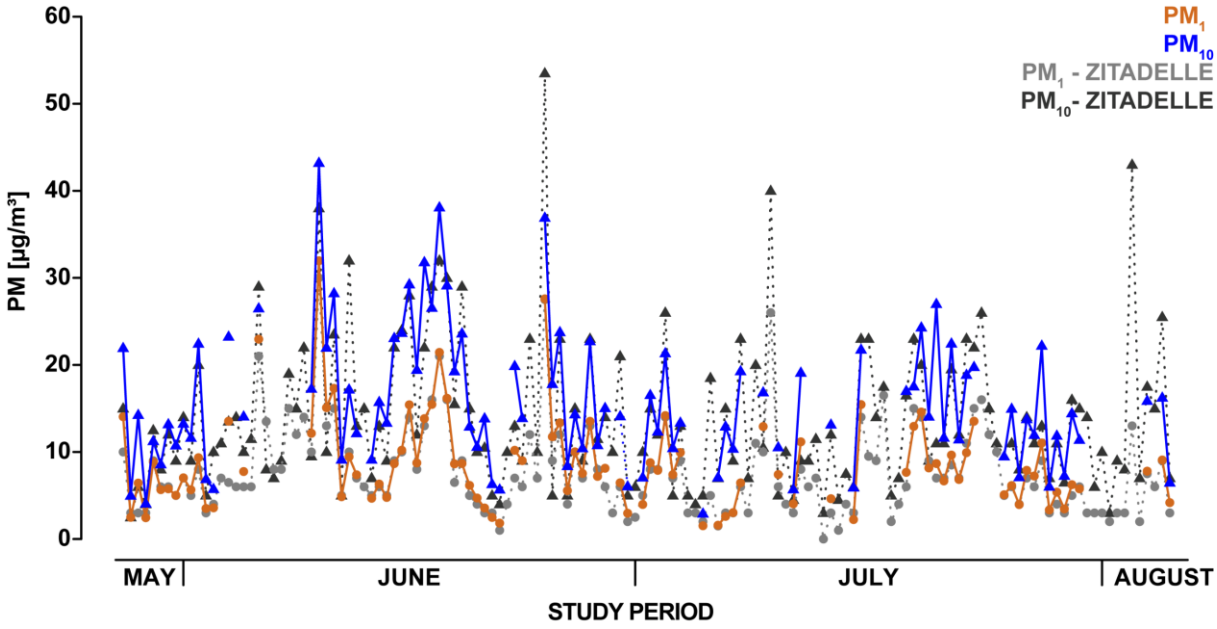

Fig. 4-3 Median PM_1 and PM_{10} concentrations from May–August 2021 recorded with the cargo bike and derived from the official ZIMEN measurement station at Mainz-Zitadelle, respectively.

4.3.2 Spatial pattern of PM_1 and PM_{10}

The spatial pattern of mean PM_1 and PM_{10} along the study track showed higher concentrations in the city than in the suburban and agricultural area (Fig. 4-4a). However, these differences were rather small for PM_1, as absolute differences were only 1.5 µg/m³ (13%) between 'Rheinallee' (Fig. 4-1 (4)) – a high traffic location with the highest mean values – and the traffic-calmed university campus (Fig. 4-1 (1)). For PM_{10}, the difference between the highest concentrations, 'Gaustraße' (Fig. 4-1 (4)), and the lowest, also university campus, was 6.3 µg/m³, meaning a relative difference of 31%. It is evident that the concentrations of both PM_1 and PM_{10} were significantly higher in the MO than in the AF, regardless of the location along the route (Fig. 4-4 b). The mean differences between MO and AF were 3.7 µg/m³ (~54%) for PM_1 and 7.7 µg/m³ (~62%) for PM_{10}, whereas the PM_1/PM_{10} ratio rose from 53% to 58% on average. The relative differences of PM_1 and PM_{10} during the day were very similar and could be explained by the average atmospheric conditions. During the night, high CIN values and low windspeeds indicate low, stable MLH leading to higher suspension of particles near ground. During the day, solar forcing in combination with diurnal TA differences of > 10 K led to fast dissolving of the stable MLH by thermal convection which in turn caused lower PM concentrations for the AF runs (Tang et al., 2016, Wagner and Schäfer, 2017; Fig. 4-A1).

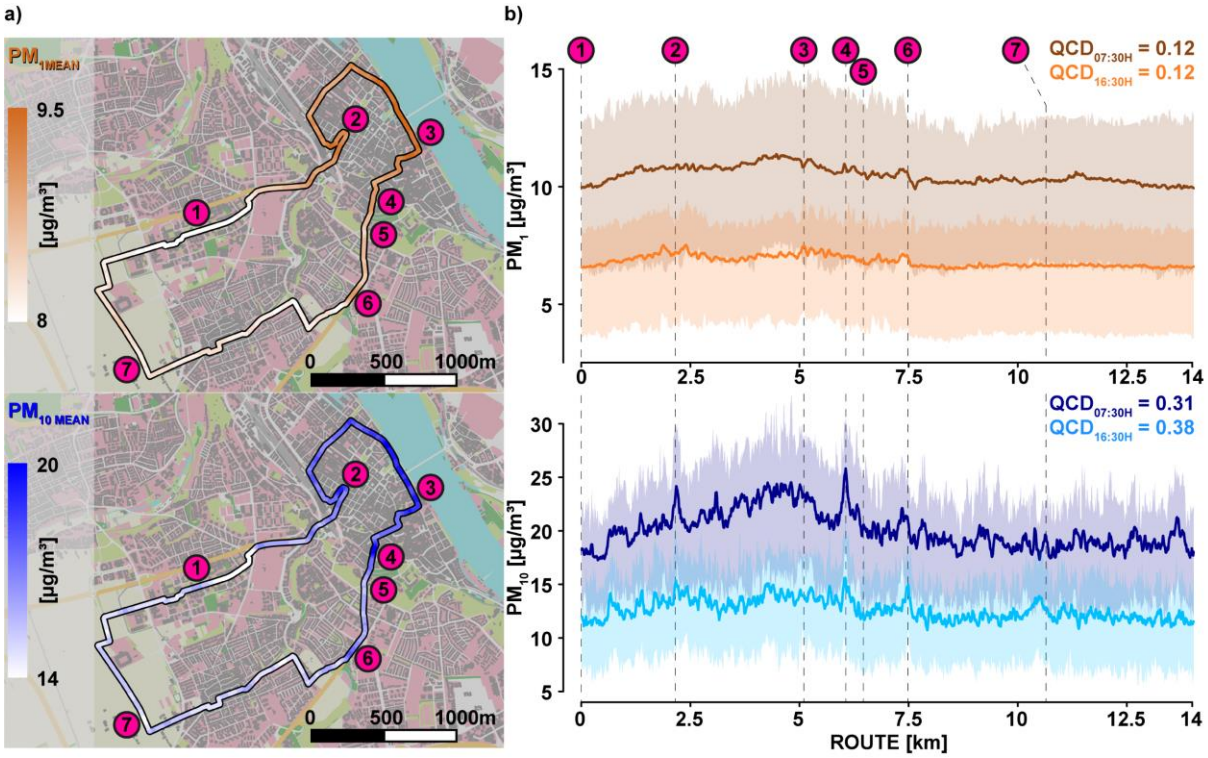

Fig. 4-4 Spatial patterns of mean PM_1 (brown) and PM_{10} (blue) concentrations along the study track (**a**) , and (**b**) subdivided into mean MO and AF timeseries (light and dark colors, respectively). Bold curves are smoothing splines (df = 35, n = 1403) surrounded by the IQR in shaded colors.

Nonetheless, the variation of PM_1 was only 12%, resulting in small differences in concentrations along the route with no clear local hotspot in the mean MO and AF runs. In contrast, the variation of PM_{10} is larger along the study track, whereby the QCD is higher in AF than in MO (0.38 to 0.31). Moreover, three local PM_{10} hotspots could be additionally identified for both times of the day, the 'Kaiserstraße', the 'Gaustraße' and the 'Pariser Straße' (Fig. 4-1 (2,4,6)) and another one close to a farm house in the agricultural fields (10.4 km) in AF. These hotspots become even more visible during mean MO runs, where PM_{10} showed differences of > 2 µg/m³ between hotspot and surrounding streets, with a maximum value of 5.7 µg/m³ at the 'Gaustraße'.

4.3.3 Particle number concentrations per D_P

The differences in variation between PM_1 and PM_{10} indicate that PM_{10} hotspots were mainly caused by particles larger than PM_1. However, the PNC per originally measured D_P bin of the sensor showed that, regardless of the time of the day and the position on the measurement track, most particles were assigned to the smallest D_P (Fig. 4-5). PNC decreased sharply with

increasing D_P. PNC with D_P < 0.25 µm, for instance, reached up to ~600,000 counts per cm³, whereas PNC for the largest bin with continuously measured PM, D_P of 4–5 µm, was around 100 particles per cm³. Consequently, particles with D_P of < 1 µm account for < 58% of the PM_{10}. PNC with D_P of < 0.25 µm is even more than 2000 times higher than PNC with D_P of 3.5–4 µm and even 6000 times higher than PNC with D_P of 4–5 µm. The consideration of particle mass is hence probably not sufficient to describe the health hazards of especially small particles in a meaningful way (Schraufnagel, 2020).

An average of 191,501,376 particles (MO) was counted in comparison to a mean of 112,013,837 particles (AF), meaning that PNC was 71% higher in MO than in AF. This difference was even 9% higher than between the PM_{10} concentrations of the MO and AF runs, which could not be explained by additional particles with D_P > 10 µm. It is more likely caused by uncertainties in the weighting process of the counted particle D_P before calculating their dM (Morawska et al., 1999).

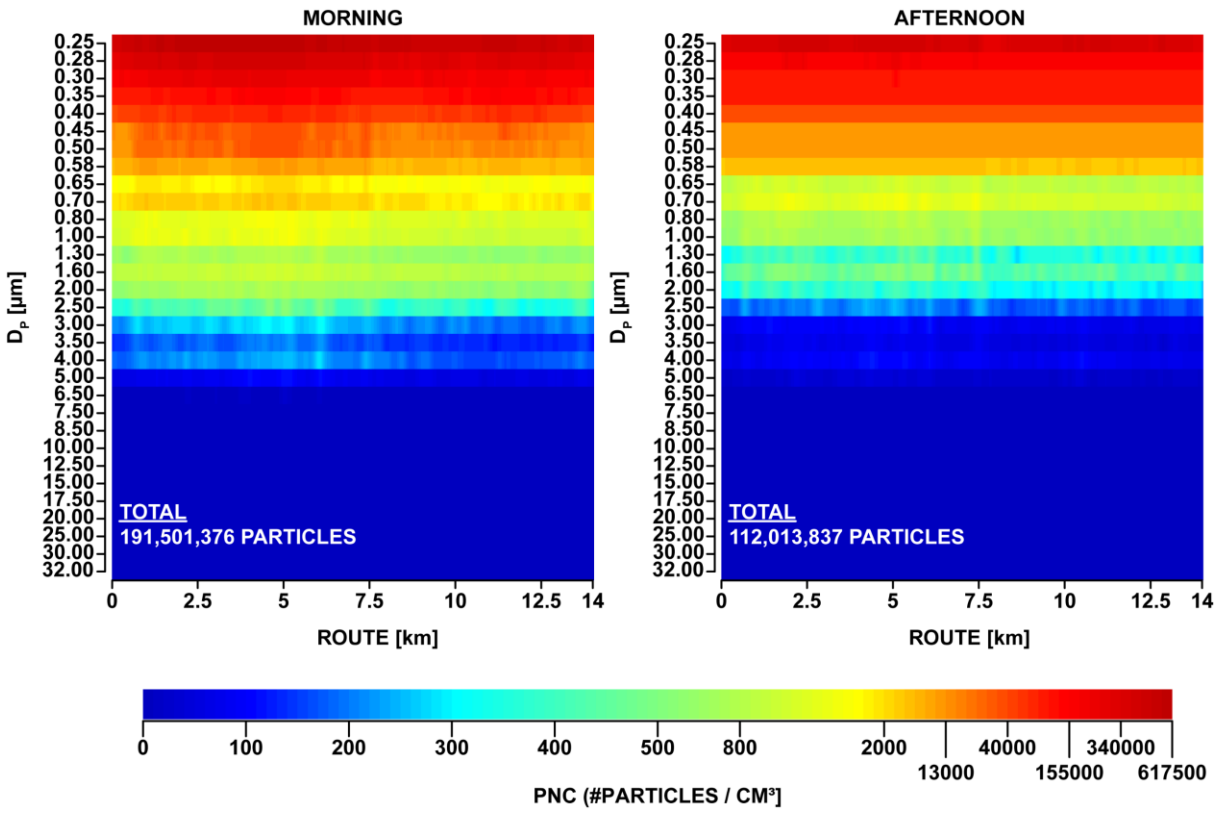

Fig. 4-5 Median PNC distributions for each bin along the study route in MO (left) and AF (right panel). Labels of the y-axes show the upper limit of the D_P per bin.

4.3.4 Median mass concentrations per D_P

The distribution of particle D_P along measured dM differed greatly from the distribution of particle counts showing that particles at D_P of 0.22–0.25 µm and 3.5–5 µm were dominating the total dM, independently of the time of the day as well as the position on the route (Fig. 4-6a). In the averaged AF run, the dM for particles of 3.5–4 µm size ranged between 0.5–0.6 µg/m³ and 0.5–1 µg/m³, respectively, with hotspots in urban (max. 1 µg/m³; ~4.5 km) and agricultural (max. 0.9 µg/m³; ~11 km) areas. The averaged MO run showed higher dM values with 0.8-1 µg/m³ for the smallest D_P and 1.2–2.3 µg/m³ for D_P 3.5–4 µm, with highest values in the street canyon 'Gaustraße' (Fig. 4-1 (3)). In contrast, particles with sizes of 0.35–1.3 µm contributed only by a maximum of 0.4 µg/m³ per D_P (MO) and only by 0.2 µg/m³ per D_P (AF) to the total dM of the runs – particles with D_P 0.65 µm only by 0.05 µg/m³ for both times of the day. Moreover, the measured median dM shows a skewed picture of the particle mass distribution since the D_P bins were not of equal width. This could cause an overestimation of the dM of large D_P, because the larger the D_P, the wider the bins and the higher the possibility of more particles in each bin. To reduce the biases, we calculated the 'normalized dM' (ndM) for every D_P (Fig. 4-6b).

Particles with D_P < 0.3 µm showed still high ndM with > 15.5 µg/m³ (MO) on average per D_P and > 9.5 µg/m³ (AF), whereas particles with D_P of 0.28–0.3 µm had higher values than particles of D_P 0.22–0.25 µm with 23.2 to 16.3 µg/m³ (MO) and 12.1 to 10.5 µg/m³ (AF). The small particle bins of D_P < 0.3 µm contributed with > 9% per D_P to the total ndM and were only exceeded by particles with D_P 3.5–4 µm having 27.6 µg/m³ and 12.0 µg/m³ on average, hence accounting with 16.3% and 14.4% (Fig. 4-A2). Although particles with sizes between 0.35-1.3 µm accounted for maximum ndM values of 5.2 µg/m³ (MO) and 2.6 µg/m³ (AF) per D_P on average, respectively, they contributed only by 3% per D_P at both times of the day and thus did not have a major impact on the total ndM.

The distinct bimodal distributions in dM and ndM with peaks at D_P 0.28–0.3 µm and D_P 3.5-4 µm indicate different kinds of emissions: Particles with size of D_P < 0.3 µm originate from whirled-up road and mineral dust, and – in urban areas – from combustion-related processes, i.e. traffic exhausts (Karagulian et al., 2015; Squizzato et al., 2016). The peak in D_P 3.5–4 µm point to (resuspended) road and mineral dust as particle origins, whereas mineral dust could be an integral part of the background concentration (Hussein et al., 2008; Titos et al., 2014).

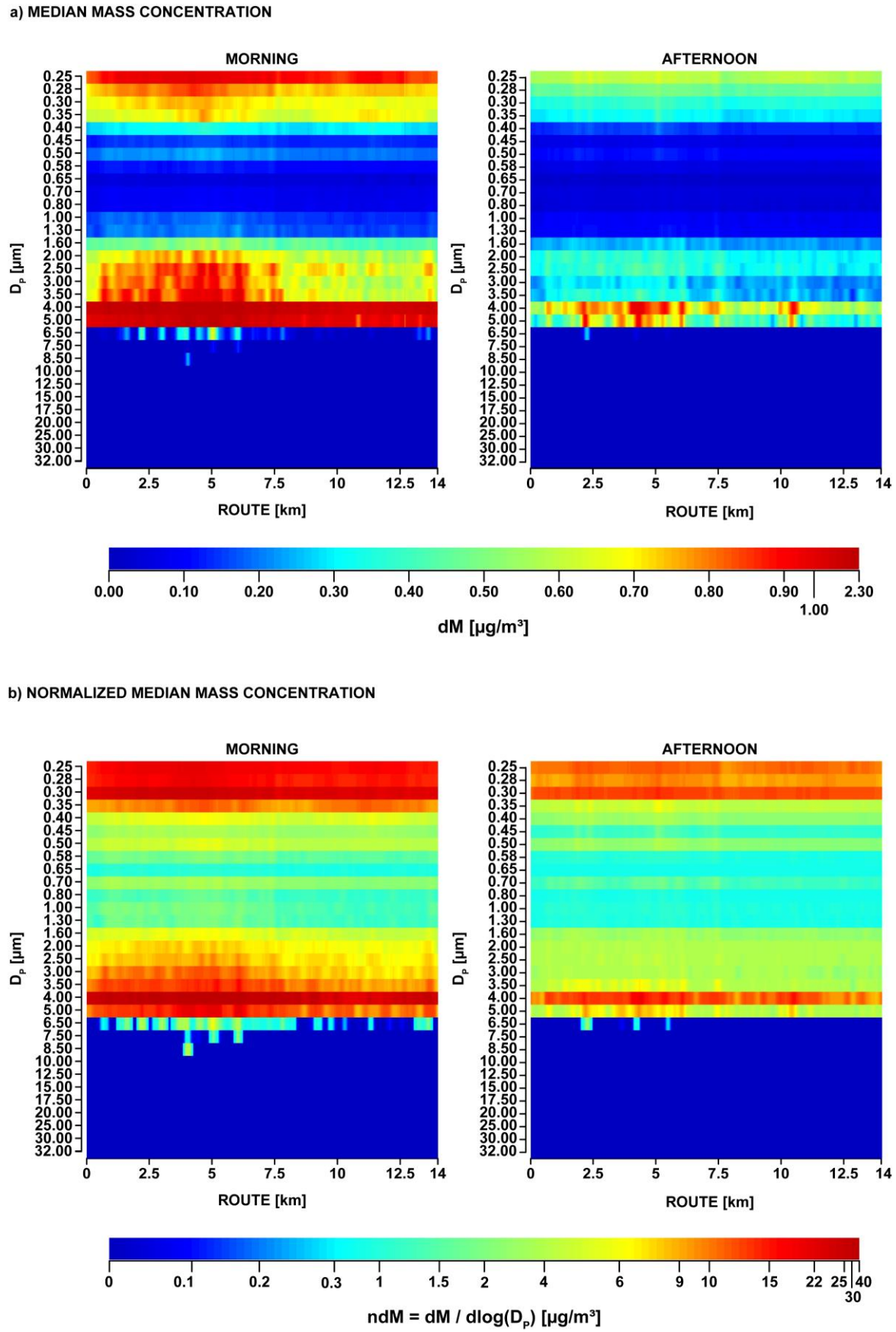

Fig. 4-6 Distribution of (**a**) median dM and (**b**) ndM per D_P along the study route in the MO (left) and AF (right panel). Labels of the y-axes show the upper limit of the D_P per bin.

According to Oroumiyeh and Zhu (2021), the main source of urban road dust could be locally emitted brake and tyre abrasion, as they have found out that brake and tyre wear have unimodal mass size distributions with a mode D_P of 3–4 µm and 4–5 µm, respectively. Studies by Sanders et al. (2003) and Lough et al. (2005) support the findings about the main size distribution of brake-related particles.

4.3.5 Relative differences per D_P

In order to indicate the spatial origin of the measured particles more clearly, we analyzed the relative differences of dM per D_P along the route (Fig. 4-7). The relative differences between dM and dM_{MEAN} per D_P showed distinct higher values in the urban (1–7.5 km) than in the suburban and agricultural areas for all continuously measured D_P. For D_P < 1 µm, the concentrations were on average 13% (MO) and 14% higher (AF). The higher dM in the city could be attributed to locally emitted, traffic-related combustion processes and whirled-up road wear in the inner city which were largely absent in the suburban and agricultural areas. This hypothesis is in line with findings by Titos et al. (2014) showing that 16% of the total PM_1 concentrations at an urban station in southern Spain in summer were related to road dust and traffic exhaust, while the background concentration consisted of mineral dust (21%) and mainly of regionally transported, resuspended dust (63%). It is noticeable that the relative differences in the urban area were increasing with increasing D_P. While for D_P 0.22–0.25 µm, the concentrations were 8% (MO) and 5% (AF) higher in the urban than rural areas on average, the difference of particles with D_P 3–5 µm, mode D_P of tyre and brake abrasion, increased to 30%, at the ‘Rheinallee’ (3.7–5.1 km; Fig. 4-1 (3)) for particles with D_P 4–5 µm even to 55% (MO) and 70% (AF). This discrepancy between dM in the city and dM in the more rural areas indicated a decreasing large-scale mixing with increasing size of the emitted particles. This behavior can be traced back to a shorter suspension time of coarser particles in the ambient air due to faster deposition. Wu et al. (2018) found out that the velocity of dry deposition in summer for PM_{10} (3.19 ± 1.18 cm/s) was nearly ten times higher compared to $PM_{2.5}$ (0.32 ± 0.33 cm/s) on average (i.e., the larger the measured particles, the more likely they have been emitted in the vicinity of the respective measurement).

Our findings also agree with the results of Carreras et al. (2020), who stated in their study with mobile measurements of particle mass and number concentrations by bike, that long-range transported particles dominated the dM for $PM_{2.5}$, but local emissions were an important factor for coarse PNC concentrations with larger D_P. For the hotspot at the agricultural field (10.4 km)

in AF runs, the relative differences for D_P > 3 µm were elevated by 20% compared to the dM_{MEDIAN}, indicating local emissions. In lack of motorized road traffic and as there were no other increased differences in smaller D_P, it is likely that the particles originated from locally whirled up natural dust from the surrounding fields. Considering the other identified hotspots at 'Kaiserstraße', 'Rheinallee', 'Gaustraße' and 'Pariser Straße' (see 4.3.2; Fig. 4-7 (2)–(4), (6)), the > 17% higher relative differences of particles with D_P > 3 µm indicated that these particles have likely been locally emitted. Since concentrations were elevated across most D_P at these sites, it stands to reason that the particles were emitted from multiple sources at the same time or, more likely, from one source that emits particles with several D_P. In urban areas, this one source is traffic: Road wear and combustion processes of vehicles have an impact on particle concentrations of D_P < 1 µm (Titos et al., 2014), while (resuspended) road dust can also contribute to concentrations of particles with D_P > 1 µm (Fussell et al., 2022), predominantly at D_P 3–5 µm due to brake and tyre abrasion (Hussein et al., 2008; Oroumiyeh and Zhu, 2021).

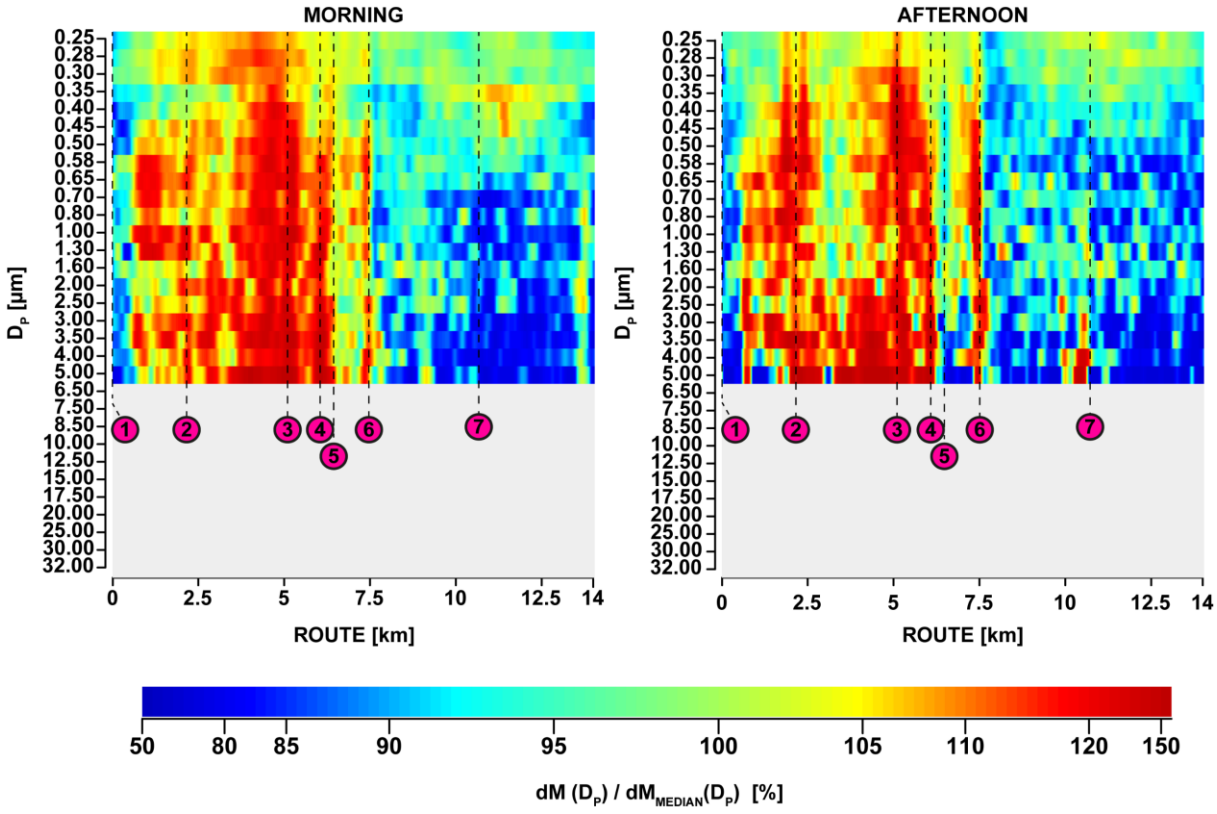

Fig. 4-7 Relative differences between dM and dM_{MEDIAN} for each continuously measured D_P bin along the study route in the MO (left) and AF (right panel). Labels of the y-axes show the upper limit of the D_P per bin. Dots and dashed lines refer to locations highlighted in **Fig. 4-1**.

The patterns of the relative differences surrounding the hotspots support this hypothesis: While the relative differences were high on the entire, highly frequented, four-lane roads ‘Kaiserstraße’ (1.7–2.3 km) and ‘Rheinallee’ (3.7–5.1 km), the relative differences decreased greatly after the ‘Gaustraße’ and the ‘Pariser Straße’, which could be explained by the characteristics of the respective locations. At ‘Pariser Straße’ hotspot, the speed limit on the four-lane road is changed from 50 to 70 km/h for out-of-town traffic lanes, which leads to an acceleration of vehicles causing an increase in traffic exhaust and whirled up road dust on the one hand as well as increased braking on the opposite lanes on the other hand. This resulted in a rise in particle concentrations in each D_P, especially in $D_P > 3$ µm with relative differences of 113% (MO) and 124% (AF) on average. The differences at each D_P decreased abruptly > 20% as the bike lane leads away from the street into a suburban part of the town. The characteristics of the ‘Gaustraße’, however, are different. The ‘Gaustraße’ (5.9–6.4 km) is a short but steeply ascending road that is demanding for vehicles, leading to a higher amount of exhaust and brake abrasion particles. These particles accumulated due to the additional canyon effect in the street, as the surrounding buildings obstruct the air flow to disperse PM (Gallagher et al., 2015). This in turn resulted in up to 51% higher concentrations (MO) and even 61% (AF) for D_P 4–5 µm in ‘Gaustraße’. The relative differences for particles of the same D_P decreased rapidly by 46% (MO) and 72% (AF) on average after leaving the street canyon and entering the ‘Fichteplatz’ (Fig. 4-1 (5)), an open place with scrubs and trees between the traffic and bike lane that reduces the impact of motorized traffic on the measurements. The more pronounced differences in AF occurred not only at ‘Gaustraße’ and ‘Pariser Straße’, but also at the other urban hotspots, which could be attributed to the generally lower concentration level with a higher diffusivity due to more solar forcing in AF (Tang et al., 2016; Wagner and Schäfer, 2017).

The dominance of traffic-related particle sources as local emissions in urban environments are not unexpected, but only the spatiotemporal high-resolution analysis of PM gave the possibility to attribute emissions from different processes to the same emission source, mainly tyre and brake abrasion and fuel combustion from traffic. This analysis can be particularly relevant since electric vehicles become a serious alternative to internal combustion engine vehicles in urban environments (e.g. Ding et al., 2017; Sanguesa et al., 2021; Yong et al., 2015). Assuming an increasing proportion of electric vehicles, emission from combustion-related particles with $D_P < 1$ µm would be reduced to a minimum, which could lead to a reduction of up to 14% for total PM concentrations in urban areas. However, particle emissions by tyre and brake abrasion would still be present (Timmers and Achten, 2016; Woo et al., 2022), which means that the

30% higher particle concentrations in urban compared to rural areas at D_P 3–5 µm will not decrease by banning fossil-fueled vehicles alone. In order to additionally minimize these PM concentrations, it would hence be required to reduce the total number of vehicles in the city, i.e., reducing private transport and increasing the use of local public transport. Nonetheless, it is important to note that measurements of PNC and dM of particles alone could not prove the emission source beyond doubt, even though traffic is very likely one of the main PM sources in the city. It is also not possible to clearly distinguish between road dust and tyre and brake abrasion of the same size (Bukowiecki et al., 2010). We therefore recommend measuring the chemical composition of the particles in addition to the PNC and dM in further studies.

4.4 Conclusion

In this study, it was demonstrated that high-resolution spatiotemporal analyzes of PNC and dM in urban environments are feasible using a mobile measurement setup and produce values comparable to the fixed-station ZIMEN network. Mean PM_1 and PM_{10} concentrations were higher in the urban than in the suburban and agricultural areas. Regardless of the unsteady weather conditions during the study period, PM concentrations were significantly higher in MO than in AF for both particle sizes. Whereas the PM_1 variability is somewhat reduced and shows no clear local hotspot, PM_{10} variability is larger and can be used to identify pollution hotspot, three of which located at urban multi-lane roads and street canyons and one in the agricultural area. The numbers of particles per classified D_P bin, however, showed that the PNC decreased greatly with increasing D_P. This finding is independent of the location and time of the day, and PNC were ~6000 times higher at 0.22–0.25 µm compared to 4–5 µm. Particles with $D_P < 0.3$ µm and 3–5 µm were vastly dominating, representing 33 and 24%, of the total dM, respectively. Higher dM in both of these D_P ranges indicate that the particles were likely emitted from traffic-related combustion processes ($D_P < 1$ µm) and tyre and brake abrasion (D_P 3-5 µm). In contrast, the AF hotspot in the agricultural area showed a relative increase of 20% at $D_P > 3$ µm indicating natural dust from the fields as the main source. These might be relevant for traffic planning as the transition from fossil-fueled to electric vehicles in urban areas can reduce the PNC for $D_P < 1$ µm significantly and the dM would decrease up to 14%. However, tyre and brake emissions would still be present and harmful particularly in street canyons and roads with high traffic intensity. A reduction of the total number of vehicles and increase of public transport would seemingly help to limit PM emissions at all particle sizes.

We strongly recommend extending high-resolution spatiotemporal analyzes of particle distributions per measured D_P bin in urban environments in the future. These analyzes provide a deeper insight into the variability of PNC and particle concentrations than the commonly observed fractions of PM_1, $PM_{2.5}$, or PM_{10}. They reveal patterns from different emission processes to indicate emission sources which facilitates more effective urban transport planning and eventually a reduction of fine particulate pollution for urban citizens.

4.5 Acknowledgements

We thank the environmental state office of Rhineland-Palatinate for providing data of the official ZIMEN meteorological measurement station Mainz-Zitadelle. We are also grateful to the members of the climatology working group at the Department of Geography of the Johannes Gutenberg university of Mainz for supporting the measurements by bike.

4.6 Funding

Jan Esper received support from the Gutenberg Research College, SustES (CZ.02.1.01/0.0/0.0/16_019/0000797), and ERC (AdG 882727).

4.7 References

Azarmi, F., Kumar, P., Marsh, D., Fuller, G., 2016. Assessment of the long-term impacts of PM10 and PM2.5 particles from construction works on surrounding areas. Environmental science. Processes & impacts 18 (2), 208–221. doi:10.1039/c5em00549c.

Bonett, D.G., 2006. Confidence interval for a coefficient of quartile variation. Computational Statistics & Data Analysis 50 (11), 2953–2957. doi:10.1016/j.csda.2005.05.007.

Bukowiecki, N., Lienemann, P., Hill, M., Furger, M., Richard, A., Amato, F., Prévôt, A., Baltensperger, U., Buchmann, B., Gehrig, R., 2010. PM10 emission factors for non-exhaust particles generated by road traffic in an urban street canyon and along a freeway in Switzerland. Atmospheric Environment 44 (19), 2330–2340. doi:10.1016/j.atmosenv.2010.03.039.

Carreras, H., Ehrnsperger, L., Klemm, O., Paas, B., 2020. Cyclists' exposure to air pollution: in situ evaluation with a cargo bike platform. Environmental monitoring and assessment 192 (7), 470. doi:10.1007/s10661-020-08443-7.

Ding, N., Prasad, K., Lie, T.T., 2017. The electric vehicle: a review. Int. J. Electr. Hybrid Veh. 9, 49. https://doi.org/10.1504/IJEHV.2017.082816

DWD, 2021a. Niederschlag: vieljährige Mittelwerte 1981 - 2010. DWD. https://www.dwd.de/DE/leistungen/klimadatendeutschland/mittelwerte/nieder_8110_fest_html.html?view=nasPublication&nn=16102. Accessed 31 August 2022.

DWD, 2021b. Temperatur: vieljährige Mittelwerte 1981 - 2010. DWD. https://www.dwd.de/DE/leistungen/klimadatendeutschland/mittelwerte/temp_8110_fest_html.html%3Fview%3DnasPublication. Accessed 31 August 2022.

DWD, 2022. Data extracted from Climate Data Center (CDC): Monthly station observations of precipitation in mm for Germany. Lerchenberg. v21.3. Accessed 2 September 2022.

European Parliament and Council (EU), 2008. Directive 2008/50/EC of the european Parliament and of the council of 21 May 2008 on ambient air quality and cleaner air for Europe. https://eur-lex.europa.eu/eli/dir/2008/50/oj.

Fussell, J.C., Franklin, M., Green, D.C., Gustafsson, M., Harrison, R.M., Hicks, W., Kelly, F.J., Kishta, F., Miller, M.R., Mudway, I.S., Oroumiyeh, F., Selley, L., Wang, M., Zhu, Y., 2022. A Review of Road Traffic-Derived Non-Exhaust Particles: Emissions, Physicochemical Characteristics, Health Risks, and Mitigation Measures. Environmental science & technology 56 (11), 6813–6835. doi:10.1021/acs.est.2c01072.

Gallagher, J., Baldauf, R., Fuller, C.H., Kumar, P., Gill, L.W., McNabola, A., 2015. Passive methods for improving air quality in the built environment: A review of porous and solid barriers. Atmospheric Environment 120, 61–70. doi:10.1016/j.atmosenv.2015.08.075.

Garcia-Algar, O., Canchucaja, L., d'Orazzio, V., Manich, A., Joya, X., Vall, O., 2015. Different exposure of infants and adults to ultrafine particles in the urban area of Barcelona. Environmental monitoring and assessment 187 (1), 4196. doi:10.1007/s10661-014-4196-5.

GRIMM Aerosol Technik GmbH & Co. KG, 2015. Portable Laser Aerosol Spectrometer: Model Mini-LAS 11-R.

Gualtieri, M., Ovrevik, J., Mollerup, S., Asare, N., Longhin, E., Dahlman, H.-J., Camatini, M., Holme, J.A., 2011. Airborne urban particles (Milan winter-PM2.5) cause mitotic arrest and cell death: Effects on DNA, mitochondria, AhR binding and spindle organization. Mutation research 713 (1-2), 18–31. doi:10.1016/j.mrfmmm.2011.05.011.

Harr, L., Sinsel, T., Simon, H., Esper, J., 2022a. Seasonal Changes in Urban PM2.5 Hotspots and Sources from Low-Cost Sensors. Atmosphere 13 (5), 694. doi:10.3390/atmos13050694.

Harr, L., Sinsel, T., Simon, H., Konter, O., Dreiseitl, D., Schulz, P., Esper, J., 2022b. PM2.5 exposure differences between children and adults. Urban Climate 44, 101198. doi:10.1016/j.uclim.2022.101198.

Harrison, R.M., Allan, J., Carruthers, D., Heal, M.R., Lewis, A.C., Marner, B., Murrells, T., Williams, A., 2021. Non-exhaust vehicle emissions of particulate matter and VOC from road traffic: A review. Atmospheric Environment 262, 118592. doi:10.1016/j.atmosenv.2021.118592.

Hussein, T., Johansson, C., Karlsson, H., Hansson, H.-C., 2008. Factors affecting non-tailpipe aerosol particle emissions from paved roads: On-road measurements in Stockholm, Sweden. Atmospheric Environment 42 (4), 688–702. doi:10.1016/j.atmosenv.2007.09.064.

Jalava, P.I., Wang, Q., Kuuspalo, K., Ruusunen, J., Hao, L., Fang, D., Väisänen, O., Ruuskanen, A., Sippula, O., Happo, M.S., Uski, O., Kasurinen, S., Torvela, T., Koponen, H., Lehtinen, K., Komppula, M., Gu, C., Jokiniemi, J., Hirvonen, M.-R., 2015. Day and night variation in chemical composition and toxicological responses of size segregated urban air PM samples in a high air pollution situation. Atmospheric Environment 120, 427–437. doi:10.1016/j.atmosenv.2015.08.089.

Karagulian, F., Belis, C.A., Dora, C.F.C., Prüss-Ustün, A.M., Bonjour, S., Adair-Rohani, H., Amann, M., 2015. Contributions to cities' ambient particulate matter (PM): A systematic review of local source contributions at global level. Atmospheric Environment 120, 475–483. doi:10.1016/j.atmosenv.2015.08.087.

Kerschbaumer, A., Lutz, M., 2008. Origin and influence of PM10 in urban and in rural environments. Adv. Sci. Res. 2 (1), 53–55. doi:10.5194/asr-2-53-2008.

Lelieveld, J., Klingmüller, K., Pozzer, A., Pöschl, U., Fnais, M., Daiber, A., Münzel, T., 2019. Cardiovascular disease burden from ambient air pollution in Europe reassessed using novel hazard ratio functions. European heart journal 40 (20), 1590–1596. doi:10.1093/eurheartj/ehz135.

Lough, G.C., Schauer, J.J., Park, J.-S., Shafer, M.M., Deminter, J.T., Weinstein, J.P., 2005. Emissions of metals associated with motor vehicle roadways. Environmental science & technology 39 (3), 826–836. doi:10.1021/es048715f.

Mie, G., 1908. Beiträge zur Optik trüber Medien, speziell kolloidaler Metallösungen. Ann. Phys. 330 (3), 377–445. doi:10.1002/ANDP.19083300302.

Minguillón, M.C., Querol, X., Baltensperger, U., Prévôt, A.S.H., 2012. Fine and coarse PM composition and sources in rural and urban sites in Switzerland: local or regional pollution? The Science of the total environment 427-428, 191–202. doi:10.1016/j.scitotenv.2012.04.030.

Morawska, L., Johnson, G., Ristovski, Z.D., Agranovski, V., 1999. Relation between particle mass and number for submicrometer airborne particles. Atmospheric Environment 33 (13), 1983–1990. doi:10.1016/S1352-2310(98)00433-6.

Oroumiyeh, F., Zhu, Y., 2021. Brake and tire particles measured from on-road vehicles: Effects of vehicle mass and braking intensity. Atmospheric Environment: X 12, 100121. doi:10.1016/j.aeaoa.2021.100121.

Peters, T.M., Ott, D., O'Shaughnessy, P.T., 2006. Comparison of the Grimm 1.108 and 1.109 portable aerosol spectrometer to the TSI 3321 aerodynamic particle sizer for dry particles. The Annals of occupational hygiene 50 (8), 843–850. doi:10.1093/annhyg/mel067.

Piscitello, A., Bianco, C., Casasso, A., Sethi, R., 2021. Non-exhaust traffic emissions: Sources, characterization, and mitigation measures. The Science of the total environment 766, 144440. doi:10.1016/j.scitotenv.2020.144440.

Sanders, P.G., Xu, N., Dalka, T.M., Maricq, M.M., 2003. Airborne brake wear debris: size distributions, composition, and a comparison of dynamometer and vehicle tests. Environmental science & technology 37 (18), 4060–4069. doi:10.1021/es034145s.

Sanguesa, J.A., Torres-Sanz, V., Garrido, P., Martinez, F.J., Marquez-Barja, J.M., 2021. A Review on Electric Vehicles: Technologies and Challenges. Smart Cities 4, 372–404. https://doi.org/10.3390/smartcities4010022

Schraufnagel, D.E., 2020. The health effects of ultrafine particles. Experimental & molecular medicine 52 (3), 311–317. doi:10.1038/s12276-020-0403-3.

Sharma, A., Kumar, P., 2020. Quantification of air pollution exposure to in-pram babies and mitigation strategies. Environment international 139, 105671. doi:10.1016/j.envint.2020.105671.

Shepard, D., 1968. A two-dimensional interpolation function for irregularly-spaced data, in: Proceedings of the 1968 23rd ACM national conference on -. the 1968 23rd ACM national conference, Not Known. ACM Press, New York, New York, USA, pp. 517–524. doi:10.1145/800186.810616.

Squizzato, S., Masiol, M., Agostini, C., Visin, F., Formenton, G., Harrison, R.M., Rampazzo, G., 2016. Factors, origin and sources affecting PM 1 concentrations and composition at an urban background site. Atmospheric Research 180, 262–273. doi:10.1016/j.atmosres.2016.06.002.

Stewart, I.D., Oke, T.R., 2012. Local Climate Zones for Urban Temperature Studies. Bulletin of the American Meteorological Society 93 (12), 1879–1900. doi:10.1175/BAMS-D-11-00019.1.

Tang, G., Zhang, J., Zhu, X., Song, T., Münkel, C., Hu, B., Schäfer, K., Liu, Z., Zhang, J., Wang, L., Xin, J., Suppan, P., Wang, Y., 2016. Mixing layer height and its implications for air pollution over Beijing, China. Atmos. Chem. Phys. 16 (4), 2459–2475. doi:10.5194/acp-16-2459-2016.

Timmers, V.R.J.H., Achten, P.A.J., 2016. Non-exhaust PM emissions from electric vehicles. Atmos. Environ. 134, 10–17. https://doi.org/10.1016/j.atmosenv.2016.03.017

Titos, G., Lyamani, H., Pandolfi, M., Alastuey, A., Alados-Arboledas, L., 2014. Identification of fine (PM1) and coarse (PM10-1) sources of particulate matter in an urban environment. Atmospheric Environment 89, 593–602. doi:10.1016/j.atmosenv.2014.03.001.

Torres-Ramos, Y.D., Montoya-Estrada, A., Guzman-Grenfell, A.M., Mancilla-Ramirez, J., Cardenas-Gonzalez, B., Blanco-Jimenez, S., Sepulveda-Sanchez, J.D., Ramirez-Venegas, A., Hicks, J.J., 2011. Urban PM2.5 induces ROS generation and RBC damage in COPD patients. Frontiers in bioscience (Elite edition) 3, 808–817. doi:10.2741/e288.

Wagner, P., Schäfer, K., 2017. Influence of mixing layer height on air pollutant concentrations in an urban street canyon. Urban Climate 22, 64–79. doi:10.1016/j.uclim.2015.11.001.

WHO, 2022. World health statistics 2022: monitoring health for the SDGs, sustainable development goals. Global report. World Health Organization (WHO).

Woo, S.-H., Jang, H., Lee, S.-B., Lee, S., 2022. Comparison of total PM emissions emitted from electric and internal combustion engine vehicles: An experimental analysis. Sci. Total Environ. 842, 156961. https://doi.org/10.1016/j.scitotenv.2022.156961

Wu, Y., Liu, J., Zhai, J., Cong, L., Wang, Y., Ma, W., Zhang, Z., Li, C., 2018. Comparison of dry and wet deposition of particulate matter in near-surface waters during summer. PloS one 13 (6), e0199241. doi:10.1371/journal.pone.0199241.

Yang, M., Guo, Y.-M., Bloom, M.S., Dharmagee, S.C., Morawska, L., Heinrich, J., Jalaludin, B., Markevychd, I., Knibbsf, L.D., Lin, S., Hung Lan, S., Jalava, P., Komppula, M., Roponen, M., Hirvonen, M.-R., Guan, Q.-H., Liang, Z.-M., Yu, H.-Y., Hu, L.-W., Yang,

B.-Y., Zeng, X.-W., Dong, G.-H., 2020. Is PM1 similar to PM2.5? A new insight into the association of PM1 and PM2.5 with children's lung function. Environment international 145, 106092. doi:10.1016/j.envint.2020.106092.

Yong, J.Y., Ramachandaramurthy, V.K., Tan, K.M., Mithulananthan, N., 2015. A review on the state-of-the-art technologies of electric vehicle, its impacts and prospects. Renew. Sustain. Energy Rev. 49, 365–385. https://doi.org/10.1016/j.rser.2015.04.130

ZIMEN, 2021. Jahresbericht 2020: Zentrales Immissionsmessnetz - ZIMEN -. ZIMEN. https://luft.rlp.de/fileadmin/luft/ZIMEN/Jahresberichte/ZIMEN-Jahresbericht_2020.pdf. Accessed 31 August 2022.

ZIMEN, 2022. - Luft-Überwachung in Rheinland-Pfalz -: Zentrales Immissionsmessnetz - ZIMEN -. State Office of Rhineland-Palatinate. https://luft.rlp.de/de/startseite/.

4.8 Appendix

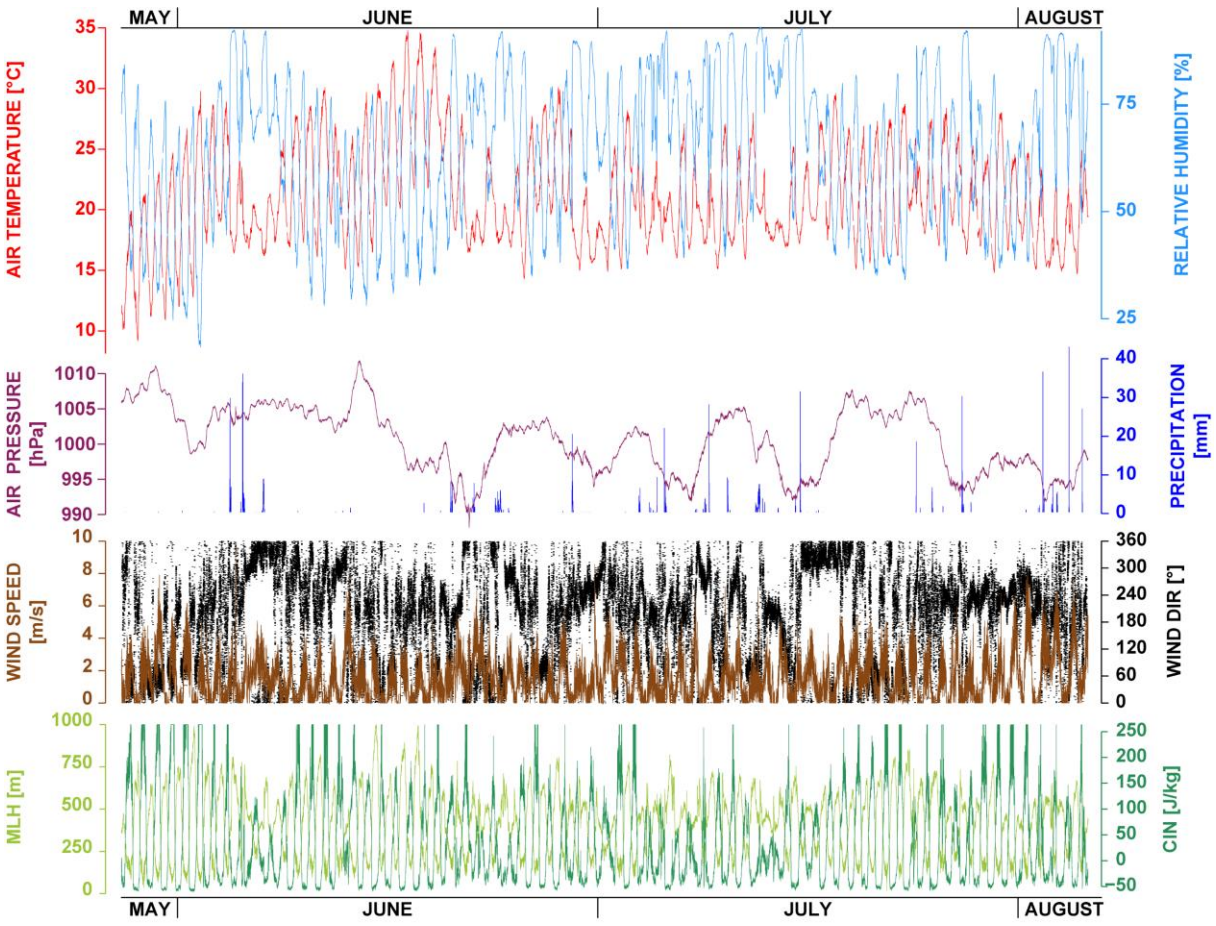

Fig. 4-A1 Weather conditions from May–August 2021. TA, RH and air pressure were measured at 2m a.g.l. at the measurement station Mainz-Zitadelle, wind speed and direction 10m a.g.l and precipitation 2m a.g.l. at Institute for

Atmospheric Physics at the Johannes Gutenberg-University. MLH and CIN were measured at the headquarter of the state office for environment in downtown Mainz.

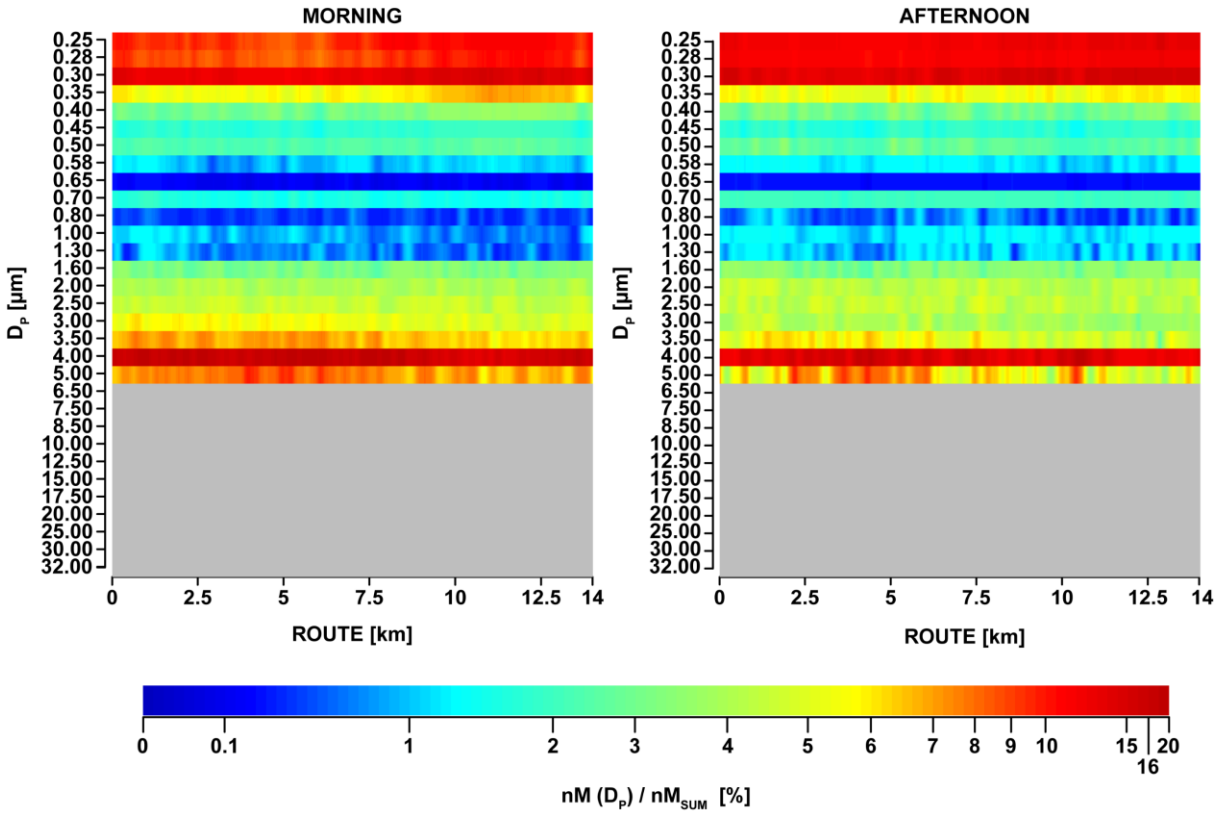

Fig. 4-A2 Relative differences between ndM of each D_P and the sum of all continuously measured D_P ndM at each track point (n=1403). Labels of the y-axis show the upper limit of the D_P per bin.

5 Conclusions and perspectives

Besides climate change, air pollution is one of the biggest challenges worldwide. Monitoring air pollution and in particular PM levels is therefore of great importance in order to be able to make recommendations for the protection of the population (Gozzi et al., 2016; WHO, 2022). As stationary monitoring sites cannot provide data about spatiotemporal variability due to their immobility and measurement interval of > 30 min (ZIMEN, 2022), mobile measurement systems offer the opportunity to measure personal exposure levels in complex urban environments at high spatiotemporal resolution. Upcoming low-cost sensors, in particular, impress with great portability and little expenses to expand mobile measurements in science and private citizen monitoring.

This thesis has revealed great advancements in mobile PM monitoring in urban environments. The explorative investigations point out potentials and limitations in vertically differentiated personal $PM_{2.5}$ exposures measurements of children and adults as well as in identifying small-scale spatial PM hotspots and their sources.

First, it was demonstrated that it can be appropriate to use state-of-the-art, low-cost sensors OPC-N3 by Alphasense to conduct mobile PM measurement studies in complex urban environments (Section 2). It has been proven that in six out of eight runs on consecutive days, children are exposed to significantly higher $PM_{2.5}$ concentrations than adults, independent of the position along the measurement route. The absolute and relative differences increased with increasing concentrations accompanying with lower spatial variability. The differences could be explained by accumulation processes of locally emitted PM during stable anticyclonic weather conditions. The findings are all the more remarkable as the breathing heights of children and adults, and thus the measurement heights, are only 60 cm apart vertically. These results could be brought into line with an exhaust particle dispersion simulation conducted with ENVI-met for high-traffic roads.

Based on the demonstrated applicability of the Alphasense OPC-N3 low-cost sensors for mobile measurements, seasonal and spatial variability of $PM_{2.5}$ in the urban area of Mainz were examined in high spatiotemporal resolution. Persisting $PM_{2.5}$ hotspots could be identified in > 60% of the runs, but the locations varied between the spring and autumn study periods. While the March hotspots could be attributed to anthropogenic sources as construction sites and traffic emissions, underlined by $PM_{2.5}$ / PM_{10} ratios, the September hotspots could be allocated to

popular areas dominated by pedestrians: seating activities outside of restaurants and a park. The according $PM_{2.5}$ / PM_{10} ratios indicate cooking and smoking at the restaurants and whirled up bare soils of graveled paths. The results of both studies contribute to a rethinking of the optimal location of PM monitoring stations to identify hotspots and the representativeness of the formalized measurement heights between 1.5 – 4 m to cover personal exposure.

Despite the great potential of being able to measure spatiotemporal variability in high vertical and spatiotemporal resolution, there are still important limitations that need to be considered when using the low-cost sensors. It is highly recommended to recalibrate the OPC-N3 sensors under ambient environmental conditions of the study as varying chemical compositions of ambient PM may influence the measured concentrations (Chatzidiakou et al., 2019; Gysel et al., 2007; Hagler et al., 2018). However, the side-by-side calibration in Section 2 demonstrated that the perform weak under RH > 85% even after the recommended RH correction following Crilley et al. (2020, 2018). The variability between the sensors showed a large heteroscedasticity for PM > 10 µg/m³, resulting in such large biases that reliable comparisons of these sensors under high RH conditions were questionable. In the perspective, there is a need of further improvements to reduce the RH sensitivity. For example, before the air flow enters the sensor, the RH could be reduced by an upstream chemical absorber or by drying the air with a heated measuring inlet (Samad et al., 2021), but these processes are still too complex and too large to be used in mobile measuring devices.

Furthermore, a side-by-side calibration of the OPC-N3 sensors to each other is not sufficient to determine absolute PM concentrations accurately enough. The three sensors used in section 3, for example, showed high agreement with each other, but significantly underestimated the measured $PM_{2.5}$ concentrations of the ZIMEN network of the state Rhineland-Palatinate, regardless of whether a RH correction was applied or not. Calibration with reference instruments could improve the accuracy of the sensors, in particular during RH < 85% conditions. However, this is very time-consuming and cost-intensive, as the measuring stations in the EU do not provide high-resolution measurement data and calibration at the measuring points is therefore not possible. Consequently, high-resolution reference measuring instruments would have to be purchased and suitable measuring locations would have to be identified prior to each study as low-cost sensors can be sensitive to chemical compositions of the ambient air. This could possibly be undertaken for scientific studies, but in the context of easy-to-use citizen science projects, the extensive calibrations are not feasible and low-cost sensors would no longer be attractive despite their existing potential.

Until improved low-cost sensors are available to address RH susceptibility and absolute PM accuracy, low-cost sensors should only be used to determine spatiotemporal highly resolved relative changes and trends in $PM_{2.5}$ and PM_{10} in complex urban environments. The detection of exceedances of concentration limits is then not possible, but low-cost sensors PM data could complement measurements by stationary monitoring systems and help to identify highly polluted areas in urban areas where follow-up measurements can then be taken.

To address high spatiotemporal absolute PM values and to indicate PM pattern (sub-) micron resolution, a study using a mobile cargo bike platform with GRIMM 11-R reference instruments was conducted in the urban environment of Mainz (Section 4). It could be demonstrated that the concentrations for PM_1 and PM_{10} were significantly higher in the MO than in the AF. The mean concentrations were higher in urban than in suburban and rural areas for both fractions. But only clear hotspots could be identified for $PM_{10,}$ three of which were located at urban multi-lane roads and street canyons and one in the agricultural area.

The PNC decreased greatly with increasing D_P, independent of the location and time of the day. Particles with $D_P < 0.3$ µm and 3–5 µm were vastly dominating the total dM. This indicates that the particles were likely emitted from traffic-related combustion processes ($D_P < 1$ µm) and tyre and brake abrasion (D_P 3–5 µm). In contrast, the elevated concentrations with $D_P > 3$ µm at the rural hotspot gave an indication that natural dust from the agricultural fields was crucial for the elevated concentrations.

These results could be of relevance for future traffic planning as well as for the new EURO 7 emission standard, as the transition from internal combustion engine vehicles to electric ones in urban areas can reduce the PNC and dM for $D_P < 1$ µm significantly. Tyre and brake emissions, however, would still be there and noxious especially in areas where emissions accumulate, i.e. street canyons and roads with high traffic intensity. Reducing the total number of vehicles and increasing of public transport would help to limit PM emissions at all particle sizes.

In summary, mobile measurement systems offer the opportunity to measure PM in high spatiotemporal resolution in urban areas. While state-of-the-art low-cost sensors can extend spatial coverage and provide PM hotspots and their sources using relative PM values, more the more expensive measurement system on the cargo bike platform can even provide absolute values in (sub-) micron resolution to gain a deeper insight into the variability of the PNC and PM distributions across the D_P spectrum on personal exposure level. D_P spectral analyzes

enable the visualization of spatial PNC and dM patterns so that emission sources can be more clearly identified. This might help future urban transportation planners target PM pollution reduction. Mobile measurement systems therefore usefully complement fixed, stationary measurements and can take particular account of personal exposure in complex urban environments.

References

Aberer, K., Sathe, S., Chakraborty, D., Martinoli, A., Barrenetxea, G., Faltings, B., Thiele, L., 2010. OpenSense: open community driven sensing of environment, in: Proceedings of the ACM SIGSPATIAL International Workshop on GeoStreaming. Presented at the GIS '10: 18th SIGSPATIAL International Conference on Advances in Geographic Information Systems, ACM, San Jose California, pp. 39–42. https://doi.org/10.1145/1878500.1878509

Alemany, S., Vilor-Tejedor, N., García-Esteban, R., Bustamante, M., Dadvand, P., Esnaola, M., Mortamais, M., Forns, J., van Drooge, B.L., Álvarez-Pedrerol, M., Grimalt, J.O., Rivas, I., Querol, X., Pujol, J., Sunyer, J., 2018. Traffic-Related Air Pollution, *APOE* ε4 Status, and Neurodevelopmental Outcomes among School Children Enrolled in the BREATHE Project (Catalonia, Spain). Environ Health Perspect 126, 087001. https://doi.org/10.1289/EHP2246

Alfano, B., Barretta, L., Del Giudice, A., Vito, S., Di Francia, G., Esposito, E., Formisano, F., Massera, E., Miglietta, M.L., Polichetti, T., 2020. A Review of Low-Cost Particulate Matter Sensors from the Developers' Perspectives. Sensors (Basel) 20. https://doi.org/10.3390/s20236819

Báthory, C., Dobó, Z., Garami, A., Palotás, Á., Tóth, P., 2022. Low-cost monitoring of atmospheric PM—development and testing. Journal of Environmental Management 304, 114158. https://doi.org/10.1016/j.jenvman.2021.114158

Briggs, D.J., de Hoogh, C., Gulliver, J., Wills, J., Elliott, P., Kingham, S., Smallbone, K., 2000. A regression-based method for mapping traffic-related air pollution: application and testing in four contrasting urban environments. Science of The Total Environment 253, 151–167. https://doi.org/10.1016/S0048-9697(00)00429-0

Bukowiecki, N., Lienemann, P., Hill, M., Furger, M., Richard, A., Amato, F., Prévôt, A.S.H., Baltensperger, U., Buchmann, B., Gehrig, R., 2010. PM10 emission factors for non-exhaust particles generated by road traffic in an urban street canyon and along a freeway in Switzerland. Atmospheric Environment 44, 2330–2340. https://doi.org/10.1016/j.atmosenv.2010.03.039

Carreras, H., Ehrnsperger, L., Klemm, O., Paas, B., 2020. Cyclists' exposure to air pollution: in situ evaluation with a cargo bike platform. Environ Monit Assess 192, 470. https://doi.org/10.1007/s10661-020-08443-7

Castell, N., Liu, H.-Y., Dauge, F.R., Kobernus, M., Berre, A.J., Noll, J., Cagatay, E., Gangdal, R., 2016. Supporting Sustainable Mobility Using Mobile Technologies and Personalized Environmental Information: The Citi-Sense-MOB Approach in Oslo, Norway, in: Marx Gomez, J., Sonnenschein, M., Vogel, U., Winter, A., Rapp, B., Giesen, N. (Eds.), Advances and New Trends in Environmental and Energy Informatics, Progress in IS. Springer International Publishing, Cham, pp. 199–218. https://doi.org/10.1007/978-3-319-23455-7_11

Chatzidiakou, L., Krause, A., Popoola, O.A.M., Di Antonio, A., Kellaway, M., Han, Y., Squires, F.A., Wang, T., Zhang, H., Wang, Q., Fan, Y., Chen, S., Hu, M., Quint, J.K., Barratt, B., Kelly, F.J., Zhu, T., Jones, R.L., 2019. Characterising low-cost sensors in highly portable platforms to quantify personal exposure in diverse environments. Atmos Meas Tech 12, 4643–4657. https://doi.org/10.5194/amt-12-1-2019

Chen, L.C., Lippmann, M., 2009. Effects of metals within ambient air particulate matter (PM) on human health. Inhal Toxicol 21, 1–31. https://doi.org/10.1080/08958370802105405

Crilley, L.R., Shaw, M., Pound, R., Kramer, L.J., Price, R., Young, S., Lewis, A.C., Pope, F.D., 2018. Evaluation of a low-cost optical particle counter (Alphasense OPC-N2) for ambient air monitoring. Atmos. Meas. Tech. 11, 709–720. https://doi.org/10.5194/amt-11-709-2018

Crilley, L.R., Singh, A., Kramer, L.J., Shaw, M.D., Alam, M.S., Apte, J.S., Bloss, W.J., Hildebrandt Ruiz, L., Fu, P., Fu, W., Gani, S., Gatari, M., Ilyinskaya, E., Lewis, A.C., Ng'ang'a, D., Sun, Y., Whitty, R.C.W., Yue, S., Young, S., Pope, F.D., 2020. Effect of aerosol composition on the performance of low-cost optical particle counter correction factors. Atmos. Meas. Tech. 13, 1181–1193. https://doi.org/10.5194/amt-13-1181-2020

Czernecki, B., Półrolniczak, M., Kolendowicz, L., Marosz, M., Kendzierski, S., Pilguj, N., 2017. Influence of the atmospheric conditions on PM10 concentrations in Poznań, Poland. J Atmos Chem 74, 115–139. https://doi.org/10.1007/s10874-016-9345-5

Di Antonio, A., Popoola, O.A.M., Ouyang, B., Saffell, J., Jones, R.L., 2018. Developing a Relative Humidity Correction for Low-Cost Sensors Measuring Ambient Particulate Matter. Sensors (Basel) 18. https://doi.org/10.3390/s18092790

EEA, 2023. Europe's air quality status 2022 . URL https://www.eea.europa.eu/publications/status-of-air-quality-in-Europe-2022/europes-air-quality-status-2022

EEA, 2022. Premature deaths due to exposure to fine particulate matter in Europe.

European Parliament and Council, 2008. Directive 2008/50/EC of the european Parliament and of the council of 21 May 2008 on ambient air quality and cleaner air for Europe . URL https://eur-lex.europa.eu/eli/dir/2008/50/oj

Eurostat, 2016. Urban Europe: statistics on cities, towns and suburbs : 2016 edition. Publications Office, LU.

Fritz, S., See, L., Carlson, T., Haklay, M., Oliver, J.L., Fraisl, D., Mondardini, R., Brocklehurst, M., Shanley, L.A., Schade, S., Wehn, U., Abrate, T., Anstee, J., Arnold, S., Billot, M., Campbell, J., Espey, J., Gold, M., Hager, G., He, S., Hepburn, L., Hsu, A., Long, D., Masó, J., McCallum, I., Muniafu, M., Moorthy, I., Obersteiner, M., Parker, A.J., Weisspflug, M., West, S., 2019. Citizen science and the United Nations Sustainable Development Goals. Nat Sustain 2, 922–930. https://doi.org/10.1038/s41893-019-0390-3

Fuller, R., Landrigan, P.J., Balakrishnan, K., Bathan, G., Bose-O'Reilly, S., Brauer, M., Caravanos, J., Chiles, T., Cohen, A., Corra, L., Cropper, M., Ferraro, G., Hanna, J., Hanrahan, D., Hu, H., Hunter, D., Janata, G., Kupka, R., Lanphear, B., Lichtveld, M., Martin, K., Mustapha, A., Sanchez-Triana, E., Sandilya, K., Schaefli, L., Shaw, J., Seddon, J., Suk, W., Téllez-Rojo, M.M., Yan, C., 2022. Pollution and health: a progress update. The Lancet Planetary Health 6, e535–e547. https://doi.org/10.1016/S2542-5196(22)00090-0

Garcia-Algar, O., Canchucaja, L., d'Orazzio, V., Manich, A., Joya, X., Vall, O., 2015. Different exposure of infants and adults to ultrafine particles in the urban area of Barcelona. Environ Monit Assess 187, 4196. https://doi.org/10.1007/s10661-014-4196-5

Goel, A., Kumar, P., 2016. Vertical and horizontal variability in airborne nanoparticles and their exposure around signalised traffic intersections. Environ Pollut 214, 54–69. https://doi.org/10.1016/j.envpol.2016.03.033

Goldman, L.R., 1995. Children--unique and vulnerable. Environmental risks facing children and recommendations for response. Environ Health Perspect 103 Suppl 6, 13–8. https://doi.org/10.1289/ehp.95103s613

Gozzi, F., Della Ventura, G., Marcelli, A., 2016. Mobile monitoring of particulate matter: State of art and perspectives. Atmospheric Pollution Research 7, 228–234. https://doi.org/10.1016/j.apr.2015.09.007

Graham, A.M., Pringle, K.J., Arnold, S.R., Pope, R.J., Vieno, M., Butt, E.W., Conibear, L., Stirling, E.L., McQuaid, J.B., 2020. Impact of weather types on UK ambient particulate

matter concentrations. Atmospheric Environment: X 5, 100061. https://doi.org/10.1016/j.aeaoa.2019.100061

Gualtieri, M., Ovrevik, J., Mollerup, S., Asare, N., Longhin, E., Dahlman, H.-J., Camatini, M., Holme, J.A., 2011. Airborne urban particles (Milan winter-PM2.5) cause mitotic arrest and cell death: Effects on DNA, mitochondria, AhR binding and spindle organization. Mutat Res 713, 18–31. https://doi.org/10.1016/j.mrfmmm.2011.05.011

Gysel, M., Crosier, J., Topping, D.O., Whitehead, J.D., Bower, K.N., Cubison, M.J., Williams, P.I., Flynn, M.J., McFiggans, G.B., Coe, H., 2007. Closure study between chemical composition and hygroscopic growth of aerosol particles during TORCH2. Atmos. Chem. Phys. 7, 6131–6144. https://doi.org/10.5194/acp-7-6131-2007

Hagler, G.S.W., Williams, R., Papapostolou, V., Polidori, A., 2018. Air Quality Sensors and Data Adjustment Algorithms: When Is It No Longer a Measurement? Environ Sci Technol 52, 5530–5531. https://doi.org/10.1021/acs.est.8b01826

Harr, L., Sinsel, T., Simon, H., Esper, J., 2022a. Seasonal Changes in Urban PM2.5 Hotspots and Sources from Low-Cost Sensors. Atmosphere 13, 694. https://doi.org/10.3390/atmos13050694

Harr, L., Sinsel, T., Simon, H., Konter, O., Dreiseitl, D., Schulz, P., Esper, J., 2022b. PM2.5 exposure differences between children and adults. Urban Climate 44, 101198. https://doi.org/10.1016/j.uclim.2022.101198

Harrison, R.M., Allan, J., Carruthers, D., Heal, M.R., Lewis, A.C., Marner, B., Murrells, T., Williams, A., 2021. Non-exhaust vehicle emissions of particulate matter and VOC from road traffic: A review. Atmospheric Environment 262, 118592. https://doi.org/10.1016/j.atmosenv.2021.118592

Jalava, P.I., Wang, Q., Kuuspalo, K., Ruusunen, J., Hao, L., Fang, D., Väisänen, O., Ruuskanen, A., Sippula, O., Happo, M.S., Uski, O., Kasurinen, S., Torvela, T., Koponen, H., Lehtinen, K.E.J., Komppula, M., Gu, C., Jokiniemi, J., Hirvonen, M.-R., 2015. Day and night variation in chemical composition and toxicological responses of size segregated urban air PM samples in a high air pollution situation. Atmospheric Environment 120, 427–437. https://doi.org/10.1016/j.atmosenv.2015.08.089

Karagulian, F., Barbiere, M., Kotsev, A., Spinelle, L., Gerboles, M., Lagler, F., Redon, N., Crunaire, S., Borowiak, A., 2019. Review of the Performance of Low-Cost Sensors for Air Quality Monitoring. Atmosphere 10, 506. https://doi.org/10.3390/atmos10090506

Kaur, K., Kelly, K.E., 2022. Performance evaluation of the Alphasense OPC-N3 and Plantower PMS5003 sensor in measuring dust events in the Salt Lake Valley, Utah (preprint).

Aerosols/In Situ Measurement/Instruments and Platforms. https://doi.org/10.5194/amt-2022-292

Kumar, P., Fennell, P., Britter, R., 2008. Measurements of particles in the 5-1000 nm range close to road level in an urban street canyon. Science of The Total Environment 390, 437–47. https://doi.org/10.1016/j.scitotenv.2007.10.013

Kumar, P., Rivas, I., Sachdeva, L., 2017. Exposure of in-pram babies to airborne particles during morning drop-in and afternoon pick-up of school children. Environ Pollut 224, 407–420. https://doi.org/10.1016/j.envpol.2017.02.021

Lelieveld, J., Klingmüller, K., Pozzer, A., Pöschl, U., Fnais, M., Daiber, A., Münzel, T., 2019. Cardiovascular disease burden from ambient air pollution in Europe reassessed using novel hazard ratio functions. Eur Heart J 40, 1590–1596. https://doi.org/10.1093/eurheartj/ehz135

Mazur, L.J., 2003. Pediatric environmental health. Curr Probl Pediatr Adolesc Health Care 33, 6–25. https://doi.org/10.1067/mps.2003.1

Mead, M.I., Popoola, O.A.M., Stewart, G.B., Landshoff, P., Calleja, M., Hayes, M., Baldovi, J.J., McLeod, M.W., Hodgson, T.F., Dicks, J., Lewis, A., Cohen, J., Baron, R., Saffell, J.R., Jones, R.L., 2013. The use of electrochemical sensors for monitoring urban air quality in low-cost, high-density networks. Atmospheric Environment 70, 186–203. https://doi.org/10.1016/j.atmosenv.2012.11.060

Morawska, L., Thai, P.K., Liu, X., Asumadu-Sakyi, A., Ayoko, G., Bartonova, A., Bedini, A., Chai, F., Christensen, B., Dunbabin, M., Gao, J., Hagler, G.S.W., Jayaratne, R., Kumar, P., Lau, A.K.H., Louie, P.K.K., Mazaheri, M., Ning, Z., Motta, N., Mullins, B., Rahman, M.M., Ristovski, Z., Shafiei, M., Tjondronegoro, D., Westerdahl, D., Williams, R., 2018. Applications of low-cost sensing technologies for air quality monitoring and exposure assessment: How far have they gone? Environ Int 116, 286–299. https://doi.org/10.1016/j.envint.2018.04.018

Parkhurst, W.J., Tanner, R.L., Weatherford, F.P., Valente, R.J., Meagher, J.F., 1999. Historic PM2.5/PM10 Concentrations in the Southeastern United States-Potential Implications of the Revised Particulate Matter Standard. J Air Waste Manag Assoc 49, 1060–1067. https://doi.org/10.1080/10473289.1999.10463894

Piscitello, A., Bianco, C., Casasso, A., Sethi, R., 2021. Non-exhaust traffic emissions: Sources, characterization, and mitigation measures. Sci Total Environ 766, 144440. https://doi.org/10.1016/j.scitotenv.2020.144440

Roberts, F.A., Van Valkinburgh, K., Green, A., Post, C.J., Mikhailova, E.A., Commodore, S., Pearce, J.L., Metcalf, A.R., 2022. Evaluation of a new low-cost particle sensor as an internet-of-things device for outdoor air quality monitoring. Journal of the Air & Waste Management Association 72, 1219–1230. https://doi.org/10.1080/10962247.2022.2093293

Samad, A., Melchor Mimiaga, F.E., Laquai, B., Vogt, U., 2021. Investigating a Low-Cost Dryer Designed for Low-Cost PM Sensors Measuring Ambient Air Quality. Sensors 21, 804. https://doi.org/10.3390/s21030804

Schlesinger, R.B., 2007. The health impact of common inorganic components of fine particulate matter (PM2.5) in ambient air: a critical review. Inhal Toxicol 19, 811–32. https://doi.org/10.1080/08958370701402382

Sharma, A., Kumar, P., 2018. A review of factors surrounding the air pollution exposure to in-pram babies and mitigation strategies. Environ Int 120, 262–278. https://doi.org/10.1016/j.envint.2018.07.038

Sicard, P., Agathokleous, E., De Marco, A., Paoletti, E., Calatayud, V., 2021. Urban population exposure to air pollution in Europe over the last decades. Environ Sci Eur 33, 28. https://doi.org/10.1186/s12302-020-00450-2

Snyder, E.G., Watkins, T.H., Solomon, P.A., Thoma, E.D., Williams, R.W., Hagler, G.S.W., Shelow, D., Hindin, D.A., Kilaru, V.J., Preuss, P.W., 2013. The Changing Paradigm of Air Pollution Monitoring. Environ. Sci. Technol. 47, 11369–11377. https://doi.org/10.1021/es4022602

Sousan, S., Koehler, K., Hallett, L., Peters, T.M., 2016. Evaluation of the Alphasense Optical Particle Counter (OPC-N2) and the Grimm Portable Aerosol Spectrometer (PAS-1.108). Aerosol Sci Technol 50, 1352–1365. https://doi.org/10.1080/02786826.2016.1232859

Squizzato, S., Masiol, M., Agostini, C., Visin, F., Formenton, G., Harrison, R.M., Rampazzo, G., 2016. Factors, origin and sources affecting PM 1 concentrations and composition at an urban background site. Atmospheric Research 180, 262–273. https://doi.org/10.1016/j.atmosres.2016.06.002

Tang, G., Zhang, Jinqiang, Zhu, X., Song, T., Münkel, C., Hu, B., Schäfer, K., Liu, Z., Zhang, Junke, Wang, L., Xin, J., Suppan, P., Wang, Y., 2016. Mixing layer height and its implications for air pollution over Beijing, China. Atmos. Chem. Phys. 16, 2459–2475. https://doi.org/10.5194/acp-16-2459-2016

Titos, G., Lyamani, H., Pandolfi, M., Alastuey, A., Alados-Arboledas, L., 2014. Identification of fine (PM1) and coarse (PM10-1) sources of particulate matter in an urban environment. Atmospheric Environment 89, 593–602. https://doi.org/10.1016/j.atmosenv.2014.03.001

Torres-Ramos, Y.D., Montoya-Estrada, A., Guzman-Grenfell, A.M., Mancilla-Ramirez, J., Cardenas-Gonzalez, B., Blanco-Jimenez, S., Sepulveda-Sanchez, J.D., Ramirez-Venegas, A., Hicks, J.J., 2011. Urban PM2.5 induces ROS generation and RBC damage in COPD patients. Front Biosci (Elite Ed) 3, 808–17. https://doi.org/10.2741/e288

Wagner, P., Schäfer, K., 2017. Influence of mixing layer height on air pollutant concentrations in an urban street canyon. Urban Climate 22, 64–79. https://doi.org/10.1016/j.uclim.2015.11.001

West, S.E., Büker, P., Ashmore, M., Njoroge, G., Welden, N., Muhoza, C., Osano, P., Makau, J., Njoroge, P., Apondo, W., 2020. Particulate matter pollution in an informal settlement in Nairobi: Using citizen science to make the invisible visible. Applied Geography 114, 102133. https://doi.org/10.1016/j.apgeog.2019.102133

WHO, 2022. World health statistics 2022: monitoring health for the SDGs, sustainable development goals. Global report. .

WHO, 2021. WHO global air quality guidelines: particulate matter (PM2.5 and PM10), ozone, nitrogen dioxide, sulfur dioxide and carbon monoxide . URL https://apps.who.int/iris/handle/10665/345329

WMO, 2018. Low-cost sensors for the measurement of atmospheric composition: overview of topic and future applications.

Xu, G., Jiao, L., Zhang, B., Zhao, S., Yuan, M., Gu, Y., Liu, J., Tang, X., 2017. Spatial and Temporal Variability of the PM2.5/PM10 Ratio in Wuhan, Central China. Aerosol Air Qual. Res. 17, 741–751. https://doi.org/10.4209/aaqr.2016.09.0406

Yang, M., Guo, Y.-M., Bloom, M.S., Dharmagee, S.C., Morawska, L., Heinrich, J., Jalaludin, B., Markevychd, I., Knibbsf, L.D., Lin, S., Hung Lan, S., Jalava, P., Komppula, M., Roponen, M., Hirvonen, M.-R., Guan, Q.-H., Liang, Z.-M., Yu, H.-Y., Hu, L.-W., Yang, B.-Y., Zeng, X.-W., Dong, G.-H., 2020. Is PM1 similar to PM2.5? A new insight into the association of PM1 and PM2.5 with children's lung function. Environ Int 145, 106092. https://doi.org/10.1016/j.envint.2020.106092

ZIMEN, 2022. - Luft-Überwachung in Rheinland-Pfalz -: Zentrales Immissionsmessnetz - ZIMEN - . URL https://luft.rlp.de/de/startseite/

List of Figures

List of Tables

Index of Abbreviation

AF	afternoon
CIN	Convective inhibition
CV	coefficient of variation
dM	mass concentration
D_P	aerodynamic diameter
IQR	interquartile range
MO	morning
MLH	mixing layer height
ndM	normalized mass concentration
PM	particulate matter
PM_1	particulate matter, where particles have an aerodynamic diameter of ≤ 1 µm
$PM_{2.5}$	particulate matter, where particles have an aerodynamic diameter of ≤ 2.5 µm
PM_{10}	particulate matter, where particles have an aerodynamic diameter of ≤ 10 µm
PNC	particle number concentration
QCD	quartile coefficient of dispersion
RH	relative humidity
RMSE	root-mean-square error
SD	standard deviation
TA	air temperature

6 Curriculum Vitae

Not available online.